Microfluidics-generated Double Emulsion Platform for High-Throughput Screening and Multicellular Spheroid Production with Controllable Microenvironment

by

Hon Fai Chan

Department of Biomedical Engineering
Duke University

Date:_______________________
Approved:

____
Kam W. Leong, Supervisor

____
George Truskey, Chair

____
Farshid Guilak

____
Xuanhe Zhao

____
Jun Chen

Dissertation submitted in partial fulfillment of
the requirements for the degree of Doctor of Philosophy in the Department of
Biomedical Engineering in the Graduate School
of Duke University

2015

ABSTRACT

Microfluidics-generated Double Emulsion Platform for High-Throughput Screening and Multicellular Spheroid Production with Controllable Microenvironment

by

Hon Fai Chan

Department of Biomedical Engineering
Duke University

Date:_______________________
Approved:

____
Kam W. Leong, Supervisor

____
George Truskey, Chair

____
Farshid Guilak

____
Xuanhe Zhao

____
Jun Chen

An abstract of a dissertation submitted in partial
fulfillment of the requirements for the degree
of Doctor of Philosophy in the Department of
Biomedical Engineering in the Graduate School
of Duke University

2015

Copyright by
Hon Fai Chan
2015

Abstract

High-throughput processing technologies hold critical position in biomedical research. These include screening of cellular response based on phenotypic difference and production of homogeneous chemicals and biologicals for therapeutic applications. The rapid development of microfluidics technology has provided an efficient, controllable, economical and automatable processing platform for various applications. In particular, emulsion droplet gains a lot of attention due to its uniformity and ease of isolation, but the application of water-in-oil (W/O) single emulsion is hampered by the presence of the oil phase which is incompatible with aqueous phase manipulation and the difficulty in modifying the droplet environment.

This thesis presents the development of a double emulsion (DE) droplet platform in microfluidics and two applications: (1) high-throughput screening of synthetic gene and (2) production of multicellular spheroids with adjustable microenvironment for controlling stem cell differentiation and liver tissue engineering. Monodisperse DE droplets with controllable size and selective permeability across the oil shell were generated via two microfluidics devices after optimization of device design and flow rates.

Next, bacterial cells bearing synthetic genes constructed from an inkjet oligonucleotide synthesizer were encapsulated as single cells in DE droplets. Enrichment of fluorescent signals (~100 times) from the cells allowed quantification and

selection of functionally-correct genes before and after error correction scheme was employed. Permeation of Isopropyl β-D-1-thiogalactopyranoside (IPTG) molecules from the external phase triggered target gene expression of the pET vector. Fluorescent signals from at least ~100 bacteria per droplet generated clearly distinguishable fluorescent signals that enabled droplets sorting through fluorescence-activated cell sorting (FACS) technique.

In addition, DE droplets promoted rapid aggregation of mammalian cells into single spheroid in 150 min. Size-tunable human mesenchymal stem cells (hMSC) spheroids could be extracted from the droplets and exhibited better differentiation potential than cells cultured in monolayer. The droplet environment could be altered by loading matrix molecules in it to create spheroid-encapsulated microgel. As an example, hMSC spheroid was encapsulated in alginate or alginate-RGD microgel and enhanced osteogenic differentiation was found in the latter case.

Lastly, the capability of forming spheroids in DE droplet was applied in liver tissue engineering, where single or co-culture hepatocyte spheroids were efficiently produced and encapsulated in microgel. The use of alginate-collagen microgel significantly improved the long-term function of the spheroid, in a manner similar to forming co-culture spheroids of hepatocytes and endothelial progenitor cells at a 5 to 1 ratio. The hepatocyte spheroid encapsulated in microgel could be useful for developing bioartificial liver or drug testing platform or applied directly for hepatocyte transplantation.

Contents

Abstract iv

List of Figures xi

Acknowledgements xvi

1. An Introduction to Microfluidics Technologies: Application in High-throughput Biomedical Processing 1

  1.1 Introduction to High-throughput Biomedical Processing 1

    1.1.1 High-throughput Screening (HTS) 1

    1.1.2 High-throughput Synthesis of Drugs, Biomaterials or Cells 3

  1.2 Introduction to Microfluidics 7

  1.3 Droplet Microfluidics 10

  1.4 Conclusions and Perspectives 14

2. Development of Microtissue with Controlled Cell-cell and Cell-ECM Interactions for Tissue Engineering 16

  2.1 Direct Cell-cell Interaction 16

  2.2 Cell-ECM Interaction 18

  2.3 Liver Tissue Engineering 20

  2.4 Fabrication of Multicellular Spheroids 23

  2.5 Conclusions and Perspectives 25

3. Development of a DE droplet platform in microfluidics as miniaturized bioreactor for screening synthetic genes 27

  3.1 Introduction 28

  3.2 Materials and Methods 32

3.2.1 Microfluidics device fabrication 32

3.2.2 DE droplets generation and characterization 33

3.2.3 Gene synthesis and error correction 34

3.2.4 Cloning of synthetic genes 34

3.2.5 Encapsulation of bacterial cells 35

3.2.6 IPTG induction of gene expression 35

3.2.7 Fluorescence microscopy 36

3.2.8 Flow cytometry analysis 36

3.3 Results 37

3.3.1 Optimization of microfluidics device design 37

3.3.2 Generation and characterization of DE droplet 38

3.3.3 Single cell encapsulation and amplification in DE droplets 41

3.3.4 Screening of accurate clones for microarray-synthesized and error-corrected genes 44

3.3.5 Tunable induction of synthetic gene expression through IPTG diffusion into droplet 45

3.3.6 Analysis of gene expression by fluorescence-activated high-throughput droplets sorting 51

3.4 Discussion 54

3.5 Conclusion 57

4. Rapid formation of hMSC spheroids with controllable microenvironment in DE droplets 59

4.1 Introduction 59

4.2 Materials and Methods 62

4.2.1 Culture and encapsulation of hMSC. 62

4.2.2 hMSC spheroid characterization 63

4.2.3 Formation of PMEF, Caco-2 and HepG2 spheroids 64

4.2.4 Encapsulation of hMSC spheroids in hydrogel 64

4.2.5 Osteogenic differentiation and characterization 65

4.3 Results 65

4.3.1 Generation of size-controllable spheroids in DE droplets 65

4.3.2 Characterization of hMSC spheroids 70

4.3.3 Controlling microenvironment of hMSC spheroid for osteogenic differentiation 73

4.4 Discussion 75

4.5 Conclusion 77

5. Generation of microencapsulated hepatocyte spheroids with enhanced functions for liver tissue engineering 79

5.1 Introduction 80

5.2 Materials and Methods 84

5.2.1 Cell culture 84

5.2.2 Microencapsulated spheroid generation and characterization 86

5.2.3 MRP-2 transporter activity 87

5.2.4 Immunostaining 87

5.2.5 Albumin ELISA quantification 88

5.2.6 Urea assay 88

5.2.7 Cytochrome P450 3A4 (CYP3A4) assay and induction 88

5.2.8 Statistical analysis 89
5.3 Results 89
5.3.1 Generation of hepatocyte spheroids and subsequent encapsulation in microgel 89
5.3.2 Characterization of hepatocytes cultured in 2D and 3D 92
5.3.3 Investigation of the co-culture of EPC and Hep 98
5.3.4 Combination of heterocellular influence and conducive matrix cue 102
5.4 Discussion 105
5.5 Conclusions 107
References 109
Biography 121

List of Figures

Figure 1-1: Conventional nanoparticle fabrication methods. a) Nanoprecipitation. Polymer dissolved in organic solvent is added to an aqueous solution in a dropwise manner under constant agitation. b) Layer-by-layer assembly. Solid form of drugs is used as the core. A polymer layer is first adsorbed onto the drug colloidal template and transferred to the oppositely charged polymer solution for additional layering. c) Emulsion-based two step methods. Emulsified oil-in-water droplets containing polymer and drugs are formed in the first step. In the second step, different methods are applied to remove the solvent and precipitate nanoparticles. Top panel: solvent evapoaration method. Middle panel: Solvent diffusion method. Bottom panel: salting out. 5

Figure 1-2: Microfabricated platforms for drug particle synthesis. a) Particle Replication In Non-wetting Template (PRINT). b) Step-Flash Imprint Lithography (S-FIL) c) Continuous flow photolithography. 7

Figure 1-3: Common types of microfluidics design. (a) Flow focusing, (b) T-junction and (c) concentric capillary device. 12

Figure 3-1: Optimization of microfluidic device design. a) Schematic diagram of DE droplet formation. b) Impact of junction angle on droplet size and generation frequency; c) Impact of channel aspect ratio (AR) on droplet size and generation frequency 38

Figure 3-2: Generation of size-controllable DE droplets. Microscopic image of (a) the first and (b) the second PDMS device showing droplet formation. c) The effect of oil flow rate (at a fixed aqueous phase flow rate) on size of DE droplets using two types of devices. d) DE droplets generated at 3 μL/min (oil flow rate) using device with 200 μm channel width. e) DE droplets generated at 3 μL/min (oil flow rate) using device with 100 μm channel width. 39

Figure 3-3: a) Diffusion curve of different dyes encapsulated in DE droplets. Molecular weight (MW) and partition coefficient (PC) of the dyes are provided in the legend. b) Fluorescent images of rhodamine B encapsulated in DE droplets at 0, 1, 2, 3, 5 h 41

Figure 3-4: a) Single cell encapsulation of bacteria carrying gfp, rfp & cfp genes showing no colocalization at 24 h post-encapsulation. b) Quantification of cell number distribution in droplets in graphic and table format. c) Relative RFP intensity measured inside the droplets over time. (n ⩾10) d) Fluorescent microscope images showing the proliferation from a single RFP-expressing *E. coli* cell encapsulated in droplet. 43

Figure 3-5: Characterization of fluorescent cell population transfected with synthetic RFP gene before or after error correction. a) Fluorescent microscope images showing increased percentage of fluorescent droplet after error correction. Circled droplets contain bacteria that are either fluorescent (pink) or not (yellow). b) Percentage of fluorescent clones was measured before and after error correction for RFP gene construct. 45

Figure 3-6: a) Relative fluorescent intensities of bacteria with pET vector controlling a gfp gene in bulk and in droplets after addition of 5 μM IPTG over time. (n=9) b) Fluorescent microscope images of droplets containing bacteria in absence of IPTG (top panel) and in presence of 5 μM IPTG (bottom panel). (Scale bar: 100 μm) c) Relative fluorescent intensities of bacteria with pET vector controlling a gfp gene 8 h after introduction of various concentration of IPTG. d) Average GFP intensity per droplet as a function of time with the external concentration of IPTG ranging from 0.5 mM and 40 mM. (n=9) e) Fluorescent images showing GFP expressing cell clusters per droplet at 8 h, 12 h and 24 h time point post-IPTG induction. Images were taken at 20x magnification. f) Fluorescent images showing GFP expressing cell clusters per droplet at 12 h and 24 h time point after IPTG induction in minimal M9 vs growth LB/PBS media. Images were taken at 20x magnification. g) GFP intensity per droplet as a function of time upon IPTG induction in minimal M9 vs growth LB/PBS media. h) GFP intensity per droplet as a function of time with IPTG introduced prior to encapsulation at various concentrations. Fluorescent intensity curves are compared to the condition with IPTG introduced from external aqueous environment (red line) 50

Figure 3-7: a) Separation of DE droplets containing GFP and RFP expressing cells. Top: Intensity histogram of GFP and RFP channels. Bottom: Overlay of green and red channels showing RFP+-GFP+ populations. b) Flow cytometry analysis of DE droplets loaded with 4 different numbers of GFP-positive cells per droplet. Top: Overlay of signal intensities obtained for each conditions respectively. Bottom: Analysis of droplet mixture containing all four species with 1, 10, 100 and 1000 bacteria/droplet........ 54

Figure 4-1: a) The cell distribution in DE droplets with and without addition of alginate in the inner phase. More empty droplets and droplets with over 10 cells were observed in the case without alginate addition. b) Plot of experimental data (distribution of cell number in 200 DE droplets) versus Poisson estimation with an average cell number in each droplet of 4. c) Viability of hMSC encapsulated in DE droplets over time. 67

Figure 4-2: Figure 4-2. DE droplets generated in device with 200 μm channel width as bioreactor for cell assembly. Live/dead staining of hMSC after monolayer culture for 1 day with (a) no addition of oil or surfactant, (b) with oil and (c) with 1% Pico-Surf TM 1 surfactant dissolved in oil. (d) Time course images showing spheroids are formed in 150 min. (e) Phase image of hMSC spheroids encapsulated in DE droplets after 6 h. (f) Live/dead staining of spheroids after release from DE droplets at 6 h. Live cells were labeled with calcein AM (green) and dead cells were labeled with propidium iodide (red). 69

Figure 4-3: Bright field and live-dead images showing spheroid formation of a) PMEF, b) HepG2 at 2 h and Caco-2 at 2 h (c) and 6 h (d) (Scale bar = 100 μm). 70

Figure 4-4: Characterisation of hMSC spheroids released from DE droplets a) Diameter of spheroids measured at different cell densities used (n = 50). (Data = mean ± SD) (b) Percentage of viable cell area in spheroids obtained at different cell encapsulation densities upon release (n = 10). (Data = mean ± SD). Live-dead image of released hMSC spheroids cultured on (c) ultra-low attachment surface and (d) TCPS for one day (Green - calcein AM, red - propidum iodide). Oil Red O staining of hMSC cultured in (e) 2D and (f) 3D spheroid configuration differentiated along the adipogenic lineage for 7 days (Arrow indicates intracellular lipid vesicles.). Immunofluorescence images of hMSC spheroid stained with (g) collagen type I and (h) laminin taken under confocal microscope. 72

Figure 4-5: Control of microenvironment for spheroid culture using DE droplets. (a) Live/dead staining of spheroids encapsulated in alginate gel. Live and dead cells were stained with calcein AM (green) and propidium iodide (red) respectively. Confocal images showing phalloidin staining (b, f) and immunostaining for E-cadherin, integrin $\alpha5\beta1$ (c, g) for spheroids encapsulated in alginate or alginate-RGD gel cultured in normal media for 3 days. Images of alizarin red staining (d, h) and alkaline phosphatase activity staining using BCIP/NBT as substrate (e, i) for spheroids cultured in osteogenic medium for 7 days. 75

Figure 5-1: a) Schematic diagram of the process of generating microencapsulated hepatocyte spheroid using DE droplet. b) Microfluidic devices assembled on a glass microscope slide. 84

Figure 5-2: a) Microencapsulated spheroid production (Left & middle: Bright field image taken at time 0 & 4 h. Right: Microgel formation after oil removal). (Scale bar = 200 μm) b) DE droplet trapped on top of a cell strainer while rinsed with calcium-containing solution. (Scale bar = 100 μm) c) Alginate microgels encapsulating single hepatocyte spheroid. (Scale bar = 200 μm) d) Size distribution of spheroid and microgel. e) Size distribution of DE droplet 91

Figure 5-3: a & b) Size distribution of DE droplets produced from microfluidic device with 100 μm channel width and depth and the representative bright field image. c & d)

Size distribution of microgel and spheroid produced from the 122 μm droplets and the representative bright field image. (Scale bar = 100 μm) e) Immunostaining of rat collagen I of HEK 293 and rat hepatocytes spheroid encapsulated in different materials. (Scale bar = 50 μm) 92

Figure 5-4: a) Characterization (morphology and live-dead staining) of hepatocyte cultured in collagen sandwich configuration or on collagen coating only for 7 days. (Scale bar = 100 μm) Hepatocytes cultured in Col-sandwich exhibited cubic cell shape while the ones cultured on a single collagen coating displayed elongated, fibroblast-like shape. b) Characterization (morphology, live-dead staining at Day 24 and staining for bile canaliculi) of hepatocyte cultured in different conditions. (Scale bar = 50 μm) 96

Figure 5-5: a) Daily albumin release (#p<0.05 between Alg and Col-Sandwich, **p<0.01 between Alg-col and Col-Sandwich). b) Cumulative albumin release of 3 conditions for 24 days (*p<0.05) c) Daily urea secretion (#p<0.05 between Alg and Col-Sandwich, *p<0.05 between Alg-col and Col-Sandwich).). d) Cumulative urea secretion of 3 conditions for 24 days. e) Basal CYP3A4 activity measured by a luminogenic assay. f) Induction of CYP3A4 activity after treatment with 10 μM Dex for 72 h........ 97

Figure 5-6: a) Immunostaining of von Willibrand factor (vWF), an EPC marker, of EPC cultured in various media. (Scale bar = 25 μm) b & c) EPC number and viability after culture in various media for 5 days. d & e) Cumulative albumin and urea secretion of hepatocytes cultured in various media for 14 days. 99

Figure 5-7: a) Tracking of cell organization in the composite spheroids at different co-culture ratios. (Scale bar = 50 μm) b) Cumulative albumin release for 14 days (**p<0.01 between 1:5 and 1:1/3:1/0:1). c) Cumulative urea secretion for 14 days (*p<0.05 between 1:5 and 1:1/3:1/0:1). d) Basal CYP3A4 activity measured by a luminogenic assay (**p<0.01 between 1:5 and 0:1). 101

Figure 5-8: a) Characterization (immunostaining against hepatocyte (albumin) and EPC (vWF) markers, live-dead staining and staining of bile canaliculi) of single or co-culture spheroids cultured in different conditions. (Scale bar = 50 μm) b) Cumulative albumin release for 14 days. c) Cumulative urea secretion for 14 days. d) Basal CYP3A4 activity measured by a luminogenic assay (*p<0.05 between HepEPC in Alg-col and HepEPC in Alg). e) Induction of CYP3A4 activity after treatment with 10 μM Dex for 72 h. 104

Figure 5-9: Relative intensity of albumin-FITC encapsulated in microgels of different size. The total intensity of the gel at each time point was substracted with the intensity at equilibrium (5 days) and normalized with the intensity at time 0. Gaussian nonlinear fitting was shown on the graph. The top and bottom figure on the right shows the fluorescent images of small and large gel. (Scale bar = 200 μm) 107

Acknowledgements

First of all, I want to thank my dissertation advisor Dr. Kam W. Leong. It has been an honor to be his Ph.D. student and I am very grateful that he admitted me to his research group in 2010. He has demonstrated to me, by presenting himself as the role model, how to conduct good scientific research. I appreciate all his contributions of time, ideas, and funding to make my Ph.D. experience productive and stimulating. I am also thankful for the freedom he has granted me in pursuing my research goal.

I would also like to thank the members of my defense committee, each of whom has constantly provided invaluable support and guidance: Dr. George Truskey, Jun Chen, Farshid Guilak and Xuanhe Zhao. I would like to thank Dr. Truskey specially, for his kindness to serve as my thesis committee chair. I also want to extend my thanks to the colleges with whom I have worked during the past few years: Ying Zhang, Dr. Megan Ho, Dr. Ya-Ling Chiu, Dr. Youngmee Jung, Dr. Sungmin Hong, Dalton Sycks etc. They have contributed immensely to my personal and professional development at Duke.

Lastly, I would like to thank my family for all their love, support and encouragement.

1. An Introduction to Microfluidics Technologies: Application in High-throughput Biomedical Processing

1.1 Introduction to High-throughput Biomedical Processing

1.1.1 High-throughput Screening (HTS)

Biological systems are inherently intricate which are regulated by numerous interactions among thousands of genes and genetic products in a temporally and spatially organized manner. Humankind strives to explore the underlying mechanisms that govern the homeostasis of human body, which lead them to comprehend how disease is initiated and progresses. To better understand biological systems, the complexity of them must be replicated and studied systematically. Conventional cell culture platform fails to mimic the multiplex features of biological systems in an efficient manner [1]. Consequently, studying complex cellular events such as cell signaling that requires analysis of effect of individual biochemical in an isolated environment is labor-intensive [2]. Similarly, screening of individual compound for their effect against various extra- and intracellular molecular targets, as in drug discovery, requires tremendous input of resources [3]. A combinatorial and multiparallel investigation of a library of drug compounds, extracellular matrix (ECM) components, gene variants or cell mutants would require a HTS system [4].

The first version of HTS system was 96-well microplate adopted in early and mid- 1990s. Subsequent development led to the use of 384- and 1596-well microplate, where working volume per well were reduced from 100 μL to 2.5 μL [4]. The reagent cost is one factor that attributes to the overall cost-efficiency of the screening process as some reagents such as enzyme and ECM protein can be very expensive. Reducing working volume could help lessen the reagent cost. This was accompanied by the advances in robotic processing to increase the process efficiency when handling samples. Nevertheless, further development of the microplate technology is restricted by the macroscopic footprint of the plate. Given that a library of molecules, such as a gene variants library, can contain up to 10,000 candidates, a large number of microplates is required to conduct the screening, which will increase the cost and reduce the screening efficiency. On the other hand, microarrays tools are widely used in the analyses of biomolecules and tissues and are an excellent manifestation of the potential of employing microtechnology to increase the screening throughput. The global market of microarray is over $ 1 billion per year [5]. Nucleic acids, proteins or cells can be immobilized on over thousands spots, the substrate composition of which can be individually controlled, on a microchip to study binding events or reactions occurring between the analysts and substrates. Yet the disadvantage of this technology is that it is difficult to analyze the secretory product of cells and isolate individual detection spot from cross-contamination of diffusing biochemical. Also screening involving cell and matrix substrate is often done in 2D which does not truly reflect the 3D nature of cellular environment. These issues will be addressed in this thesis.

1.1.2 High-throughput Synthesis of Drugs, Biomaterials or Cells

Apart from screening, the complexity of biological systems also creates challenge for synthesizing drug particle, biomaterials and cells for medical use. The specific cell type targeted, dimension of blood vessels, immune regulation or even state of disease etc poses a strict requirement on the characteristics of drugs/biomaterials/cells for treatment. These include the size of drug particle, dimension of biomaterials and cell/biomaterial composite, N/P ratio of nanoparticle and chemical composition of drug/biomaterials etc. Commercially, robotic platform has been widely utilized to automate and accelerate the liquid handling during synthesis [6]. The cost-effectiveness is justified given the large scale of production. In a laboratory setting, alternative synthesis method is required which can provide flexibility as well as acceptable production speed.

In the case of nanoparticle synthesis, conventional fabrication techniques often involve bulk mixing of two or more immiscible phases, such as nanoprecipitation and emulsion-based methods (Figure 1-1) [7]. The particles produced are prone to polydispersity and batch-to-batch variations. For instance, the final size of nanoparticles generated by the emulsion-based techniques is directly determined by the size of the emulsion droplets, which itself could be very heterogeneous in bulk mixing. This will lead to poor predictability and control of particle penetration *in vivo*, drug loading efficiency and drug release rate. Consequently, several approaches made use of microfabrication were proposed to fabricate drug-loaded particles with defined shapes and sizes in a high-throughput manner (Figure 1-2).

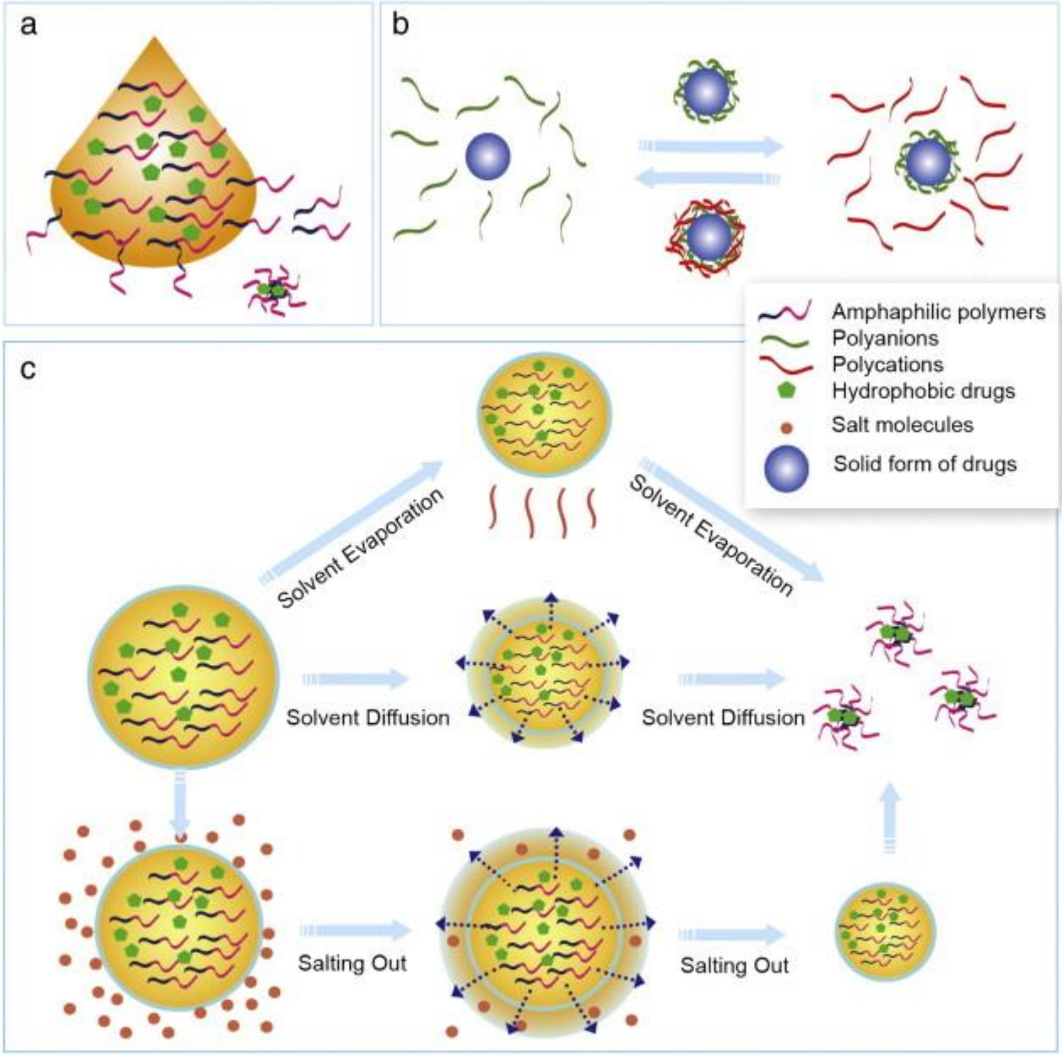
a
b
c
Amphaphilic polymers
Polyanions
Polycations
Hydrophobic drugs
Salt molecules
Solid form of drugs
Solvent Evaporation
Solvent Evaporation
Solvent Diffusion
Solvent Diffusion
Salting Out
Salting Out

Figure 1-1: Conventional nanoparticle fabrication methods. a) Nanoprecipitation. Polymer dissolved in organic solvent is added to an aqueous solution in a dropwise manner under constant agitation. b) Layer-by-layer assembly. Solid form of drugs is used as the core. A polymer layer is first adsorbed onto the drug colloidal template and transferred to the oppositely charged polymer solution for additional layering. c) Emulsion-based two step methods. Emulsified oil-in-water droplets containing polymer and drugs are formed in the first step. In the second step, different methods are applied to remove the solvent and precipitate nanoparticles. Top panel: solvent evapoaration method. Middle panel: Solvent diffusion method. Bottom panel: salting out.

The first one is called Particle Replication In Non-wetting Template (PRINT) [8]. A non-wetting PFPE mold with cavities of predesigned patterns is pressed against a polymer solution deposited on another non-wetting surface. The liquid polymer solution is then solidified by applying pressure or temperature. The solidified particles could be recovered from the mold by using an adhesive film.

Secondly, a quartz mold with cavities of predesigned shapes is pressed against a photo-crosslinkable monomer solution on top of a silica wafer for Step-Flash Imprint Lithography (S-FIL) [9]. A PVA layer is placed beneath the polymer solution for the release of imprinted particles. The monomers are crosslinked by UV light. Residual layer from crosslinking reaction is removed by oxygen plasma etching and particles are freed by dissolving away the PVA layer.

Finally, in continuous flow photolithography, a stream of photo-crosslinkable monomer solution continuously flows through the rectangular channel of microfluidic device [10]. A photomask with defined patterns is placed underneath through which pulses of UV light are applied. Particles of defined shapes are formed via crosslinking reaction and are flushed out for collection.

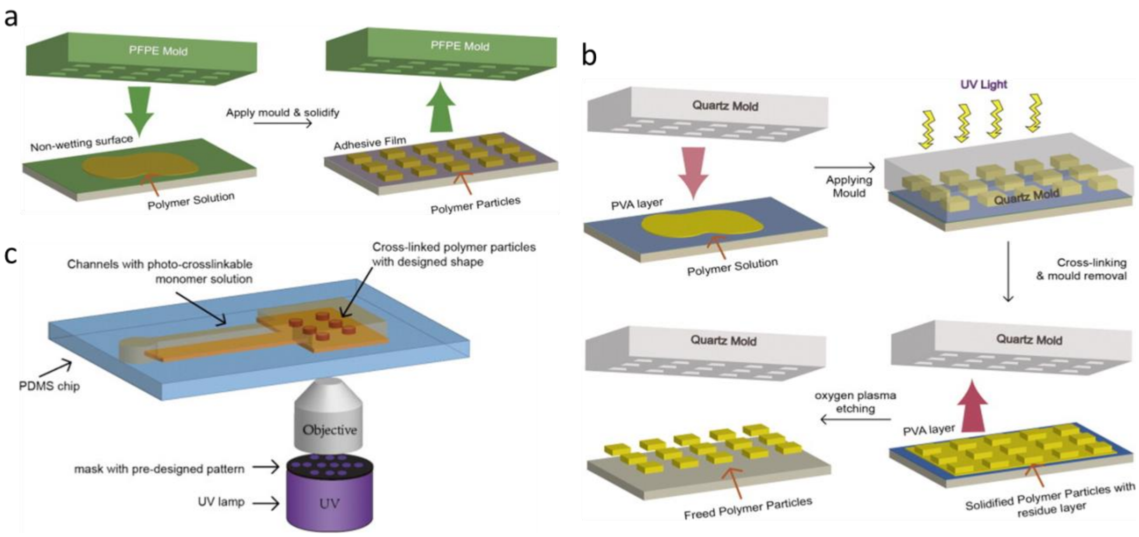
a
PFPE Mold
Non-wetting surface
Polymer Solution
Apply mould & solidify
PFPE Mold
Adhesive Film
Polymer Particles
b
Quartz Mold
PVA layer
Polymer Solution
Applying Mould
UV Light
Quartz Mold
Cross-linking & mould removal
Quartz Mold
oxygen plasma etching
Freed Polymer Particles
Quartz Mold
PVA layer
Solidified Polymer Particles with residue layer
c
Channels with photo-crosslinkable monomer solution
Cross-linked polymer particles with designed shape
PDMS chip
Objective
mask with pre-designed pattern
UV lamp
UV

Figure 1-2: Microfabricated platforms for drug particle synthesis. a) Particle Replication In Non-wetting Template (PRINT). b) Step-Flash Imprint Lithography (S-FIL) c) Continuous flow photolithography.

The above approaches can be modified to encapsulate cells in biomaterials with defined features for cell delivery. Whereas the first two approaches mentioned are static techniques, the third one incorporates microfluidics flow which significantly enhances the production rate of particles. The sections below will elaborate on the advantages of employing microfluidics in high-throughput processing.

1.2 Introduction to Microfluidics

Microfluidics is a technology characterized by the engineered manipulation of fluids at the submillimeter scale. This is often achieved using a device with channels in microscale. The devices are connected together to achieve desired functions such as mixing, sorting or controlling bio-chemical environment [11]. Fluids are driven via external active systems such as syringe pump or pressure controller connected through tubings or even simple holes in the device.

Over the last decade, PDMS has been the most popular material for fabricating microfluidic devices, due to the ease with which it can be cast on to a micro-scale mould using soft lithography and then bonded to glass [12]. The high oxygen permeability of PDMS renders it attractive for cell-related applications. However, the hydrophobic nature of PDMS can be a concern as hydrophobic drugs as well as some metabolites including urea and albumin can be absorbed into the device's material due to hydrophobic–hydrophobic interactions which may influence cell behaviors during drug screening. Also PDMS is incompatible with most common organic solvents, which limits the use of these devices for chemical synthesis applications. Apart from elastomer like PDMS, amorphorous thermoplastics (e.g. polymethylmethacrylate (PMMA)) were used to fabricate microfluidics device by micro-embossing or injection-moulding [11, 13]. These materials are stiffer thus producing channels with higher depth-to-width aspect ratios is possible.

Microfluidics device made with glass are advantageous in terms of high temperature resilience, chemical inertness and large limit of channel aspect ratios allowed [14]. Besides, its wettability (hydrophilicity) can be easily controlled by a surface reaction with an appropriate surface modifier. The most common fabrication approach is called bulk micromachining, in which micro- and nano-fluidic channels are generated by etching the wafer and bonding it to another wafer to encapsulate the channels. More recent reports explored the use of paper and woven fabrics as inexpensive and disposable substrate materials for microfluidics device fabrication. Sub-millimeter channel structures can be created on paper by the printing of hydrophobic (e.g., wax) patterns [15].

The general benefits of performing reactions and processes in microfluidics are as such [16]: (1) Fast diffusion due to small volume or large surface to volume ratio; (2) Miniaturization of device which reduces space and enhances portability; (3) Reduced use of reagents required for testing and analysis due to smaller sample volumes; (4) Possible integration of multiple processes (like labeling, purification, separation, and detection) in a microfluidic device for various applications.

Functions like electrophoresis and chromatography have been attempted using microfluidics platform for enhanced efficiency, faster speed, and low sample consumption. Biosensor is another application that is applied in microfluidics, in which substrate is immobilized in microchannels for detecting analyte in the flow [17]. Portability and reduction of samples required are the advantages. This can potentially be adopted for point-of-care diagnostic device. Besides, using a specially-designed microfluidics platform, cells were mechanically deformed as they passed through a constriction in the microchannel [18]. This resulted in the formation of transient holes that enabled the delivery of a range of materials, such as carbon nanotubes, proteins, and siRNA to cells without the need of a vector.

For high-throughput drug screening, microfluidics has been used to develop cell or tissue model to simulate metabolism and to test drug combinations at different concentrations [19]. An advantage offered by microfluidic technologies is better control of the cell or tissue environment. The microscale feature of microfluidics channel allows more facile generation of physiological-like conditions, including fluid flow rate, liquid-to-tissue ratios, ratios of various cell types, cellular organization and fluid shear stresses. Importantly, the microfluidic system of a few human model systems (e.g. blood vessel, muscle etc) provided comparable dose-dependent drug toxicity data to *in vivo* studies [20], which would stimulate further interest in applying it in more drug discovery studies.

1.3 Droplet Microfluidics

One of the major aspects of microfluidics is the generation of monodisperse emulsion droplet which is defined as the mixture of two immiscible liquids, where one liquid is dispersed in the form of small drops in another liquid that forms a continuous phase [21]. Two common types of emulsions are oil-in-water emulsion (O/W), such as milk, and water in oil emulsion (W/O), like butter. In addition to food products, emulsion also finds use in cosmetics and pharmaceutics in the form of cream, ointment or vaccine adjuvant-loaded nanoemulsion etc. As mentioned before, conventional methods for generating emulsion droplet involve drop breakup using shear or bulk mixing by manual or mechanical agitation. Since the applied stresses are not uniform, the droplets formed are highly polydisperse in size, resulting in poor control over the emulsion properties such as content loading efficiency and release rate [7]. Improved emulsification methods such as membrane extrusion, viscoelastic shear, microchannel emulsification and microthread generation have been developed for narrowing the distribution of droplet size [21]. However, greater control over droplet size distribution is still in demand.

Microfluidics has emerged as the ideal platform to fabricate monodisperse emulsion droplet [22]. In the common approach, two streams containing continuous and disperse phases (either or both contains a surfactant) are infused into two separate inlets, and the disperse phase is confined into isolated droplets at the junction of T-junction, flow-focusing device or at the tip of the capillary orifice in a capillary microfluidic device (Figure 1-3). Since the emulsion droplet in a microfluidic device is fabricated one drop at a time, highly monodisperse emulsion can be formed. What is more attractive is the ability to fabricate double, triple, and even higher order emulsions, where the size and number of the encapsulated droplets can be manipulated precisely [23].

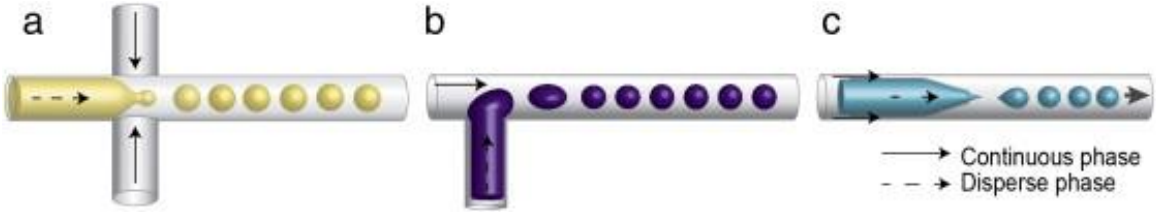

Figure 1-3: Common types of microfluidics design. (a) Flow focusing, (b) T-junction and (c) concentric capillary device.

In a capillary microfluidic device, a glass capillary with a fine orifice is slid into another capillary to form a simple device with a co-flow geometry. Monodisperse droplets are formed at the tip of the capillary orifice when the fluid flow rate is low, in a process termed dripping [21]. As the flow rate increases past a threshold, a long stream of the inner fluid with droplets forming downstream would occur, resulting in wider size distribution.

Another device geometry is called flow focusing, where two immiscible fluids are introduced at 90 or 180 degree and converge at a junction [24]. The disperse phase is hydrodynamically focused by the continuous phase. Droplet formation occurs in the dripping mode at the junction while the droplet forms further downstream in the jetting mode. This method enables the formation of monodisperse droplet smaller than the size of the junction, and is useful for making particle-loaded droplet where the probability of clogging the channels by suspended particles and debris is reduced since a wider microfluidic channel can be used.

One primary application of droplet microfluidics is digital polymerase chain reaction (PCR) [25], where nucleic acid samples are partitioned into thousands of nanoliter-sized emulsion droplets before they are amplified by PCR. This technology can give an absolute count of target DNA copies per input sample by analyzing each droplet with a flow cytometer to determine the fraction of PCR-positive droplets in the original sample, circumventing the need for running standard curves. Apart from reducing sample input, increased signal-to-noise ratio and sensitivity are the edges of the technology due to enriched sample concentration in droplets.

Partitioning via emulsion droplet generation can also be applied on cells. Single bacterium or mammalian cell can be encapsulated in droplet based on the probability equation derived from Poisson distribution [26]. When sufficiently diluted cell suspension is loaded into droplets, single cell can be found in some droplets while the rest are empty. This kind of compartmentalization is important for high-throughput single cell analysis, such as studying cellular heterogeneity and identifying rare cell (e.g. cancer stem cell) from a mixed population [27, 28]. Lysis of single cell can be performed in W/O single emulsion droplet to retrieve cellular mRNA or protein by physical and chemical methods, which can then be examined after amplification, labelling or conversion into detectable products by the cocktail reagent pre-loaded inside the droplet [21]. W/O emulsion droplet also allows single cell culture for drug screening, immunological testing and directed evolution experiment. One advantage cited is the significant reduction in the reaction time due to the increase in both the cell concentration and the products of reactions, resulting from the confinement of single cells into droplet compartments. However, since the external oil phase does not supplement nutrients and metabolites are accumulated in the droplets, the cell viability cannot be sustained inside the droplets [29]. Forming microgel based on an emulsion droplet template is one way to tackle the problem by removing the oil phase and transferring the microgel into fresh medium [30]. Nevertheless, this approach also poses a disadvantage, which is the cross-contamination of soluble secreted molecules with other cell-containing microgels, thereby influencing screening results. This thesis will address the issue by proposing the use of double water-in-oil-in-water (W/O/W) emulsion droplet for prolonged cell culture and studies.

1.4 Conclusions and Perspectives

High-throughput technologies are actively sought in the biomedical field, from screening candidates during discovery of drugs, biomaterials and cells for medical use, to manufacturing drugs or other medical products. The past decade has witnessed the rapid development of microfluidics technologies to leverage on the unique advantages such as close spatial and temporal control of fluids. Such technologies hold potential for significantly increasing the throughput of processing cells, proteins or nucleic acids. In particular, emulsion droplets generated in microfluidics platform possess special feature that allows compartmentalization of samples in uniform-sized chambers for individual control and analysis. The emulsion droplet technology could spur the growth of high-throughput processing techniques, enabling project concepts that were not previously realizable.

2. Development of Microtissue with Controlled Cell-cell and Cell-ECM Interactions for Tissue Engineering

2.1 Direct Cell-cell Interaction

Direct interactions between cells regulate biological processes such as development, homeostasis and disease progression via juxtacrine signalling (or contact-dependent signalling) [31]. Cell adhesion molecules such as selectins, integrins and immunoglobulin superfamily, and membrane-bound proteins such as Notch and ephrin, from one cell can bind to its ligand from another cell whereby the cytoskeletons of adjacent cells are not linked to one another [32]. Examples include those between leukocytes and endothelial cells or blood platelets in the process of cell migration. Binding of ligands by its respective receptors triggers a cascade of intracellular signaling events and eventually alter the gene expression of cells. Cadherins, on the other hand, can form more stable junctions between cells such as adherens junctions and desmosomes. One example is E-cadherin found between epithelial cells. These junctions serve as mechanical anchorage to connect the cytoskeletons of neighboring cells, and also relay signals via the cytoskeletons to affect gene expression of cells [33]. In addition, connexins, another surface adhesion molecule, form gap junctions that directly couple cells to one another and the adhesive function of gap junctions contributes to self-assembly on par with the adhesive effects of cadherins [34].

Juxtacrine signaling via direct cellular contact assumes a critical role in development process especially for guiding cell migration and directing cell differentiation. For instance, the interactions between Notch and its ligands are shown to regulate cell differentiation into optic neurons and glial cells respectively [35]. Gap junctions are also important for many physiological processes by providing electrical coupling between cells such as neurons. Signal transduction via gap junctions facilitates coordinated depolarization of cardiac muscle. In the context of tissue engineering, the use of stem cells, which are primitive cells and capable of differentiating into a wide variety of mature cell types, for reconstruction of living tissues including cartilage, liver, heart muscle and bone etc benefits from restoring the cell-cell contact for enhanced survival and differentiation [36].

Embryonic stem cell (ESC) is one example. Embryoid body (EB) formation is used to trigger *in vitro* ESC differentiation since an EB consists of the three germ layers (ectodermal, mesodermal, and endodermal) that recapitulate many aspects of cell differentiation during early mammalian embryogenesis [37]. ESC spontaneously establish cell-cell contact and gap junctions by aggregating into EB and differentiate when cultured in the absence of leukemia inhibitory factor or mouse embryonic fibroblasts (MEFs) feeder layer. Similarly, mesenchymal stem cells (MSC) exhibit enhanced differentiation towards the adipose and bone tissue when cultured in aggregate (spheroid) configuration [38]. The conventional pellet culture of MSC for chondrogenic differentiation also takes advantage of the extensive cell-cell interactions found in the tightly aggregated cell mass which mimics embryonic cartilage development [39]. Besides, the neurosphere assay is used to confirm the presence of neural stem cells as their presence would induce the formation of cell spheroid [40]. The neurosphere is also used to expand and cryopreserve neural stem cells. All these examples reaffirm the importance of restoring cell-cell contact in culturing cells for tissue engineering.

2.2 Cell-ECM Interaction

The ECM consists of a complex mixture of biomacromolecules such as proteoglycans, collagen family, elastin fibres and glycosoaminoglycans etc. The different combination and spatial organization of ECM components give rise to different types of scaffolds that characterize the different body tissues and organs [41]. The ECM, organized into micro- and nano-structures, provides a route for cell migrations, and molecules in the ECM activate intracellular signaling pathways that induce cell growth, proliferation, and gene expression [42]. The major class of cell-adhesion molecules that mediate cell-ECM interaction is integrin, which is formed by a combination of various α and β subunits that bind to various ECM components. The coupling of integrin to cytoskeleton allows activation of intracellular protein kinases and subsequent phosphorylation of cytoskeleton upon ECM binding. Eventually signals are transmitted to the transcriptional machinery in the nucleus to effect the changes of cell behaviors [43]. In addition, the ECM also controls the mobilization of growth factors presented to cells.

The preferential binding of specific growth factors to ECM affects the local concentration of growth factors available to cells [44]. The ECM also selectively stimulates specific types of signal transduction pathways activated by growth factors binding. For instance, the cell may need to interact with an ECM component in order for an appropriate intracellular signal transduction cascades to be triggered [45].

Tissue engineers typically create exogenous three-dimensional ECM scaffold to engineer new natural tissues from natural cells. The exogenous ECMs are designed to support cell survival and proliferation in an appropriate three dimensional environment, and also to provide mechanical support until the newly formed tissues are structurally stabilized [46]. A number of key criteria of the scaffold materials should be met to optimize cell-ECM interaction [47].

First, the scaffold materials must be biocompatible so that it would not elicit a noticeable immune reaction and hence a severe inflammatory response from human body which might reduce healing or cause rejection by the body. Second, since the implanted scaffold should be replaced by body's own cells eventually, the materials should be biodegradable and the by-products of this degradation should be non-cytotoxic and able to be removed from the body without interference with other organs. The synchronized degradation and tissue formation characterized by an inflammatory response combined with controlled infusion of cells such as macrophages and stem cells is required. Third, the mechanical properties of the scaffold should be consistent with that of the anatomical site to which it is implanted to. Not only is the scaffold required to have sufficient mechanical integrity to serve their functions such as in cartilage and bone, it should also resemble native tissue in terms of mechanical property for transplanted or regenerated cells to function in a biomimetic environment. Studies have shown the stiffness of the hydrogel guides the differentiation of MSC into neurogenic (0.1-1 kPa), myogenic (8-17 kPa), and osteogenic lineage (25-40 kPa) in accordance with the stiffness observed in native tissues [48]. Finally, the scaffold materials should be fabricated in a way that the micro- and nano-scaled features found in endogenous ECM are mimicked. Reports have shown various cell types respond to micro- and nano-topographies via changes in adhesion, attachment, proliferation and differentiation etc [49]. For example, contact guidance often occurs at microscale while more complex mechanotransduction occurs at nanoscale which influences stem cell differentiation. To fabricate functional tissue construct, cell-ECM interaction should be optimized.

2.3 Liver Tissue Engineering

Liver tissue engineering aims to develop artificial liver system as novel therapies for liver diseases and as effective models for understanding fundamental aspects of liver biology and pathologic processes, in particular for studying drug metabolism and toxicity [50]. Liver is the largest internal organ as well as largest gland in the body. The functions performed by liver include detoxification, protein production and secretion of biochemical important for digestion etc. Liver failure, resulting from acute or chronic end-stage liver diseases, represents the cause of death for over 40,000 individuals in the United States annually [51]. The lack of treatment options except liver transplants from donors has stimulated interest in developing artificial liver system for extracorporeal liver support device and implantable tissue engineered liver systems [52, 53].

Extracorporeal devices are designed to offer transient support during liver regeneration or before liver transplantation. These *ex vivo* devices process the blood of patients in a manner analogous to kidney dialysis systems. Different types of such devices are available, including hollow-fiber devices, flat plate and monolayer systems, perfusion bed or porous matrix devices, and suspension reactors [54]. In addition to temporary support, researchers are pursuing more permanent cell-based therapies in an attempt to replace damaged or diseased liver tissues, such as in the form of hepatocyte transplantation and implantable tissue engineered hepatocellular constructs [55].

The cell sources used to incorporate into the devices range from primary human or animal hepatocytes, and hepatocyte-like cells derived from stem cells or reprogrammed adult cells. Primary hepatocytes perform better functionally than those derived from stem cells or reprogrammed adult cells but they are either limited in supply (in the case of human cells) or prone to immune rejection (in the case of animal cells). Hepatocyte-like cells derived from stem cells or reprogrammed cells can be supplied in larger number but the optimized differentiation protocol is yet to be determined. No matter which cells type to use, one common bottleneck of fabricating an extracorporeal liver support device or implantable liver tissue constructs lies in the rapid decline in viability and liver-specific functions over time [56]. To solve this, various approaches of restoring the biomimetic cell-cell and cell-ECM interactions have been proposed to maintain the hepatocyte phenotype during culture.

Homotypic (same type of cells) and heterotypic (different types of cells) cell-cell interactions have been found to be essential in the maintenance of hepatocyte function and survival in culture [57]. In liver tissue, hepatocytes, the principal parenchymal cells, contribute 80% of liver mass. Hepatocytes exist as a single layer and bound by tight junctions to form an impenetrable barrier. Within each sinusoid where oxygen and nutrients exchange takes place, hepatocyte layer is shielded from direct blood flow by a thin, porous extracellular matrix (space of Disse) and a specialized endothelium that lines the sinusoids. Other non-parenchymal cells such as Kupffer cells and hepatic stellate cells are also present in the sinusoid. Pre-aggregation of primary hepatocytes to 3D spheroids enhanced both cell survival and hepatocyte function compared with monolayer culture [58]. Attempts have also been made to co-culture non-parenchymal cell populations such as fibroblasts, endothelial cells, and stellate cells, with hepatocytes, with improved hepatocyte functions shown in some studies [59, 60].

On the other hand, ECM also plays an important role in hepatocyte culture. ECM of different composition and topology have different effects on hepatocyte morphology and function. For example, the presence of collagen I on a substrate enhances hepatocyte attachment while ECM mixture extracted from the liver has been shown to improve hepatocyte function over culture on a monolayer of pure collagen [61, 62]. In the collagen sandwich culture, hepatocytes are sandwiched between two layers of collagen gel. In this format, hepatocytes demonstrate desirable morphology and liver functions for 1 to 2 weeks [63]. In general, the use of natural, biologically-derived materials containing binding sites for cell attachment can enhance hepatocyte function since hepatocytes are anchorage-dependent cells. In contrast, synthetic scaffolds offer improved control over scaffold physicochemical and biological properties, but the absence of natural cell-binding sequences in these systems often mean incorporation of biologically active elements in the materials is required to improve hepatocyte adhesion and functions [64].

2.4 Fabrication of Multicellular Spheroids

Multicelluar spheroids recapitulate three-dimensional tissue *in vivo* in enabling cell–cell and cell–matrix interactions [65]. Forming multicellular spheroids *in vitro* can establish cell-cell contact required for preserving cellular viability, function and phenotype that are often lost in monolayer culture [66]. In stem cell differentiation, aggregating cells to become spheroid or pellet is usually the prerequisite for efficient differentiation to restore the juxtacrine signaling via direct cellular contact [67]. However, generating spheroids in a high-throughput manner has been a challenge.

Conventional ways of making spheroids comprise culture in suspension, in spinner flask, or in hanging drop [68]. Culturing cells in suspension or in spinner flask is relatively simple but typically results in heterogeneity in spheroid size [69]. Cell suspension is either cultured on a non-adhesive dish or stirred in a spinner flask and the cells would spontaneously aggregate upon minimal cellular attachment to the solid surface and to maximize cell to cell contact. There is wide consensus that necrosis in spheroid core will occur if the spheroid size is larger than ~150 μm, which is the limiting diffusion distance of oxygen reaching to the spheroid core based on the estimated average distance between the capillaries and surrounding tissues *in vivo* [70]. Large (>150 μm) spheroid can result if the spheroids produced are heterogeneous in size. This will hinder the application of these spheroids for clinical use.

On the other hand, the hanging drop method provides some control over the spheroid size [71]. Using this method, the user needs to pipette a small volume (~10-30 μL) of cell suspension on to a petri dish before culturing them upside down. The cells would settle and aggregate under gravity. The spheroid size can be controlled by maintaining the same pipetting volume (i.e. number of cells) every time. However, the disadvantage of this method is that the process becomes labor-intensive when large number of spheroid is required. Robotic system can potentially expedite and automate the process but the cost can be high. Besides, changing media in the hanging drop is difficult unless some specially-fabricated culture plate is used [72].

Recently the research focus has turned to the approach of using non-adhesive micromolded surface, taking advantage of microfabriation technique that supports spheroid size control as well as scaling up [73]. Cells will settle into non-adhesive microwells after seeding, where they will aggregate into spheroid over time. One limitation of this approach is the requirement of delicate skills in culturing spheroids on the micromolded surface as the tiny spheroids from different microwells aggregate into larger spheroids easily. What's more, none of the current approaches offer a controlled presentation of exogenous ECM in spheroid culture, meaning the spheroids have to be further encapsulated or loaded into an ECM scaffold if needed [74]. A platform that allows rapid and high-throughput production of multicellular spheroids and simultaneous modulation of their ECM microenvironment will greatly obviate the need for labor-intensive fabrication of stem cell spheroids as well as replating of spheroids into matrix scaffold for efficient control of cell functions and differentiation.

2.5 Conclusions and Perspectives

Both cell-cell contact and cell-ECM interaction are important considerations for developing functional tissue engineered construct. In particular, the survival of hepatocytes depends highly on the establishment of cell-cell contact, either in 2D monolayer or 3D spheroid culture. The generation of hepatocyte spheroid can be applied in bioreactor culture or delivery of hepatocyte for liver regeneration. Various co-culture cell types and exogenous ECM were proposed to support hepatocyte functions but the optimized culture conditions for hepatocyte obtained from various cell sources have not been determined. Given that large spheroids suffer from poor oxygen penetration, generation of tiny spheroids (<150 μm) with controllable presentation of exogenous ECM will contribute to the screening of culture conditions and clinical use of the spheroids. From the first chapter we learnt about the potential of adopting microfluidics emulsion droplet for screening and synthesis. The high-throughput production of emulsion droplet would be a perfect platform to fabricate hepatocyte spheroids. Nevertheless, the concern is that W/O single emulsion is not a cell-friendly platform due to the presence of the external oil phase while hepatocytes are very sensitive to the culture environment. Obviously, further advancement of the microfluidics technology is needed for it to be useful for hepatocyte spheroid generation.

3. Development of a DE droplet platform in microfluidics as miniaturized bioreactor for screening synthetic genes

Droplet microfluidics can be exploited for high-throughput processing. Nevertheless, the potential of W/O single emulsion is limited by the presence of the external oil phase which is not compatible with aqueous phase assay and culture. In this chapter, the development of a DE W/O/W droplet platform was described. Two microfluidic devices were fabricated to generate DE for long-term cell culture and analysis. To demonstrate its screening potential, synthetic genes constructed from a custom-built microarray inkjet synthesizer were transformed into bacterial cells for screening. Bacteria bearing individual fluorescent gene variants were encapsulated as single cells into DE droplets where fluorescent signals were enhanced by 100 times within 24 h of proliferation. Enrichment of error-free genes by employing error correction method was demonstrated by screening DE droplets containing fluorescent clones of bacteria with the *rfp* gene. Permeation of isopropyl β-D-1-thiogalactopyranoside (IPTG) from the external solution initiated target gene expression. The induced expression of the synthetic fluorescent proteins from at least ~100 bacteria per droplet generated detectable fluorescent signals to enable fluorescence-activated cell sorting (FACS) of the intact droplets. Our high-throughput DE technology obviated time- and labor-intensive cell culture typically required in conventional bulk experiment.

3.1 Introduction

For over sixty years, the tools to synthesize, manipulate and analyze DNA have grown to encompass new extremes in both scale and precision. Driven by miniaturization technologies, our ability to read and write DNA has improved dramatically over the last decade. High-throughput sequencing technologies such as next-generation sequencing (NGS), has enabled the analysis of many genetic and biochemical processes at unprecedented scale and low cost [75]. Emerging technologies on parallelized and miniaturized synthetic techniques to construct DNA sequences has led to significant improvement in our ability to understand and engineer biology. Following the early demonstrations of gene assembly using microarray-derived oligo pools, exciting developments have been made to improve the quality and efficiency of microarray-based oligo synthesis and gene assembly [76]. Dr. Jingdong Tian has pioneered in developing the microarray inkjet synthesizer to synthesize pools of thousands of codon-usage variants for protein expression optimization [77].

Despite tremendous improvement in both DNA synthesis and sequencing, throughput and scale of current experimental workflow in real practice remain limiting. This is due to a bottleneck existing in the screening step where the downstream cost of testing individual biological constructs for function is often far more expensive than the synthesis cost. In addition, since the engineering information is encoded in the genotype while the selection depends on the phenotype, this requires the genotype and phenotype to be linked in any screening activity.

Cells are most commonly used to link genotype to phenotype. Synthetic constructs are usually introduced in recombinant forms and individual cells are picked from culture plates and analyzed either by hand or by robotic-pickers [76, 77]. The process is labor-intensive and time-consuming. While eukaryotic cells screened by FACS can potentially access libraries larger than 10^8 [78], flow cytometric analysis of bacteria cells is still infrequent due to their small size and the range of screening is limited to survival or cell-bound products [79]. Automation through the use of colony pickers increases the throughput to 10^4 clones/day but cannot handle larger libraries unless multiple machines are used in parallel. The cost and space issues will become unfavorable when using multiple machines.

In vitro compartmentalization (IVC) of individual element of the library in discrete [80], miniaturized W/O emulsions is an attractive alternative for coupling genotype and phenotype, while offering improved cost-effectiveness and screening sensitivity by reducing sample consumption and enhancing signal response. Bulk emulsions suffer from polydispersity and the lack of control of reaction volumes, timing and generality [81, 82]. These problems can be overcome by using droplet-based microfluidics system which allows the production of homogeneous and uniform droplets [22, 83]. However the W/O emulsions are incompatible with sustained cell culture or any aqueous phase-based analysis (e.g. flow cytometry), as the immiscible oil phase is prone to evaporation and insoluble for typically polar nutrients [29].

The problem can be circumvented by entrapping W/O droplets in another aqueous phase, forming W/O/W DE. The external aqueous phase minimizes desiccation and enables droplet sorting via FACS. The middle oil shell functions as a selective barrier to regulate molecule transport, allowing supply of nutrients or input of small inducer molecules. In this study, we present the development of a high-throughput screening platform for synthetic genes using microfluidics generated DE droplets.

Microfluidic devices were fabricated with PDMS using soft lithography. Two devices were connected serially to generate DE droplets. The angle of the flow-focusing junction and aspect ratio (height/width) of the channel were optimized for efficient droplet generation. Controllable droplet size and selective permeability of the oil shell were demonstrated.

Fluorescent protein genes were synthesized with a custom-built inkjet synthesizer, and inserted into *E. coli* cells for screening. Individual bacterium was then encapsulated bearing individual gene variants into DE droplets. The intrinsic limitation of chemical gene synthesis by stepwise addition of nucleotide monomer results in errors such as deletion, substitution in some of the genes. The DE platform enabled the identification of bacteria clones with correct *rfp* sequences. In addition, the diffusion of IPTG into the droplet could trigger the pET vector regulating the expression of the synthetic *gfp* gene inserted into the bacteria. Since the pET expression system is one of the most widely used systems for the cloning and expression of synthetic and recombinant proteins in *E. coli*, the induction of pET expression by an external triggering mechanism should offer an effective protocol to induce various target protein expression for screening within the droplets. The capacity of DE system (bacteria proliferation and activation of gene by chemical diffusion) combined with high-throughput sorting by FACS provide the basis for screening complex gene libraries for a broad range of functionality and activity.

3.2 Materials and Methods

3.2.1 Microfluidics device fabrication

Microfluidics devices were fabricated by conventional soft lithography techniques. Patterned silicon mold of 50 μm in height was prepared from SU-8 2150 (MicroChem, Newton, MA) according to protocol. PDMS prepolymer and curing agent (Sylgard 184 Silicon Elastomer Kit, Dow Corning, Midland, MI) were mixed at 10: 1.05 mass ratio before poured on top of the silicon mold to cure. A cover slide was bonded with the device after holes at inlets and outlets were punched and oxygen plasma treated for 40 s at 20 W (Plasma Asher, Quorum Technologies, West Sussex, and RH). To create a hydrophilic surface along the channels, the devices were coated following a two-step sol-gel coating procedure [84]. (All chemicals listed below were obtained from Sigma-Alrich, St. Louis, MO.) Briefly, the sol-gel solution was prepared from tetraethylorthosilicate (TEOS), methyltriethoxysilane (MTES), (heptadecafluoro-1,1,2,2-tetrahydrodecyl)- triethoxysilane, trifluoroethanol and 3-(trimethoxysilyl)-propylmethacrylate at a volume ratio of 2: 1: 4: 1. Sol-gel solution, methanol, trifluoroethanol and hydrochloric acid solution (pH 5.2) was mixed at a volume ratio of 5: 9: 9: 1 and heated at 85 ^{0}C for 2 min. The activated mixture solution was filled to the devices after bonding with cover slide and the device was heated to 180 ^{0}C for 1 min. Finally, deionized water (500 mL), acrylic acid (200 mL), ammonium persulfate (10 wt%, 100 mL), and tetramethylethylenediamine (TEMED) (16 mL) were mixed and injected continuously to the devices at 20 mL/min while the device was heated at 80 ^{0}C for 10 min.

3.2.2 DE droplets generation and characterization

DE droplets were generated as described in the main text. Bacteria culture medium was used as the inner aqueous phase. The oil phase used was HFE-7500 (Miller-Stephenson Chemical Co. Inc., Danbury, CT) supplemented with Pico-Surf TM 1 surfactant (1%) (Dolomite Microfluidics, Charlestown, MA). The outer aqueous phase comprised culture medium supplemented with Pluronic F-127 (2.5 wt. %). The flow rates of inner aqueous phase (2 μL/min), middle oil phase of HFE7500 (3 M, St. Paul, MN) (7 μL/min) and outer aqueous phase (70 μL/min) were controlled by a Harvard Apparatus PHD 2000 Syringe Pump. To study the mass transport through the oil layer, various dyes (rhodamine B, rhodamine 6G, FITC) or dextran conjugated to FITC (MW 5 4000 Da & 70000 Da) (50 mM) (all obtained from Sigma-Aldrich, St. Louis, MO) (50 mM) were prepared and encapsulated in the droplets. Images were taken at various time points using a Nikon Eclipse TE2000-U fluorescence inverted microscope fitted with appropriate filters and connected to a camera. The optimal exposure time for each dye was determined at time 0 and the same exposure time was used for the following time points. All other parameters (no binning, same lamp intensity, same brightness/contrast level) were kept the same during the course of experiments. The intensity of the core of at least 10 droplets was measured at different time points using ImageJ software (NIH). To determine the partition coefficient of various molecules, culture medium (with 20% FBS) containing rhodamine B, rhoadmine 6G or FITC (50 mM) was added on top of HFE7500 containing Pico-Surf TM 1 (1%) in an eppendorf tube. The tube was left on an orbital shaker operating at 100 rpm for 24 h before the fluorescent signal in the aqueous phase was determined by a plate reader. The amount of fluorescent dye left in the aqueous phase was determined by interpolation from a standard curve. Partition coefficient was calculated by the following formula: Partition coefficient = (Initial dye concentration - dye concentration after incubation)/ Initial dye concentration

3.2.3 Gene synthesis and error correction

The construction and error correction of synthetic fluorescent protein genes was detailed in Dr. Jiandong Tian's previous publications [77, 85].

3.2.4 Cloning of synthetic genes

Synthetic gene products (*gfp, cfp, and rfp*) were cloned into pAcGFP1 vector using circular polymerase extension method (CPEC) [86]. To prepare the pET expression plasmid, synthetic *gfp* gene was inserted into pET-28a(+) (Novagen Inc., Madison, WI, USA) vector containing a *lacI* gene, a T7 promoter, a lac operator and an ampicillin resistance gene. Cloning product was transformed into BL21(DE3) Chemically Competent *E. coli* cells (Invitrogen) according to the manufacturer's instruction. Cells were grown on agar plate with 50 μg/ml kanamycin for approximately 16 h.

3.2.5 Encapsulation of bacterial cells

Single colonies containing *rfp*, *gfp* and *cfp* genes were selected from the previous prepared LB agar plate and transferred into 200 mL M9 broth or diluted LB broth (1:1 LB medium : PBS). The inoculated culture was then thoroughly mixed and diluted to reach the desired cell density (e.g. ~10^6 cells/mL to obtain 0.06 cell per 60 pL droplet) before encapsulated into DE droplets. The flow rates of three phases (inner aqueous: middle oil: outer aqueous) were set at 1: 2: 30 μL/min respectively. The droplets were collected and transferred to 96-well plates containing M9 or diluted LB media for subsequent culture and analysis.

3.2.6 IPTG induction of gene expression

Single colony containing pET-gfp plasmid were picked from the LB agar plate and transferred into 200 mL M9 broth or diluted LB broth (1: 1 LB medium : PBS) containing 50 μg/ml kanamycin. The inoculated culture was then thoroughly mixed and diluted to reach the desired cell density, then encapsulated into DE droplets. The droplets were collected and transferred to 96-well plates containing 200 mL M9 or diluted LB media. IPTG was added immediately to the outer aqueous media to obtain a series of concentration: 0 mM, 0.5 mM, 2 mM, 5 mM, 10 mM and 20 mM. Droplet fluorescent intensity was then analyzed at various time points with fluorescence microscopy.

3.2.7 Fluorescence microscopy

Droplets containing fluorescence-bearing bacteria were suspended in a 96-well plate and examined by Nikon Eclipse TE2000-U fluorescence inverted microscope at various time points following encapsulation. Fluorescence intensity was analyzed by Image J.

3.2.8 Flow cytometry analysis

E. coli constitutively expressing GFP were diluted in PBS buffer and encapsulated in the DE droplets. Equal number of droplets was then suspended in PBS solution or M9 growth medium for comparison of cell growth over time by flow cytometry (FACSCanto II, BD Biosciences, Franklin Lakes, NJ). The FSC/SSC was gated with empty droplets and free bacteria (negative control) to specifically determine the population of droplets with bacteria encapsulated. More than 10,000 droplets were measured each time to ensure reliable statistics. FlowJo (v.7.6, Tree Star, Ashland) was used to analyze the data.

3.3 Results

3.3.1 Optimization of microfluidics device design

The high-throughput generation (>20 Hz) of pL-sized DE droplets was carried out in two PDMS flow-focusing devices connected serially (Figure 3-1a). To fabricate the devices, standard soft lithographic procedures were followed. In each device, two streams (disperse and continuous phases) converged at a narrow junction where droplets were formed and stabilized by surfactants present on the boundary of two immiscible phases. The surfactants used were 1% Picosurf 2 (Dolomite Microfluidics) in the oil phase and 2.5% Pluronic F127 (Sigma-Aldrich) in the outer aqueous phase. The angle of junction affected the size of droplet generated. The wider the angle, the larger the droplet and the lower the droplet generation frequency (Figure 3-1b). The angle of 30° was selected for subsequent studies for efficient generation of droplets. In addition to angle of junction, the channel aspect ratio (height/width) also affected droplet generation. During a preliminary screening it was found that the droplet generation was the most efficient when aspect ratio was around 1.5 (Figure 3-1c), as indicated by the shortest distance between consecutive droplets generated. As a result, 1.33 (200 μm in height and 150 μm in width) was selected as the optimal aspect ratio of the device design.

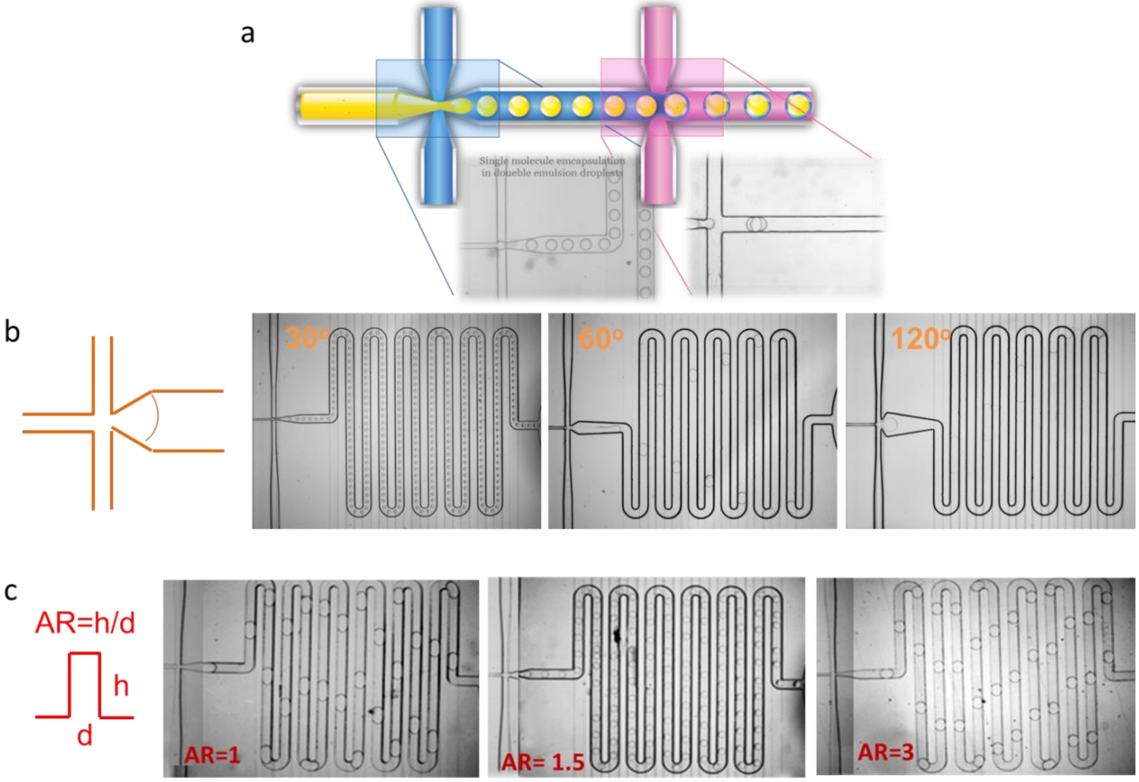
a
Single molecule emcapsulation in doueble emulsion droplests
b
30°
60°
120°
c
AR=h/d
h
d
AR=1
AR= 1.5
AR=3

Figure 3-1: Optimization of microfluidic device design. a) Schematic diagram of DE droplet formation. b) Impact of junction angle on droplet size and generation frequency; c) Impact of channel aspect ratio (AR) on droplet size and generation frequency.

3.3.2 Generation and characterization of DE droplet

Monodisperse DE droplets were generated from two PDMS devices connected serially: the first device produced W/O emulsions; the second device was used to supplement an outer aqueous phase to form W/O/W emulsions (Figure 3-2a & 3-2b). The size of the ‘‘bioreactor’’, or the droplet core, could be tuned by varying the flow rates of the inner aqueous phase versus the oil phase in the first device, or varying the microfluidics channel dimensions. As an example, two microfluidics devices with different channel widths (100 μm and 200 μm) were used and the inner aqueous phase flow rate was fixed at 2 μL/min. The diameter of the core of droplets could be tuned from 65 μm to 90 μm (100 μm device) and from 150 μm to 210 μm (200 μm device) by increasing the oil flow rate from 3 μL/min to 15 μL/min (Figure 3-2 c-e).

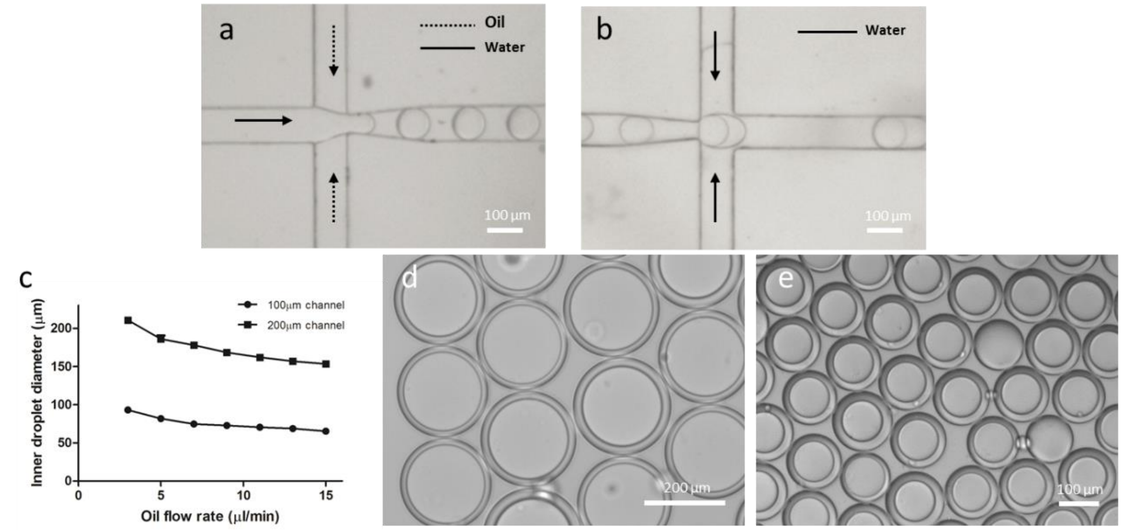

Figure 3-2: Generation of size-controllable DE droplets. Microscopic image of (a) the first and (b) the second PDMS device showing droplet formation. c) The effect of oil flow rate (at a fixed aqueous phase flow rate) on size of DE droplets using two types of devices. d) DE droplets generated at 3 μL/min (oil flow rate) using device with 200 μm channel width. e) DE droplets generated at 3 μL/min (oil flow rate) using device with 100 μm channel width.

The oil shell of DE droplets serves as a selective barrier, across which certain molecules can diffuse easily. Various dyes or dextrans of different molecular weights conjugated with fluorescein isothiocyanate (FITC) were encapsulated inside the DE droplets. The intensity of dyes in the core over time was recorded (Figure 3-3). A molecular weight-dependent diffusion of molecules out from the core was observed. Molecules with lower molecular weight (MW~ 400 Da) were able to diffuse across the oil layer while larger molecules (MW~70 k Da) were trapped within the droplets. Among molecules with similar molecular weight, their oil/water partition coefficient determines the permeability. Rhodamine 6G, rhodamine B and FITC with partition coefficient of 0.87, 0.26 and 0.08 diffused out from the droplets at a descending rate respectively (Figure 3-3a & 3-3b). To determine partition coefficient, culture medium supplemented with 2.5% pluronic F127 (outer aqueous phase) containing 50 μM of dyes was added on top of HFE7500 containing 2% Picosurf 2 surfactant (middle oil phase). The solution was then left on an orbital shaker operating at 100 rpm for 24 h to allow partition of chemical into the oil phase. The amount of dyes left in the aqueous phase was determined by intrapolating from a standard curve of the dye. The concentration of dyes in the oil phase was thus determined by the difference before and after incubation. Partition coefficient was calculated by the following formula: Partition coefficient = (Initial dye concentration – dye concentration in aqueous phase after incubation)/ Initial dye concentration. The selective permeability ensures nutrients but not large molecules to be delivered from the outer aqueous phase into the core and wastes to be removed in the opposite direction, thereby constituting an isolated bioreactor in each DE droplet for cell culture.

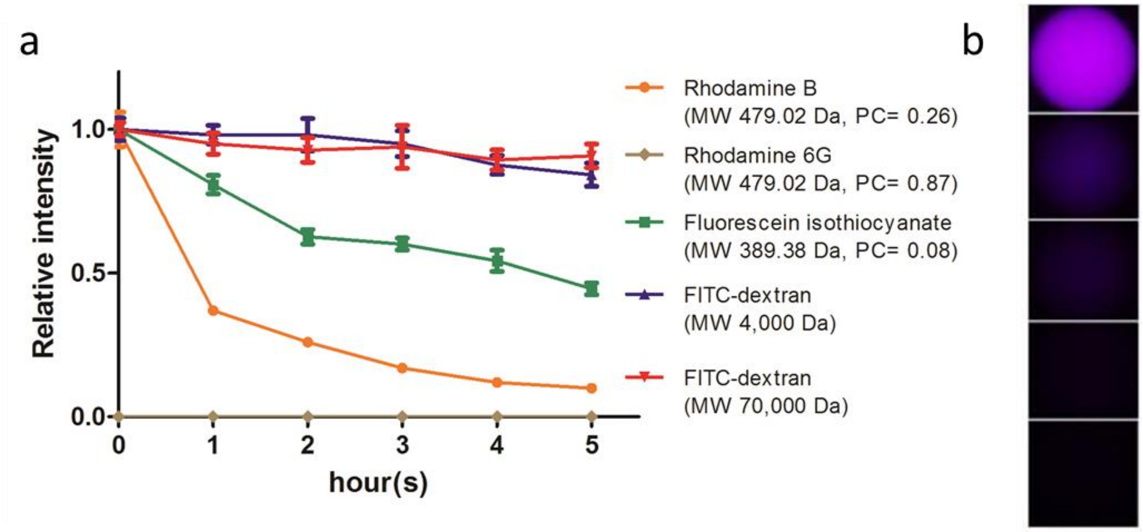

Figure 3-3: a) Diffusion curve of different dyes encapsulated in DE droplets. Molecular weight (MW) and partition coefficient (PC) of the dyes are provided in the legend. b) Fluorescent images of rhodamine B encapsulated in DE droplets at 0, 1, 2, 3, 5 h

3.3.3 Single cell encapsulation and amplification in DE droplets

To demonstrate single cell encapsulation and the subsequent population enrichment of bacteria cells in DE droplets, *E.coli* cells expressing synthetic *gfp*, *rfp* and *cfp* fluorescent proteins were loaded into 50 μm-diameter DE droplets (~60 pL) at a density of lower than 1x 10^6 bacteria/ mL, which gives an average of <0.06 bacteria per droplet. The distribution of cells in a droplet follows Poisson distribution where the probability of finding a droplet with *k* cells is defined by the equation:

$$f(k) = \frac{\lambda^{k} e^{-\lambda}}{k!}$$

Where λ is the average cell number per droplet and k is the specific cell number in the droplet.

After 24 h of incubation, the proliferation of bacteria cells generated distinctively red, green and cyan fluorescent signals in individual droplet (Figure 3-4a). No co-localization of different types of bacteria was observed, indicative of the successful separation of bacteria at single cell level. Analysis over a large pool of droplets indicated a bacteria distribution matching the Poisson distribution of 0.01 bacteria per droplet on average (Figure 3-4b). In this case, the probability of having two or more bacteria per droplet was negligible; suggesting that such a loading cell density could effectively separate all bacteria into single cell per droplet.

When DE was used to encapsulate single bacterium in growth medium (1:1 LB/PBS), fluorescent intensity from the entire droplet was enriched by approximately 100 times over a period of 24 h due to cell proliferation (Figure 3-4c & 3-4d). This observation confirms that culturing bacterium inside the droplets allows both bacteria separation as well as signal amplification from single bacterium.

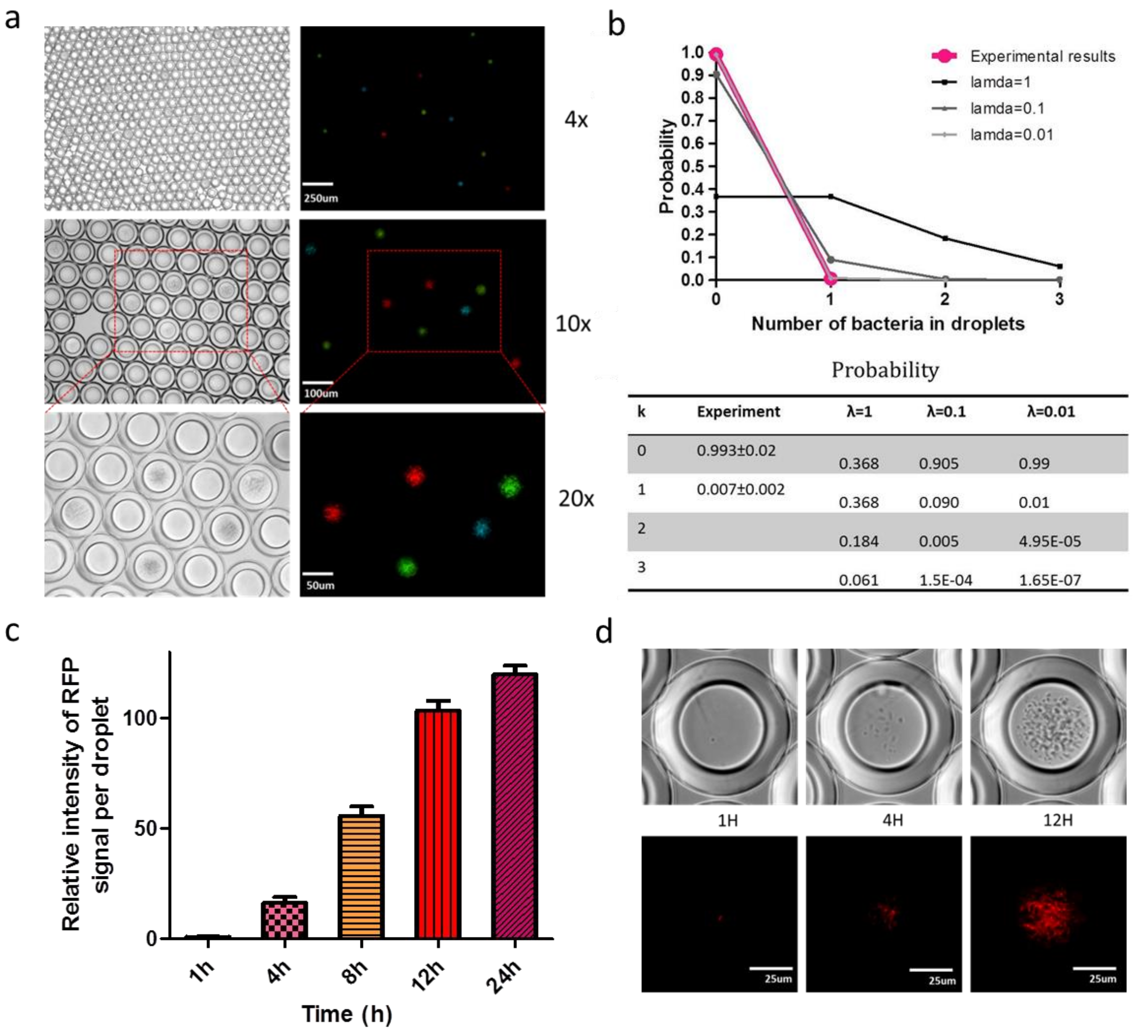

Probability

k	Experiment	λ=1	λ=0.1	λ=0.01
0	0.993±0.02	0.368	0.905	0.99
1	0.007±0.002	0.368	0.090	0.01
2		0.184	0.005	4.95E-05
3		0.061	1.5E-04	1.65E-07

Figure 3-4: a) Single cell encapsulation of bacteria carrying gfp, rfp & cfp genes showing no colocalization at 24 h post-encapsulation. b) Quantification of cell number distribution in droplets in graphic and table format. c) Relative RFP intensity measured inside the droplets over time. (n ⩾10) d) Fluorescent microscope images showing the proliferation from a single RFP-expressing *E. coli* cell encapsulated in droplet.

3.3.4 Screening of accurate clones for microarray-synthesized and error-corrected genes

To determine how the screening system compares with the conventional culture plate method in terms of productivity and reliability, the platform was applied to identify error-free sequence in microarray-synthesized genes. We chose red fluorescent protein (*rfp*) as a test gene for convenient screening of functionally correct genes. Freshly synthesized *rfp* gene construct before and after error-correction following our previously reported protocol were transformed into *E. coli* cells and encapsulated into DE droplet as single cell. The resultant droplets were incubated in growth medium overnight to allow cell proliferation to saturate the inner droplet. Using droplet counting, it was found that 52.8% of bacteria-positive droplets formed from uncorrected product contained cells that fluoresced brightly. Synthesis quality approximated from droplet system was consistent with that calculated using colony counting on agar plates (Figure 3-5a & 3-5b). Employing error correction increased the percentage of brightly fluorescent RFP droplets to 90.6%, which was also consistent with previous results conducted in conventional agar plate condition.

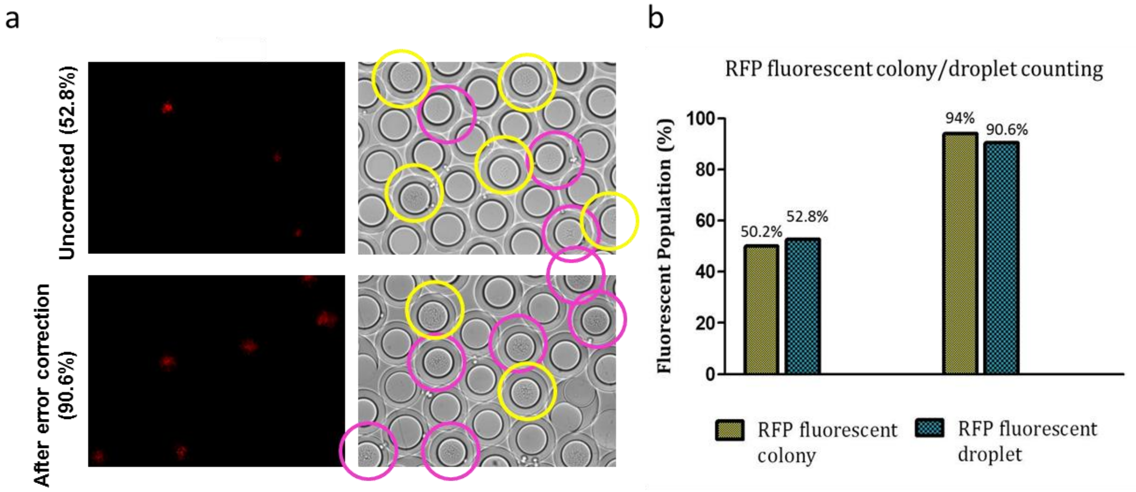

Figure 3-5: Characterization of fluorescent cell population transfected with synthetic RFP gene before or after error correction. a) Fluorescent microscope images showing increased percentage of fluorescent droplet after error correction. Circled droplets contain bacteria that are either fluorescent (pink) or not (yellow). b) Percentage of fluorescent clones was measured before and after error correction for RFP gene construct.

3.3.5 Tunable induction of synthetic gene expression through IPTG diffusion into droplet

To investigate the potential application of microfluidics-generated DE droplets as a perturbable microenvironment to screen and characterize synthetic gene expression, the feasibility of inducible gene expression in DE through the diffusion of IPTG from the external aqueous phase was studied. In bulk environment, the expression of GFP in these cells could be activated within a few hours by the application of IPTG. ~30 BL21(DE3) *E. coli* cells carrying a microarray-synthesized *gfp* controlled by a pET vector was encapsulated in each droplet. Upon addition of 5 mM IPTG in the external aqueous phase, GFP expression became detectable after 4 h, but not in control droplets without IPTG (Figure 3-6b). Relative GFP intensity observed per droplet increased over time, which was both contributed by increased GFP expression per cell (indicated by brighter bacterial cells) and bacteria growth (Figure 3-6a). The rapid appearance of GFP signal in the bacterial cells suggested effective transport of IPTG molecule across the oil shell.

To further study the induction of GFP expression by IPTG diffusion, the relative florescent intensity change overtime in droplets was compared to that in bulk culture environment. Gene expression was delayed by about 4 h in droplets compared to in conventional culture environment, which is likely the time course required for IPTG molecule to permeate into the inner core (Figure 3-6a). To understand the impact of IPTG concentration on gene expression induction, bacteria-containing droplets were suspended in medium with a gradient of IPTG concentration. A concentration-dependent activation of GFP expression was observed (Figure 3-6c). However, even at a low IPTG concentration of 0.5 mM, the system was still able to achieve ~80 % of the maximum gene expression level obtained in higher concentration conditions within 8 h of induction. This observation further confirms the relatively robust and efficient transportation of IPTG across droplet shells.

Next, the effect of IPTG diffusion on gene expression in droplets encapsulated with single cell, and how this process would interfere with bacteria proliferation were investigated. Bacteria encoding synthetic GFP in pET vector were suspended in minimal medium and encapsulated into DE droplets to yield no more than 1 bacterium cell per droplet. The minimum medium (M9) was chosen to optimize imaging conditions due to its low autofluorescence property. The resultant droplets were cultured in medium containing a broad range of IPTG concentration from 0.5 to 40 mM.

As shown in Figure 3-6d, IPTG concentration above 5 mM was inhibitive to the growth of bacteria. Lower IPTG concentrations, between 0.5 to 2 mM, were able to activate gene expression in pET vectors without interference with bacteria amplification. Noticeably upon onset, the collective GFP intensity was positively correlated with the supplied IPTG concentration with 2 mM IPTG providing the highest induced expression level. Cell populations at this point were relatively low and uniform across different conditions. The collective GFP intensity was contributed mainly by gene expression in individual cells. Yet this correlation gradually inverted itself as cells proliferated over time. At 12 h post-induction, droplets supplemented with 1 mM IPTG started to exhibit higher GFP intensity than that induced by 2 mM IPTG, whereas droplets activated by 0.5 mM IPTG generated the highest collective GFP intensity at the end point. This was due to effective exponential growth of bacteria cells post-induction, generating a large cell population encoding green fluorescent protein.

The appearance and morphology of bacteria cell clusters for droplets in each IPTG concentration were next characterized and compared (Figure 3-6e). Besides generating the largest cell density and in turn exhibiting the highest collective GFP intensity, single bacteria cell induced by 0.5 mM IPTG grew into stable and uniform cell clusters that saturated the entire inner phase of the droplet. Small deviation of intensity was thus observed across individual droplets at the same condition. Nevertheless as IPTG concentration increased, average cell density dropped significantly while variation across droplets escalated within each condition, as indicated by the error bar on Figure 3-6e.

To further investigate the optimal induction condition, the induction time course was shortened by switching to a more nutritious media i.e. LB/PBS (1:1) in an attempt to boost bacterial metabolism and reduce lag time by facilitating the initial growth of bacteria using LB/ PBS. Single bacterium was encapsulated into DE droplets with either M9 or LB/PBS (1:1) media and the droplets were suspended in 0.5 and 2 mM IPTG culture. Bacteria cultured in LB/PBS broth reached exponential growth around 4 h upon encapsulation, which coordinated with the diffusion rate of IPTG thus generated much higher overall intensity at both 12 h and 24 h time point in comparison with M9 media (Figure 3-6f & 3-6g). This enhanced signal was due to a combined effect of both a larger cell population and a higher expression per cell observed in each droplet. Particularly for 0.5 mM IPTG added to the outer core, intensity achieved at 12 h in LB/PBS broth outweighed that obtained from M9 broth at 24 h time point. Consistent with previous observation, lower IPTG concentration allowed single cell to proliferate into saturated cell density, resulting in uniform and consistent signal in each droplet. Whereas cells induced by higher IPTG concentration, albeit being brighter themselves, generated enhanced signal variation due to the presence of lower cell number and dispersed cell pattern in each droplet. These observations suggest that IPTG diffusion rate and bacteria growth curve could be synchronized to achieve the best signal amplification effect.

To further understand how IPTG would affect the growth of single bacterium in droplet, moderate amount of IPTG was introduced to bacteria culture prior to encapsulation. Single cell that came into direct contact with IPTG, even at ultralow concentration, proliferated at much lower growth rate than one that was activated by slowly diffused IPTG from external environment (Figure 3-6h). This further confirms our previous note that IPTG was inhibitive to bacteria growth when they came into contact with the cell before they reached the lag phase. The effect was also proportional to the concentration of IPTG in the environment.

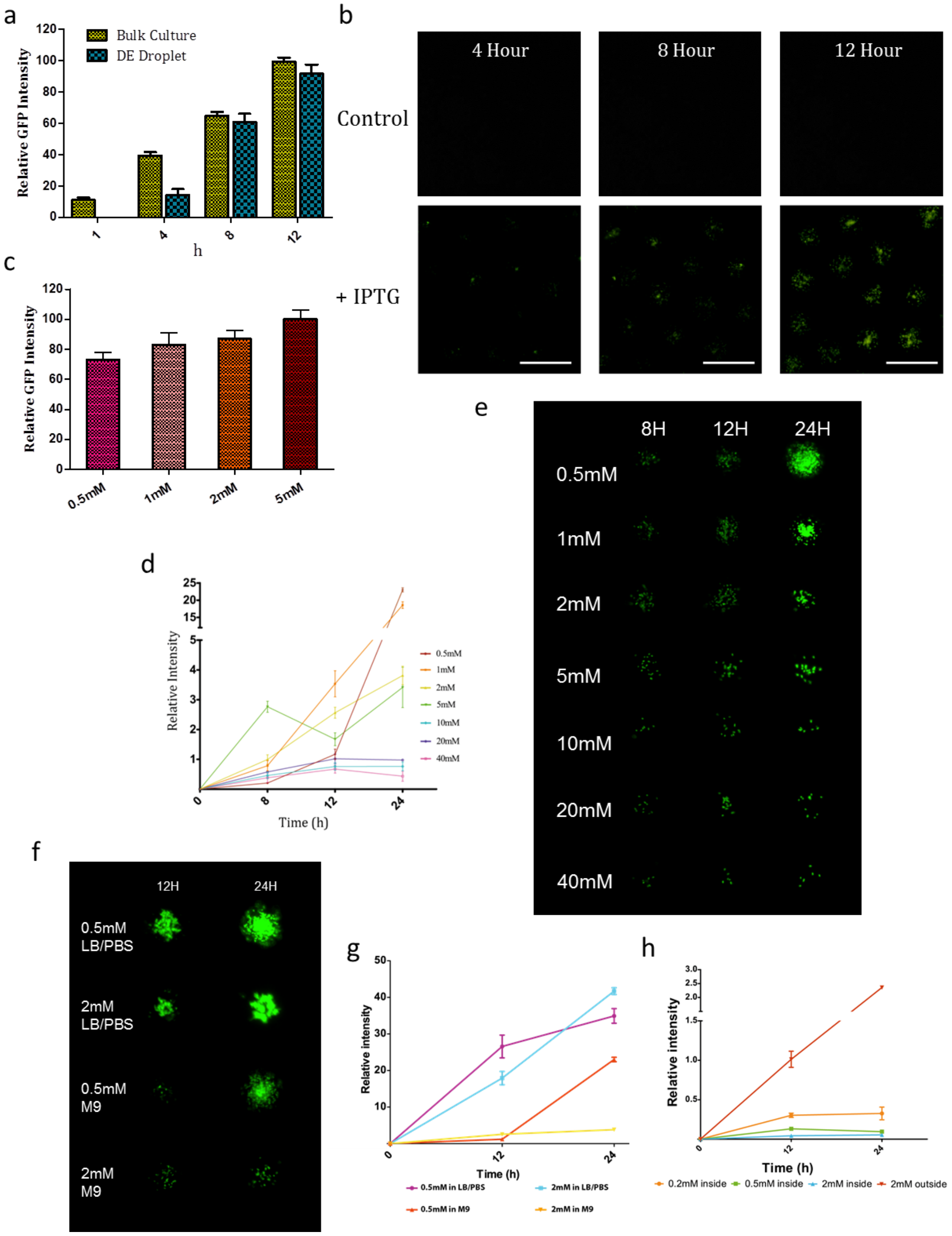

Figure 3-6: a) Relative fluorescent intensities of bacteria with pET vector controlling a gfp gene in bulk and in droplets after addition of 5 µM IPTG over time. (n=9) b) Fluorescent microscope images of droplets containing bacteria in absence of IPTG (top panel) and in presence of 5 µM IPTG (bottom panel). (Scale bar: 100 µm) c)

Relative fluorescent intensities of bacteria with pET vector controlling a gfp gene 8 h after introduction of various concentration of IPTG. d) Average GFP intensity per droplet as a function of time with the external concentration of IPTG ranging from 0.5 mM and 40 mM. (n=9) e) Fluorescent images showing GFP expressing cell clusters per droplet at 8 h, 12 h and 24 h time point post-IPTG induction. Images were taken at 20x magnification. f) Fluorescent images showing GFP expressing cell clusters per droplet at 12 h and 24 h time point after IPTG induction in minimal M9 vs growth LB/PBS media. Images were taken at 20x magnification. g) GFP intensity per droplet as a function of time upon IPTG induction in minimal M9 vs growth LB/PBS media. h) GFP intensity per droplet as a function of time with IPTG introduced prior to encapsulation at various concentrations. Fluorescent intensity curves are compared to the condition with IPTG introduced from external aqueous environment (red line)

3.3.6 Analysis of gene expression by fluorescence-activated high-throughput droplets sorting

The high capacity microfluidics-based droplet technology requires automated, high-throughput screening system to process and sort large volume of activities. DE droplets are compatible with most flow cytometric analysis platforms. In addition to throughput, the ability to precisely discriminate among DE based on their fluorescence and their uniform size are crucial for accurate screening.

To demonstrate stringent fluorescent-activated sorting of synthetic genes in DE droplets, a mixture of *E.coli* cells carrying synthetic GFP and RFP genes in equivalent amount was encapsulated into DE droplets as single cell. After overnight incubation, the droplets were suspended in PBS and analyzed them with a flow cytometry sorter. As shown in the intensity histograms, both GFP-positive and RFP-positive droplets revealed confined and distinctive peaks, representing strong and uniform signal intensities (Figure 3-7a). With proper channel compensation, droplets containing GFP and RFP expressing cells were sorted into different reservoirs.

Interesting to note is that unlike conventional mammalian cells, where the FSC vs SSC value reveals the size and morphology information of the sample, DE droplets are transparent thus do not generate similar scatter pattern when excited by the lasers. In contrast, the forward and side scatter information observed here is mostly likely generated from the spherical structure of the cell cluster confined by the inner droplet. The robust yet confined signal intensity measured during FACS indicated sufficient cell population in each droplet. This is consistent with our previous observation that efficient signal amplification through cell proliferation could be readily achieved from a single copy of bacteria/genotype with this system. The concentrated localization of data points from positive droplets on FSC vs SSC plot further confirms that the emulsion droplets were highly uniform in terms of size and internal structure.

To demonstrate the importance of signal amplification prior to FACS, a parallel analysis of multiple DE species present in the same sample was conducted. DE droplets encapsulated with four different densities of GFP-positive cells at 1, 10, 100, 1000 bacteria/droplet were created and analyzed in FACS. Both signal intensity and spatial resolution were enhanced with increased average number of cells present per droplet, as indicated by the decreased peak width yet increased peak height. Upon overlying the intensity histogram for all four emulsions conditions, peaks corresponding to droplets containing 100 and 1000 bacteria/droplet were distinguishable from adjacent peaks (Figure 3-7b). To further validate the hypothesis, these four bacteria-loaded droplet samples were mixed at equal volumes and analyzed the joint sample in a flow cytometer. As expected, only droplets loaded with higher cell density could be accurately discriminated, while droplets with lower cell population generated faint and broad signals that could not be resolved from each other or from empty droplets.

Although droplets used in all FACS analysis were created at same size and internal structure, the latter sample exhibited a much spread out pattern in terms of FSC and SSC measurement compared to the GFP/RFP mixture, further confirming our previous postulation that scatter information are representative of the size and structure of the inner cell clusters rather than the emulsion droplet.

These observations demonstrated the possibility of coupling FACS with microfluidics DE system to achieve the desired capacity, throughput and automation of synthetic genes screening. More importantly, these findings also highlight the significance of signal enrichment in stringent sorting during FACS, as sufficient cell population is essential to generate robust and uniform signals to guarantee detection sensitivity and resolution.

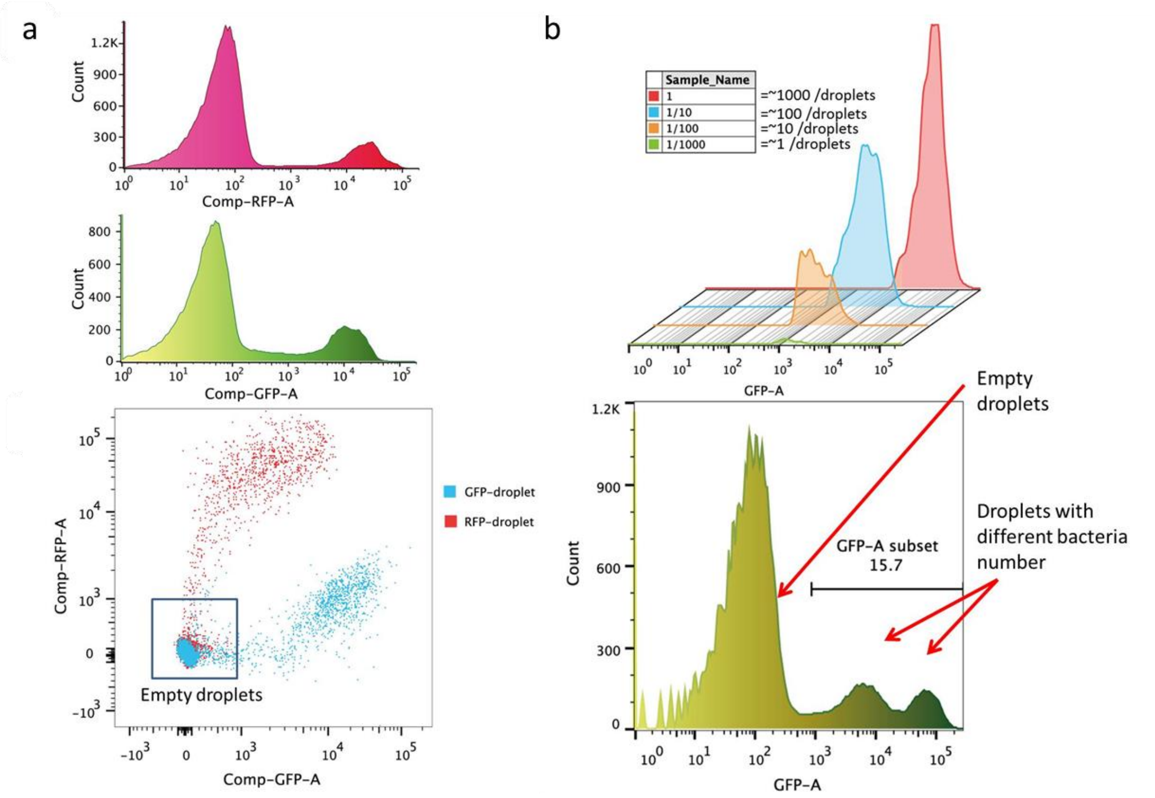

Figure 3-7: a) Separation of DE droplets containing GFP and RFP expressing cells. Top: Intensity histogram of GFP and RFP channels. Bottom: Overlay of green and red channels showing RFP+-GFP+ populations. b) Flow cytometry analysis of DE droplets loaded with 4 different numbers of GFP-positive cells per droplet. Top: Overlay of signal intensities obtained for each conditions respectively. Bottom: Analysis of droplet mixture containing all four species with 1, 10, 100 and 1000 bacteria/droplet.

3.4 Discussion

In this study, the development of DE droplet platform and the application of DE droplets to encapsulate and culture single bacterium carrying synthetic gene for high-throughput screening were demonstrated. The main difference between DE droplets and other microcapsule systems is that the microcapsule membrane which is often hydrogel itself is substituted with an oil layer [87]. In our case, no gelation step is involved when producing the droplets, which simplifies the encapsulation process and renders it unnecessary to control the viscosity of various phases to obtain a stable structure. The choice of fluorinated oil (HFE-7500) as the oil phase with high oxygen permeability ensures adequate supply of oxygen [88]. The oil phase also serves as a selectively permeable barrier to encapsulate cells while allowing passage of small molecules across it, constituting a programmable bioreactor for cell culture.

Efficient proliferation of single bacterium in DE droplets is critical in phenotype screening as sufficient number of target molecules per unit volume of sample is essential to all biological detections. Single bacterium is difficult to be visualized under optical microscope as it measures around one micron and moves rapidly at erratic trajectory. The signal intensity often falls below the detection threshold of many screening technologies. Furthermore, the rapid and stochastic motion of individual cells in aqueous environment causes them to periodically gather at the center or diffuse to the peripheral of the droplet, creating signals that are temporally and spatially unstable. The lack of uniformity and stability of signals from a particular genotype would greatly hinder the detection resolution and sensitivity when phenotyping with high-throughput platforms like FACS. Therefore, efficient enrichment, ideally saturation, of bacterial population inside the droplet through self-replication significantly amplifies the selective signals and enables stringent screening of sequence-correctness or enhanced protein expression of synthetic gene. A saturated cell population confines the collective motion of the cells, allowing cell distribution to be spatially uniform and temporally static, which in turn increases both the resolution and sensitivity of the screening process.

The proposed DE system is a tunable microenvironment suitable for single cell analysis as it allows selective transport of inducer chemicals to activate gene expression and enables efficient signal amplification through robust cell proliferation. The delayed-onset of IPTG-triggered gene activation through molecular diffusion can be fine-tuned to synchronize with the cell growth curve, facilitating the effective activation and amplification of synthetic genes from single bacterium. The fine-tuning process depends on the optimization of both the bacteria culture medium and IPTG concentration which resulted in the saturation of bacteria in droplets and consequently the creation of a stable, spherical fluorescent signal originated from the cell cluster. At high IPTG concentration, cells were most likely overburdened with plasmid expression, which diverts cellular resources from making necessary proteins for proliferation and leads to a reduction in the growth rate. This observation is consistent with that reported in the literature. The inhibition of cell proliferation due to early exposure of bacteria to IPTG again highlighted the importance of diffusion of IPTG from the external aqueous phase into the droplet core to induce gene expression. Analysis of droplets containing different number of bacteria in FACS verified our hypothesis that signal enhancement through bacteria proliferation increases the resolution and sensitivity of the screening process. The proposed technology holds potential to replace manual counting and picking bacteria colony to automate and advance the field of high-throughput synthetic gene screening.

3.5 Conclusion

In conclusion, this study demonstrated the development of a microfluidic-based platform that generates well-controlled monodispersed DE for high-throughput synthetic gene screening. The oil shell is selectively permeable that allows molecular diffusion across the oil phase. Single bacterium encapsulation in DE droplet was demonstrated, enabling the screening of error-free genes generated from microarray gene synthesizer before and after error correction process. The diffusion of IPTG into droplet core induced gene expression, in which 0.5 μM IPTG applied in the external phase resulted in the creation of a stable, spherical fluorescent signal after 24 h. We showed that fluorescent signals generated from at least 100 bacteria/droplet were distinguishable in FACS, indicative of the importance of signal amplification from single bacterium in DE droplets. The coupling of high-throughput gene synthesis and DE droplet screening system should open up opportunities to produce and screen large amount of synthetic genes efficiently. Our comprehensive study on single cell encapsulation and IPTG-triggered gene expression should pave the way for future research of screening complex gene libraries for a broad range of functionalities and activities.

4. Rapid formation of hMSC spheroids with controllable microenvironment in DE droplets

An attractive option for tissue engineering is to use of multicellular spheroids as microtissues, particularly with stem cell spheroids. Conventional approaches of fabricating spheroids suffer from low throughput and polydispersity in size, and fail to supplement cues from extracellular matrix (ECM) for enhanced differentiation. In this study, we report the application of DE droplets as pico-liter sized bioreactor for rapid cell assembly and well-controlled microenvironment for spheroid culture. Cells aggregated to form size-controllable (30–80 μm) spheroids in DE droplets within 150 min and could be retrieved via a droplet-releasing agent. Moreover, precursor hydrogel solution can be adopted as the inner phase to produce spheroid-encapsulated microgels after spheroid formation. As an example, the encapsulation of human mesenchymal stem cells (hMSC) spheroids in alginate and alginate-arginine-glycine-aspartic acid (-RGD) microgel was demonstrated, with enhanced osteogenic differentiation further exhibited in the latter case.

4.1 Introduction

Multicelluar spheroids recapitulate three-dimensional tissue *in vivo* in enabling cell–cell and cell–matrix interactions [65]. Cell-cell interactions regulate many biological processes such as development, homeostasis and disease progression via juxtacrine signaling mediated by direct cell contact or communication through functional junctions between cells. Forming multicellular spheroids *in vitro* can establish cell-cell contact required for preserving cellular viability, function and phenotype that are often lost in monolayer culture [89]. The use of scaffold-free spheroids as microtissues for microscale tissue engineering presents many advantages and opportunities, particularly with proliferative and pluripotent stem cell spheroids as building units for regenerative medicine. For instance, the differentiation of mesenchymal stem cells could be greatly enhanced with spheroid culture to facilitate tissue construction [65]. For microscale tissue engineering, the spheroid size and microenvironmental cues such as extracellular matrix (ECM) play an important role in directing stem cell behavior [90]. The size of mesenchymal stem cell (MSC) spheroid has been shown to influence its differentiation potential, with smaller spheroid directing more homogeneous chondrogenic differentiation towards hyaline chondrocytes whereas larger pellet producing more heterogeneous tissue [91]. Further, external microenvironmental cues in the form of matrix scaffold are often applied to direct stem cell differentiation. More precisely, the matrix scaffold can be modified to achieve desired mechanical properties or to present chemical and biological stimuli for controlled stem cell differentiation [92, 93]. For examples, the encapsulation of MSC in poly(ethylene glycol) (PEG) hydrogel conjugated to RGD or hyaluronic acid hydrogel favors differentiation along the osteogenic or chondrogenic lineages, respectively [94, 95]. The wide range of scaffold materials and modification options available suggests a need for a high-throughput system that can generate cell spheroids encapsulated in matrix scaffold efficiently.

Nevertheless, a scalable biofabrication technology for rapid, high-throughput production and yet offering a tunable microenvironment for spheroid culture is lacking. Conventional ways of making spheroids including culture in suspension, in spinner flask, or in hanging drop results in either heterogeneity of spheroid size or labor-intensiveness. Although development such as high-throughput droplet printing could accelerate the spheroid production process, control issues of multiple aggregates remain to be optimized [96]. Recently the research focus has turned to the approach of using non-adhesive micromolded surface, taking advantage of microfabriation technique that supports spheroid size control as well as scaling up. However, the encapsulation of spheroid in matrix scaffold following its formation either requires multiple steps or replating [97], complicating the process and possibly inducing spheroid fusion or damaging the mechanically weak spheroids due to shear stress induced by pipetting spheroids into ECM (e.g. hydrogel). In this study we demonstrated the use of W/O/W droplets for hMSC spheroid production via cell assembly and subsequent release as spheroid alone or encapsulation in microgel. Although spheroid formation has been demonstrated with cells encapsulated in alginate or gelatin microgels generated by single-emulsion technology previously [98-100], those techniques rely on some highly proliferative cell such as tumor cells to rapidly divide in the gel to form spheroids.

hMSC was chosen in this study since hMSC would not form a spheroid in an alginate gel normally; serving the purpose to demonstrate the uniqueness of our spheroid formation technology. Importantly, the time required for spheroid formation of existing technologies is around 1 to 4 days [99, 101, 102]. In our approach, cells aggregate to form spheroid in 150 min. This rapid and versatile cell assembly technology should find many interesting stem cell tissue engineering applications such as in the field of cartilage and liver regeneration as well as high-throughput drug testing applications.

4.2 Materials and Methods

4.2.1 Culture and encapsulation of hMSC.

Bone marrow–derived hMSCs were kindly provided by Tulane University Health Sciences Center. The culture medium used was a-minimum essential medium with fetal bovine serum (20%) and penicillin/ streptomycin (1%) at 37uC and 5% CO2. The 3–5 th passages of the hMSCs were used in this study. To encapsulate hMSC in DE droplets, hMSC were trypsinized and suspended at (2, 5, 10, 20* 10^6 cell/mL) in culture medium supplemented with PluronicH F-127 (1 wt%) (Sigma-Aldrich, St. Louis, MO). The flow rates of three phases (inner aqueous: middle oil: outer aqueous) were set at 5: 10: 25 mL/min respectively. The droplets were collected and transferred to 24-well plates for subsequent culture and analysis.

4.2.2 hMSC spheroid characterization

The frequency of spheroid formation was determined by counting the number of DE droplets containing a spheroid from the pool of 50–150 droplets each time. The hMSC spheroids were released from the DE droplets using a droplet releasing agent (1H,1H,2H,2H-Perfluoro-1-octanol from Sigma-Aldrich, St. Louis, MO). In a sterilized microcentrifuge tube, the droplet releasing agent (50 mL), PBS (200 mL) and DE droplets (variable volume) were added sequentially and left at room temperature for two minutes. The aqueous phase was then retrieved which contained released hMSC spheroids. The retrieval yield was determined by counting the number of intact droplets remained after the droplet release process using an initial droplet number of 100–300. The viability of hMSC spheroids was determined qualitatively by staining the spheroids with calcein AM and propidium iodide. The area of live cell (green) was divided by the total area of spheroids (green : red) to determine the ratios of live cell area in the spheroids. The hMSC spheroids were cultured on either TCPS or ultra-low attachment multiwell plate (Corning, Tewksbury, MA) to determine cell migration from the spheroids. The released spheroids and hMSC culture on TCPS were cultured in adipogenic differentiation medium (Lonza, Walkersville, MD) for 7 days before fixed with paraformaldehyde (4%) and stained with Oil Red O solution (Sigma-Aldrich, St. Louis, MO). For immunostaining, paraformaldehyde-fixed hMSC spheroids were stained with collagen type I (Abcam, Cambridge, MA) and laminin (Abcam, Cambridge, MA) antibodies. Different Alexa Fluor secondary antibodies (Abcam, Cambridge, MA) were used to obtain fluorescent colors. The stained samples were analyzed under an inverted confocal microscope (Zeiss LSM 510) available at Duke Light Microscopy Core Facility.

4.2.3 Formation of PMEF, Caco-2 and HepG2 spheroids

PMEF (passage number = 4), Caco-2 (passage number = 45) and HepG2 cells (passage number = 90) were obtained from ATCC (Manassas, VA) and Duke Cell Culture Facility and cultured according to supplier's recommendation. Each cell type was trypinsized and resuspended at 8 * 10^6 cells/mL and encapsulated in DE droplets. Bright-field images were taken at 2 h and 6 h (in the case of Caco-2) after droplet formation.

4.2.4 Encapsulation of hMSC spheroids in hydrogel

It followed the same procedures as generating hMSC spheroids except the trypsinized cells were suspended in alginate (1%) (PRONOVA SLG100, Novamatrix) or alginate-RGD (1%) (NOVATACH-GRGD, Novamatrix) solution. After spheroids were formed, the gelation of inner phase was carried out by adding the droplet releasing agent (50 mL), CaCl2 (200 mM) in NaCl solution (200 mL, 150 mM) and DE droplets (variable volume) sequentially in a sterilized microcentrifuge tube and left at room temperature for two minutes. The retrieved microgels were washed with NaCl solution (150 mM) twice before transferred to cell culture medium for subsequent culture.

4.2.5 Osteogenic differentiation and characterization

Osteogenic differentiation of hMSC spheroids encapsulated in hydrogel was performed using optimized differentiation medium (StemProH Osteogenesis Differentiation Kit, Life Technologies, Grand Island, NY) following manufacturer's protocol. To perform Alizarin red staining, samples were fixed in 4% paraformaldehyde before washed with water. Alizarin red solution (0.02%) (Sigma-Aldrich, St. Louis, MO) with pH adjusted to 4.1-4.3 was prepared in distilled water. Samples were stained in the solution for 45 min before washed with PBS and analyzed under light microscope. Staining of alkaline phosphatase activity by using BCIP/NBT as substrate (SigmaFastTM BCIPNBT; Sigma Aldrich, St. Louis, MO) was carried out following manufacturer's protocol before the samples were analyzed under light microscope.

4.3 Results

4.3.1 Generation of size-controllable spheroids in DE droplets

One advantage of using uniform-sized droplet to encapsulate cells for spheroid production is that similar number of cells can be loaded in each droplet, ensuring the size of spheroids formed is monodisperse. Theoretically the number of cells in each droplet should follow Poisson distribution. When cells were suspended in culture media, the distribution of cells in droplets was not even and the average number of cells encapsulated dropped over time, due to cells clumping and settling down in syringe during droplet generation. To solve this issue, 1% alginate or sucrose solution was added to the culture media to increase the viscosity of the inner aqueous phase, thus slowing down the aggregation and settling of cells (Figure 4-1a). A stirring bar was also used to stir the liquid in the syringe to suspend the cells. In this case, the cell distribution in droplets matched that of Poisson prediction and was consistent over a period of at least 0.5 h (Figure 4-1b). Using Optiprep™, a density gradient medium, the density of the inner aqueous phase can be adjusted to be similar to that of a cell. In that case, aggregating and settling of cells could be minimized.

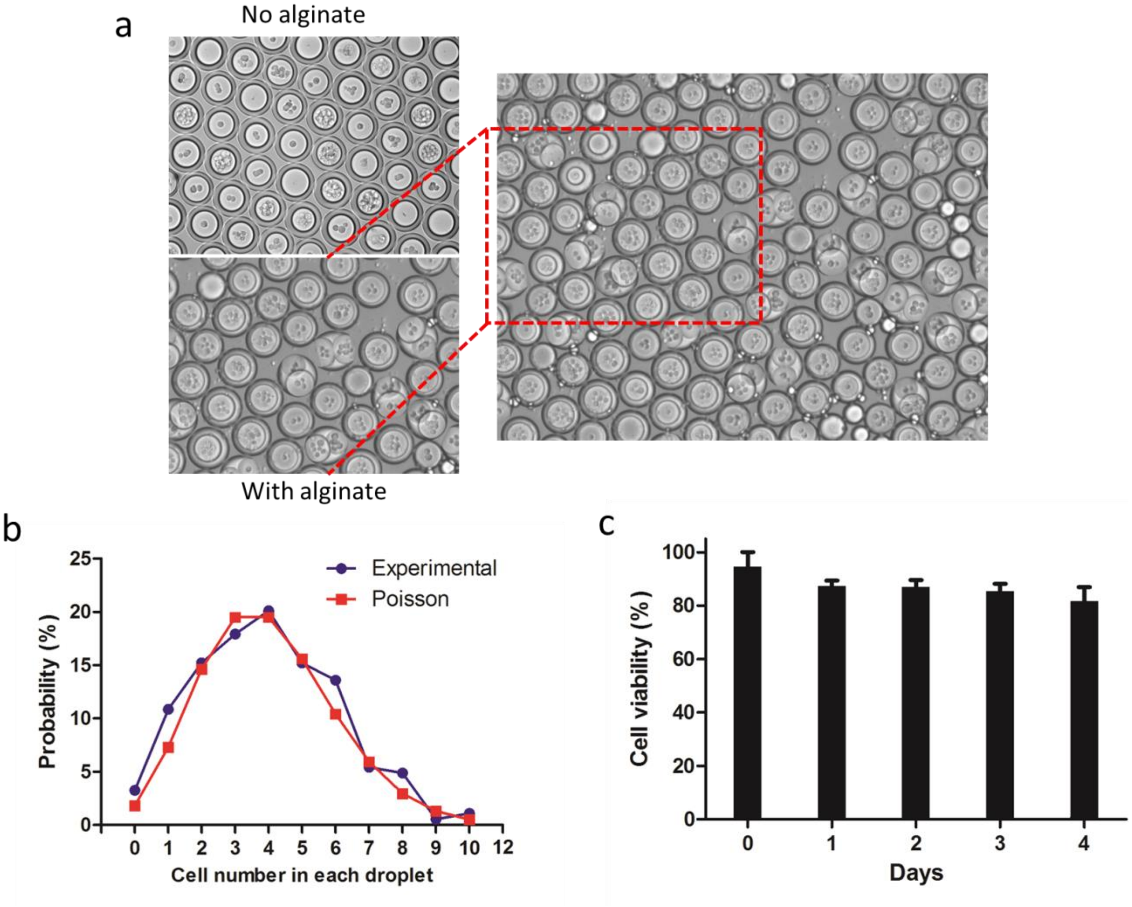

Figure 4-1: a) The cell distribution in DE droplets with and without addition of alginate in the inner phase. More empty droplets and droplets with over 10 cells were observed in the case without alginate addition. b) Plot of experimental data (distribution of cell number in 200 DE droplets) versus Poisson estimation with an average cell number in each droplet of 4. c) Viability of hMSC encapsulated in DE droplets over time.

When hMSC were encapsulated in droplets and cultured in media, high cell viability was maintained for a period of four days (Figure 4-1c). Culturing hMSC along with surfactant dissolved in the oil phase in 2D for one day led to aggregate formation, an effect that was not seen when cells were cultured with the oil alone (Figure 4-2 a-c). In the DE droplets, cell assembly occurred rapidly within 150 min due to microscale confinement in the droplets that encouraged cell-cell interactions (Figure 4-2d). To demonstrate the versatility of this cell-clustering technology, we examined different cell types (PMEF, HepG2 and Caco-2). It took 2 h for PMEF and HepG2 to form compact spheroid whereas Caco-2 required around 6 h (Figure 4-3 a-d). The effect might be attributed to the differences in cell-cell affinity of various cell types. The frequency of spheroid formation in the droplets was nearly 100 %. Compact spheroids (produced from any cell type) could be retrieved with the aid of a droplet-releasing agent (Figure 4-2e & 4-2f) and high cell viability was maintained during the process.

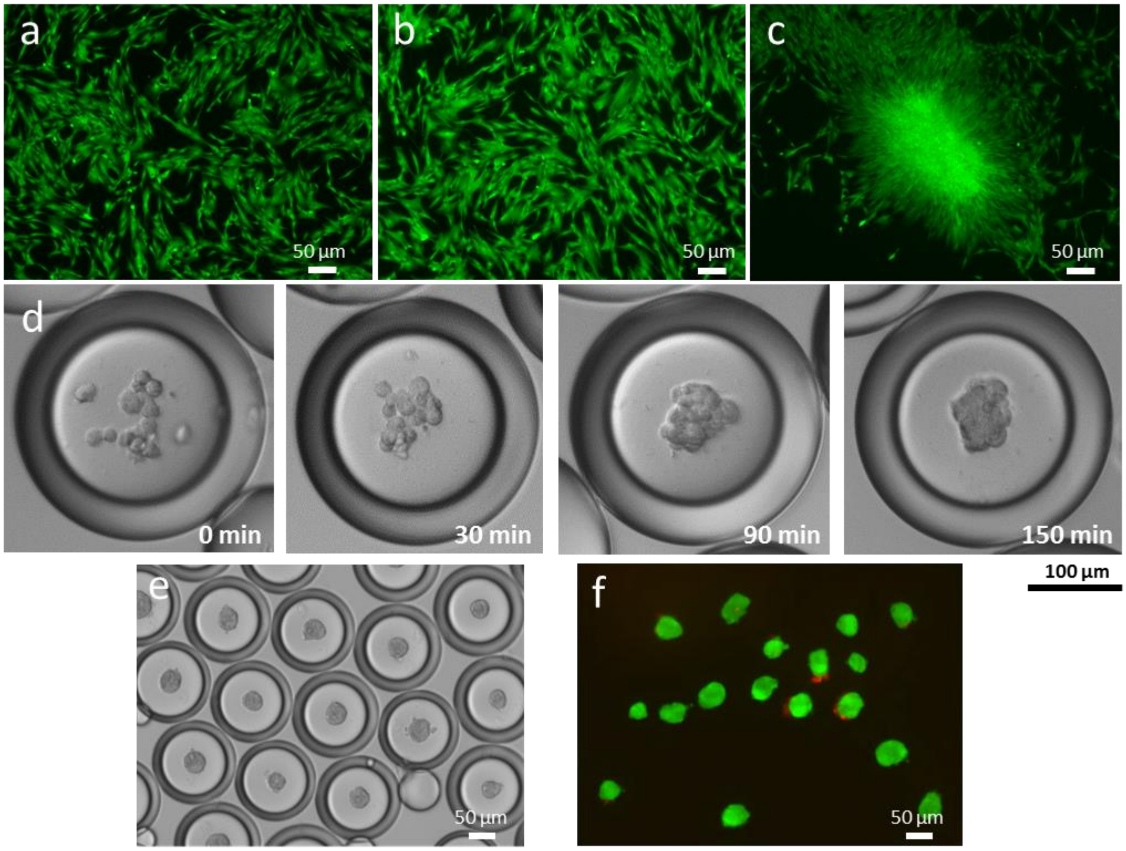

Figure 4-2: DE droplets generated in device with 200 µm channel width as bioreactor for cell assembly. Live/dead staining of hMSC after monolayer culture for 1 day with (a) no addition of oil or surfactant, (b) with oil and (c) with 1% Pico-Surf TM 1 surfactant dissolved in oil. (d) Time course images showing spheroids are formed in 150 min. (e) Phase image of hMSC spheroids encapsulated in DE droplets after 6 h. (f) Live/dead staining of spheroids after release from DE droplets at 6 h. Live cells were labeled with calcein AM (green) and dead cells were labeled with propidium iodide (red).

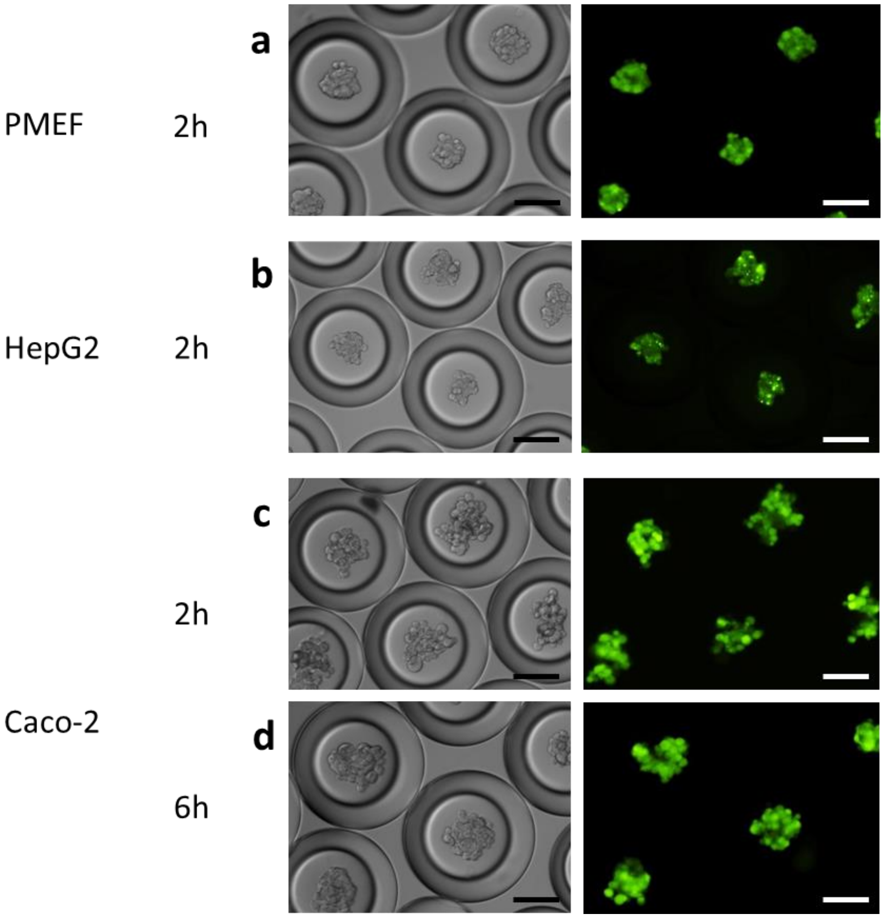

Figure 4-3: Bright field and live-dead images showing spheroid formation of a) PMEF, b) HepG2 at 2 h and Caco-2 at 2 h (c) and 6 h (d) (Scale bar = 100 μm).

4.3.2 Characterization of hMSC spheroids

The spheroid size could be controlled by changing the cell density used in the encapsulation process. In 200 μm droplets, 2, 5, 10 and 20 million cells/mL density, corresponding to 8, 20, 40, and 80 cells in each droplet on average, yielded spheroid size of 36, 46, 62, and 84 μm on average, respectively (Figure 4-4a). Larger spheroid size could be achieved by increasing the cell density or the size of droplets so that more cells could be incorporated. Percentage of viable cell area within each spheroid ranged from 88 % to 96 % for various spheroid sizes (Figure 4-4b). The released spheroids displayed spherical shape, and attached and spread when cultured on low attachment surface and normal tissue culture plate, respectively (Figure 4-4c & 4-4d), consistently with findings from previous reports [103]. Furthermore, the released hMSC spheroids could be differentiated into adipogenic lineage more readily than cells cultured in 2D (Figure 4-4e & 4-4f), indicating the functionality of the cells was not affected after encapsulation. Apart from viability and differentiation capability, another measure of the "healthiness" of the spheroids is their endogenous ECM arrangement which modulates cell behavior such as adhesion, attachment and host response. To characterize hMSC spheroids generated from DE droplets, endogenous ECM molecules including collagen type I and laminin were stained in the spheroids to show that hMSC preserved and formed complex 3D network with their endogenous ECM in the spheroids, mimicking the situation in vivo (Figure 4-4g & 4-4h).

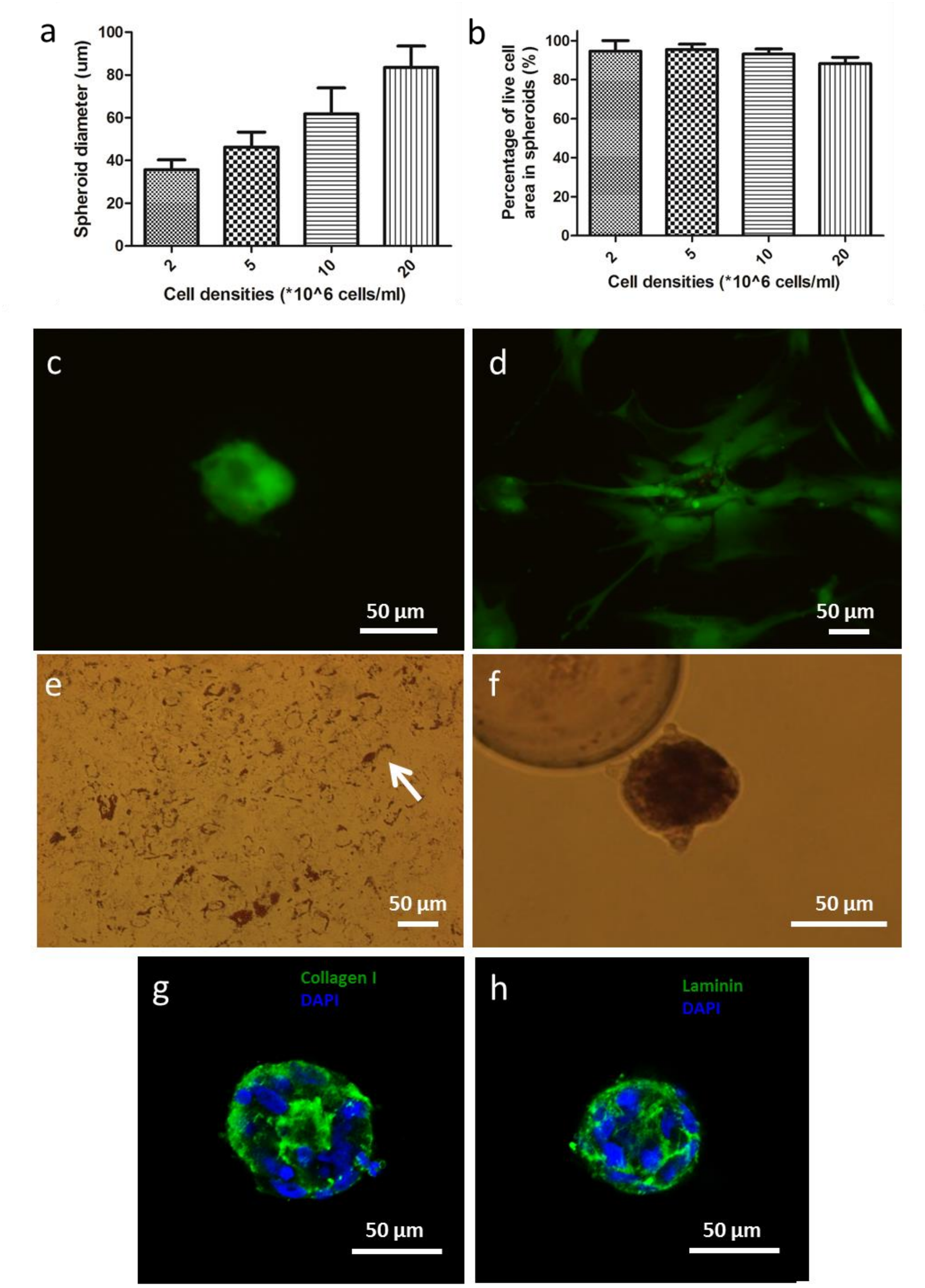

Figure 4-4: Characterisation of hMSC spheroids released from DE droplets a) Diameter of spheroids measured at different cell densities used (n = 50). (Data = mean ± SD) (b) Percentage of viable cell area in spheroids obtained at different cell encapsulation densities upon release (n = 10). (Data = mean ± SD). Live-dead image of

released hMSC spheroids cultured on (c) ultra-low attachment surface and (d) TCPS for one day (Green - calcein AM, red - propidum iodide). Oil Red O staining of hMSC cultured in (e) 2D and (f) 3D spheroid configuration differentiated along the adipogenic lineage for 7 days (Arrow indicates intracellular lipid vesicles.). Immunofluorescence images of hMSC spheroid stained with (g) collagen type I and (h) laminin taken under confocal microscope.

4.3.3 Controlling microenvironment of hMSC spheroid for osteogenic differentiation

To demonstrate the feasibility of controlling the microenvironment for hMSC spheroid differentiation, hMSC spheroids were embedded in alginate or alginate-RGD microgel for osteogenic differentiation (Figure 4-5a). Specifically, hMSC suspended in alginate or alginate-RGD solution was adopted as the inner phase during the droplet formation process. Once spheroids were formed, they were released into a solution bath containing calcium ions. The contact between the alginate or alginate-RGD solution and calcium ions induced crosslinking among alginate molecules rapidly, leading to the formation of a solid gel. Phalloidin staining after 3-day culture of hMSC spheroids in the two different gels revealed similar cellular cytoskeletal organization and displayed no obvious changes in spheroid morphology (Figure 4-5b & 4-5f). To determine the extent of cell-cell and cell-matrix interactions present in the spheroids in the microgels, immunostainings for E-cadherin, the transmembrane protein that regulates cell adhesion [69, 104], and integrin $\alpha5\beta1$ (the crucial attachment site for RGD sequence) were performed [105]. As shown in Figure 4-5c and 4-5g, both spheroids encapsulated in alginate or alginate-RGD gel displayed E-cadherin expression; however, hMSC spheroids encapsulated in alginate-RGD gel showed enhanced expression of integrin $\alpha 5\beta 1$ around the spheroids, suggesting the RGD sequence in the gel interacted with the spheroids actively to modulate its receptor expression, which could result in different cellular responses. One documented response is the enhanced osteogenic differentiation of MSC mediated by RGD sequence [95]. To show the applicability of our system in modulating stem cell differentiation, we induced osteogenic differentiation of hMSC spheroids encapsulated in alginate and alginate-RGD gels. After 7 days in culture, the spheroids in alginate-RGD gel contained more calcium deposits as shown by Alizarin red staining, and higher alkaline phosphatase activity, characteristic of enhanced osteogenic differentiation (Figure 4-5d, 4-5e, 4-5h & 4-5i) [106]. This example serves to validate our approach in controlling hMSC spheroid behavior by modulating its microenvironment.

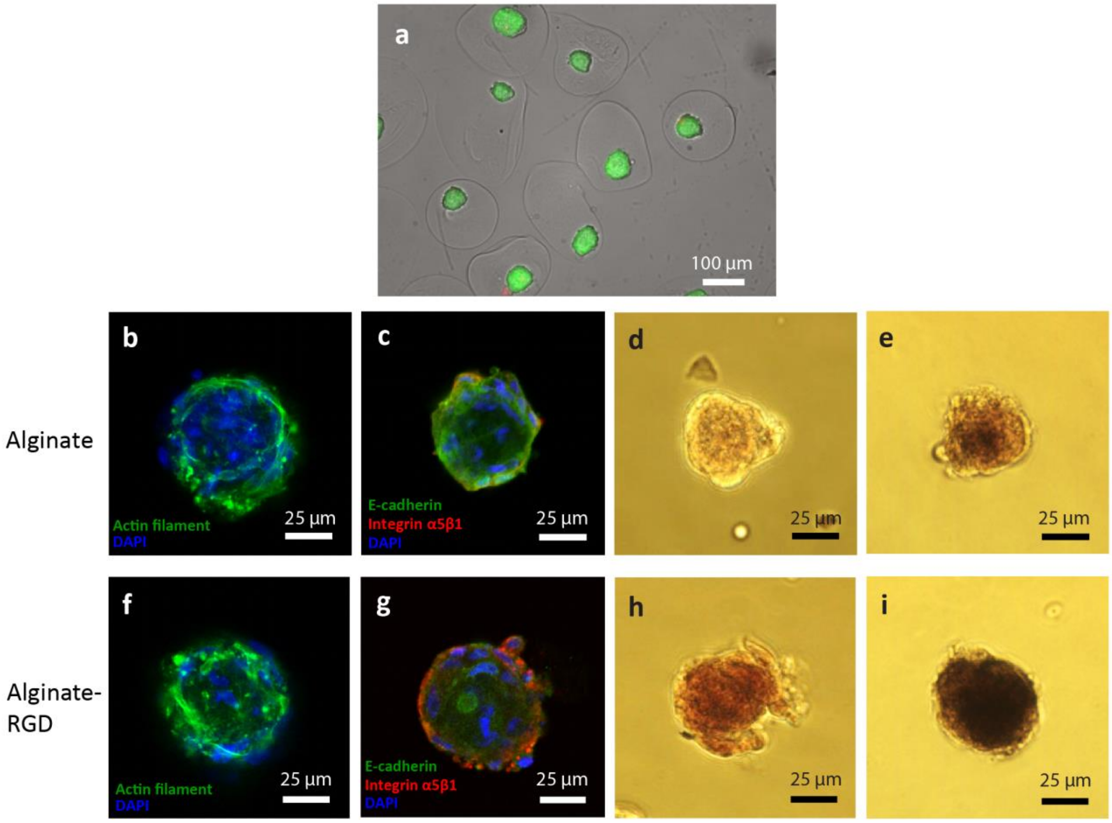
a
100 µm
b
Alginate
Actin filament
DAPI
25 µm
c
E-cadherin
Integrin α5β1
DAPI
25 µm
d
25 µm
e
25 µm
f
Alginate-RGD
Actin filament
DAPI
25 µm
g
E-cadherin
Integrin α5β1
DAPI
25 µm
h
25 µm
i
25 µm

Figure 4-5: Control of microenvironment for spheroid culture using DE droplets. (a) Live/dead staining of spheroids encapsulated in alginate gel. Live and dead cells were stained with calcein AM (green) and propidium iodide (red) respectively. Confocal images showing phalloidin staining (b, f) and immunostaining for E-cadherin, integrin α5β1 (c, g) for spheroids encapsulated in alginate or alginate-RGD gel cultured in normal media for 3 days. Images of alizarin red staining (d, h) and alkaline phosphatase activity staining using BCIP/NBT as substrate (e, i) for spheroids cultured in osteogenic medium for 7 days.

4.4 Discussion

In this study, rapid formation of multicellular spheroids in DE droplet was demonstrated. The use of amphiphilic surfactant during droplet generation not only stabilizes the droplet structure but also induces rapid spheroid formation, i.e. 150 min in our case versus 1 to 4 days in existing technologies. We speculated that the surfactant (Pico-Surf™ 1) contains a hydrophilic end that performs similar function as polyethylene glycol to resist cell adhesion based on findings from previous reports [107]. Together with the microconfinement effect offered by the pico-liter sized droplets, these explain why cells aggregated rapidly to form spheroids in the DE. The spheroids generated by our approach, apart from using as microtissues for tissue regeneration [108, 109], offer other advantages such as better retention during implantation as well [69]. The technology may also prove useful in the drug testing application where rapid formation of microtissue such as hepatocyte spheroids allows high-throughput drug testing and screening. Given that more stringent requirement for mass transfer must be satisfied for mammalian cell culture than bacteria culture, we speculated that the gradual reduction in cell viability observed in DE droplets is due to the limited supply of large molecules such as growth factors that are prevented from entry across the oil layer. Nevertheless, as we have demonstrated, the formation of spheroid and its subsequent release or encapsulation inside a microgel could be accomplished within several hours, after which the oil layer can be removed to avoid the issue of mass transport impairment.

The general idea behind various approaches of inducing stem cell differentiation is to provide a biomimetic environment for directing stem cell differentiation into a particular lineage, often accomplished by the use of growth factors and exogenous matrix scaffold. The DE droplets offer convenient control of the microenvironment where the inner aqueous phase can be easily tuned in microfluidics platform and is isolated from the outer aqueous phase. To accommodate the wide range of modulation options available, hydrogels such as collagen, agarose, gelatin and poly(ethylene glycol)-based hydrogels can be adopted as the inner phase [110, 111]. Soluble ECM components such as laminin and fibronectin can also be incorporated to screen for the optimal ECM microenvironment and generate ECM-encapsulated spheroids at high frequency (>20Hz in our case) [112]. The ease of entrapping spheroids in hydrogel directly in this study also circumvents the risk of dissociating or inducing fusion of spheroids during the transfer of spheroids into the hydrogel [90].

4.5 Conclusion

Overall, this study demonstrates an innovative DE platform for rapid and high-throughput production of multicellular spheroids and modulation of their microenvironment. The platform can easily be scaled-up with multiple channels. The DE droplets, with their selectively permeable oil layer, serve as bioreactors for rapid cell assembly for hMSC and other cell types. The inner aqueous phase could be replaced with hydrogels to fine-tune the microenvironment for desired differentiation. The proposed platform obviates the need for labor-intensive fabrication of stem cell spheroids and replating of spheroids into matrix scaffold. This rapid, versatile and scalable cell assembly technology should help advance the field of microscale tissue engineering.

5. Generation of microencapsulated hepatocyte spheroids with enhanced functions for liver tissue engineering

Microencapsulation of hepatocyte spheroids can contribute to liver research by serving in a variety of applications. Conventional approach of microencapsulating spheroids is hampered by diffusion barrier imposed by large gel size, poor control of spheroid number per gel and the requirement of spheroid loading into microgel, compounded by the rapid loss of hepatocyte functions in culture. Here, we report a microfluidics technology bypassing the step of spheroid transfer. DE droplets were used to generate microencapsulated single or co-culture hepatocyte spheroids (<200 μm in diameter all containing single spheroid) with enhanced functions. The composition of the microgel is tunable as demonstrated by improved hepatocyte functions during 24 day culture (alumin secretion, urea secretion and cytochrom P450 activity) when alginate-collagen composite hydrogel was used instead of alginate. Hepatocyte spheroids in alginate-collagen also performed better than hepatocytes cultured in 2D collagen sandwich configuration. Moreover, hepatocyte functions were significantly enhanced when hepatocytes and endothelial progenitor cells were co-cultured to form composite spheroid at a ratio of 5 to 1 after a range of ratios were tested. The hepatocyte functions could be further boosted when the co-culture spheroids were encapsulated in alginate-collagen. Our high-throughput technology with high yield, flexiblity and uniformity should help advance liver tissue engineering research as well as the broader field of biomanufacturing.

5.1 Introduction

The past decades have witnessed the exciting advances of cell microencapsulation technology in the medical field - beginning with the use of alginate-polylysine capsules for islet transplantation [113]. The envelopment of tissues or cells in microcapsules and microgels with semi-permeable membrane can protect the enclosed cells from the host immune system upon transplantation, facilitating the use of xenogeneic cell sources in clinical applications [114]. Besides, given that many cell types are fragile and highly vulnerable to shear forces, the microcapsule/microgel layer can shield the enclosed cells from shear damage in bioreactor culture [115]. Lastly, the encapsulation material itself or entrapped growth factors provide localized delivery of mechanical and biochemical cues to support or stimulate the functions or differentiation of the encapsulated cells [116].

The intrinsic characteristics associated with microcapsules/microgels such as short diffusion distance and high surface-to-volume ratio have spurred interests to use microencapsulated cells to treat various diseases [114, 117]. One notable example is the development of bioartificial liver. Most of the extracorporeal bioartificial liver systems currently examined in clinical trials involve a hollow fiber design where individual hepatocytes are immuno-isolated via hydrogel entrapment or membrane compartmentalization [118]. While the membrane offers protection from immune attack and shear force, it also creates a diffusion barrier to mass exchange [119]. In addition, flow rates within the bioreactors are low (100–200 mL/min) compared with those of *in vivo* perfusion (~1,500 mL/min) due to resistance within the fibers [120]. Entrapment of hepatocytes into microgels has been shown to preserve hepatocyte functions when they were cultured in bioreactor [56]. A fluidized or packed bed bioreactor containing microencapsulated hepatocytes appears promising in overcoming the limitations encountered with current liver support systems [121, 122]. In addition, injection of encapsulated hepatocytes intraperitonealy was proposed to treat liver-based inborn metabolic disease and acute liver failure as a better alternative to intrahepatic delivery of hepatocyte in suspension [36, 123]. The microgel layer (e.g. alginate) provides anchorage and protection against host immune attack for hepatocytes that can lead to better cell viability and functions in the engraftment site. Maintaining functional longevity of hepatocytes *in vitro* to more closely reflect the characteristics of liver *in vivo* is also the key to more effective drug screening platform [84].

It is particularly attractive to encapsulate hepatocyte spheroids owing to the improved cellular functions mediated by cell-cell interactions [97, 124, 125]. Traditionally, hepatocyte spheroids are generated before loading into microdroplets of hydrogel solution followed by polymerization [126]. To avoid clogging of spheroids in the nozzle or needle where microdroplet is generated, there exists a minimum diameter requirement of the nozzle/needle which leads to diffusional limitations and large transplant/device volume imposed by the size of capsule generated (500-1000 μm in diameter) [127]. In addition, non-uniform distribution of spheroid in capsule following Poisson equation is observed, resulting in empty capsules and possible agglomeration of multiple spheroids [74]. Since billions of hepatocytes are required to recapitulate liver function in the case of liver failure [118], the challenge of generating millions of hepatocyte spheroids and subsequently encapsulating them in a well-controlled and reproducible manner would be a hurdle to satisfy the Good Manufacturing Practice (GMP) for clinical translation.

Microfluidics has emerged as a high-throughput platform for biochemical assays and bioprocessing. Employing microfluidics to generate tiny monodisperse emulsion droplets creates microscale bioreactor and can be leveraged for scalable biomanufacturing of microencapsulated spheroids [22]. In this study, we report a high-throughput DE (water-in-oil-in-water) platform that promotes cell assembly within the droplet in 4 h and subsequently induces the polymerization of the inner hydrogel phase to generate microencapsulated hepatocyte spheroids (Figure 5-1a & 5-1b). We have previously shown that DE droplets can serve as platform for cell culture [84, 128]. Without any restriction on nozzle/needle size, the diameter of the microgel can be readily reduced to below 200 μm. Importantly, the inner phase of each droplet polymerizes individually to generate microgels all containing single spheroids. We demonstrate that the biochemical composition of the inner phase can be tuned to deliver appropriate cues for controlling hepatocyte behavior.

Besides matrix microenvironment, hepatocytes are surrounded by various types of cells such as endothelial cells, Kupffer cells and stellate cells in liver. In order to recapitulate the different types of heterocellular interactions present in liver, many attempts have focused on co-culturing hepatocytes with other cell types such as liver sinusoidal endothelial cells (LSEC), umbilical vein endothelial cells (HUVEC), Kupffer cells, stellate cells, or even fibroblasts [59, 129, 130]. In general, hepatocyte functions are enhanced and sustained with co-culture. Among the supporting cell types tested, endothelial cells are attractive as co-culture of hepatocytes and endothelial cells emulates the *in vivo* situation where the two cell types form a continuous lining along the sinusoid separated by the space of Disse [131]. Endothelial cells also contribute to vascularization of *ex vivo* engineered constructs to increase oxygen and nutrients supply [132]. In view of the invasive collection or limited supply of LSEC and HUVEC, we explored the feasibility of using EPC as an alternative supporting cell source. EPC are highly proliferative, able to differentiate into endothelial cells and available from umbilical cord as well as adult peripheral blood [133, 134]. Moreover, EPC express liver morphogen such as hepatocyte growth factor (HGF) which has been shown to stimulate albumin production in hepatocytes [135, 136]. Therefore, we hypothesized that co-culture of hepatocytes and EPC could enhance hepatocyte functions in a similar manner to a conducive microenvironment. To our best knowledge, this is the first study which researched into the co-culture of hepatocytes and EPC.

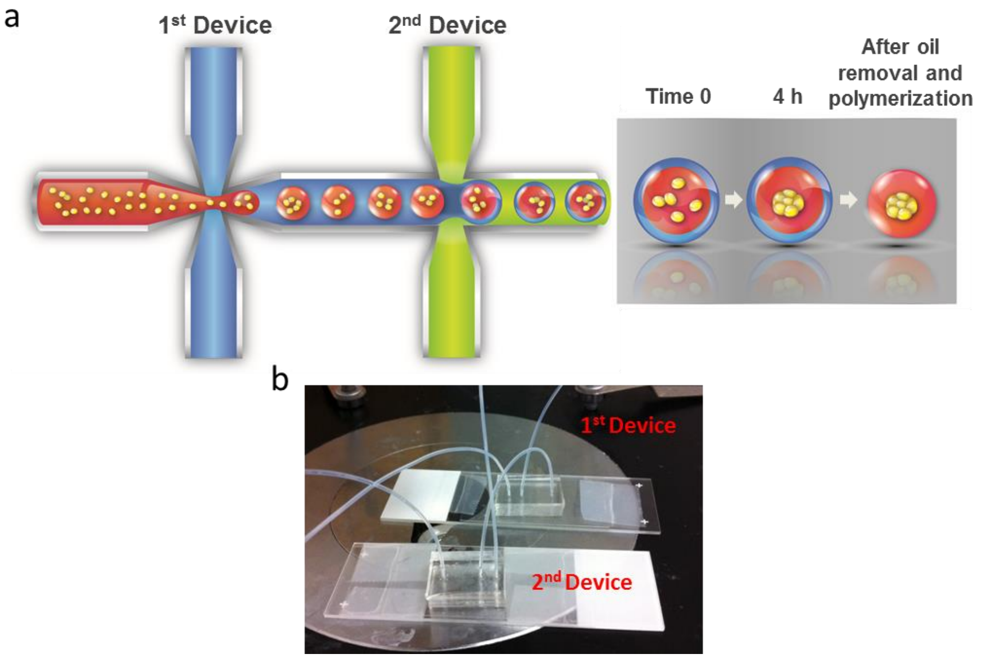
a
1st Device
2nd Device
Time 0
4 h
After oil removal and polymerization
b
1st Device
2nd Device

Figure 5-1: a) Schematic diagram of the process of generating microencapsulated hepatocyte spheroid using DE droplet. b) Microfluidic devices assembled on a glass microscope slide.

5.2 Materials and Methods

5.2.1 Cell culture

Fresh primary rat (Sprague-Dawley) hepatocytes (Hep) were purchased from Triangle Research Labs (Durham, NC) and cultured in DMEM (Life Technologies, Grand Island, NY) supplemented with 10% heat inactivated FBS (Life Technologies, Grand Island, NY), 0.02 μg/mL EGF (Life Technologies, Grand Island, NY), 7.14 μg/mL glucagon (Sigma Aldrich, St. Louis, MO), 17.36 μg/mL insulin (Sigma Aldrich, St. Louis, MO), 7.5 ng/mL hydrocortisone (Sigma Aldrich, St. Louis, MO) and 100 U/mL penicillin/ streptomycin (Life Technologies, Grand Island, NY). Hep were seeded on collagen-coated plates before overlaid with a layer of collagen gel the next day to set up the Col-Sandwich culture. Human umbilical cord blood-derived endothelial progenitor cells (EPC) were isolated as previously described [137]. Umbilical cord blood was obtained from the Carolina Cord Blood Bank. All patient identifiers were removed prior to receipt. The protocol for the collection and the usage of human blood in this study was approved by the Duke University Institutional Review Board. EPC were cultured in EGM-2 BulletKit (Lonza, Walkersville, MD) supplemented with 10% FBS and used within passage 3-5. HEK-293 cells were purchased from American Type Culture Collection (Manassas, VA) and cultured in DMEM supplemented with 10% FBS and 100 U/mL penicillin/ streptomycin. To determine the optimal co-culture medium composition, the Hep and EPC media were mixed at various ratios (1:0, 1:1, 2:1) and used to culture Hep and EPC respectively. The viability and von Willibrand factor (vWF) expression of EPC were analyzed while the albumin and urea secretions of Hep were assessed to determine the optimal culture conditions for both types of cells.

5.2.2 Microencapsulated spheroid generation and characterization

Hep or HEK-293 cells at a density of 8 million cells/ mL were loaded into droplets containing 1% alginate or 0.8% alginate/ 0.25 mg/mL collagen I solution (Rat tail collagen I, Life Technologies, Grand Island, NY). Collagen I was neutralized with sodium hydroxide solution (Sigma Aldrich, St. Louis, MO) before mixing with alginate solution. To generate co-culture spheroids composed of Hep and EPC, Hep and EPC were mixed at various ratios (1:0, 5:1, 3:1, 1:1, 1:3) to make up to 8 million cells/ mL and loaded into droplet. At 4 h after droplet formation, microgels encapsulating Hep spheroid were produced as described above. The sizes of DE, spheroids and microgels were quantified from at least three bright field images consisting of > 30 samples using ImageJ software. The viability of cell culture samples were evaluated by staining with 3 μM calcein AM and 2.5 μM propidium iodide solution for 30 min before imaged using the inverted confocal microscope (Zeiss LSM 510) available at Duke Light Microscopy Core Facility. To track the organization of co-culture cell types in the composite spheroid, EPC and Hep were labelled with CellTracker™ Green CMFDA Dye and CellTracker™ Red CMTPX Dye respectively before loaded into DE to form composite spheroids. The microencapsulated spheroids were imaged using the inverted confocal microscope at day 0 and 1.

5.2.3 MRP-2 transporter activity

5(6)-Carboxy-2′,7′-dichlorofluorescein diacetate (CDFDA) (Sigma Aldrich, St. Louis, MO) was used as the substrate to detect MRP-2 transporter activity and thus bile canaliculi formation. The samples were incubated with 5 μM CDFDA for 30 min. Thereafter, dye solution was aspirated and the cells were washed with PBS for a few times before imaged using the inverted confocal microscope.

5.2.4 Immunostaining

For immunostaining against collagen I, the microgels were first added to 50 mM sodium citrate solution for 5 min to dissolve the alginate layer before stained with collagen I primary antibody (PA1-27397) and the corresponding secondary antibody (31573). For immunostaining against albumin and vWF, the microgels were again treated with sodium citrate before permeabilized with 0.1 % Triton X-100 solution for 30 min. The antibodies used were vWF antibody (PA5-16634) and the corresponding secondary antibody (31670), and albumin antibody conjugated with FITC (PA1-86695). All antibodies were purchased from Thermo Scientific (Waltham, MA). The samples were then fixed in FluoroGel mounting medium (Electron Microscopy Sciences, Hatfield, PA) before imaged using the inverted confocal microscope (Zeiss LSM 510) available at Duke Light Microscopy Core Facility.

5.2.5 Albumin ELISA quantification

The single and co-culture microgels were cultured in Hep and the optimized co-culture media respectively. Hep in Col-Sandwich condition were cultured in Hep medium. The culture media were changed and collected once every two days. The samples were analyzed using rat albumin ELISA quantification kit (Bethyl Laboratories, Montgomery, TX) following the manufacturer's protocol and the absorbance was determined with the FLUOstar OPTIMA microμder (BMG Labtech, Germany).

5.2.6 Urea assay

The samples were analyzed for urea secretion using Urea Nitrogen (BUN) Test (Stanbio Laboratory, Boerne, TX) following the manufacturer's protocol and the absorbance was determined with the FLUOstar OPTIMA microplate reader (BMG Labtech, Germany).

5.2.7 Cytochrome P450 3A4 (CYP3A4) assay and induction

At day 8, 16 ad 24, the cell culture samples were treated with CYP3A4 assay substrate (Promega, Madison, WI) following the manufacturer's protocol before the luminescence was analyzed with the FLUOstar OPTIMA microplate reader (BMG Labtech, Germany). Dexamethasone (Dex) is a known inducer for CYP3A4 enzymatic activity. To perform the induction, the cell culture samples were pretreated with 10 μM Dex for 72 h prior to analysis.

5.2.8 Statistical analysis

The results were reported as the mean ± S.E.M. for three independently performed experiments. Statistical significance was determined using one or two way ANOVA followed by Tukey's Post Test (Prism 5.0, GraphPad Software, La Jolla, CA). The albumin, urea and CYP3A4 results were reported as amount per 10^6 cells where the number of cells in each sample was determined by counting cells after trypsination or Accutase (Life Technologies, Grand Island, NY) treatment.

5.3 Results

5.3.1 Generation of hepatocyte spheroids and subsequent encapsulation in microgel

Primary rat hepatocytes at 6 million cells/mL were encased in the DE droplets (~4 nL/droplet) (Figure 5-2a). At 4 h post droplet formation, monodisperse spheroids were formed (Figure 5-2b). The oil shell could be removed by pipetting the droplets on top of a cell strainer then the oil would evaporate after transient contact with air (Figure 5-2c & 5-2d). The inner phase (1% alginate) could be induced to polymerize upon oil shell removal and exposure to calcium chloride solution, generating microgels with single spheroids. The average size of the microgels was around 200 μm, the same as the DE droplets (Figure 5-2e & 5-2f). The microgel size and hence the thickness of the microgel layer is tunable as demonstrated by the production of smaller gel (122 μm) containing spheroids of ~80 μm diameter using a device with a reduced channel width and depth (100 μm) (Figure 5-3 a-d).

The biochemical composition of the droplet inner phase could be precisely controlled to modulate hepatocyte functions. To demonstrate, 0.25 mg/mL rat tail collagen I was added to the alginate solution, which was applied as the inner phase of droplet. Collagen I was chosen as it had been shown to enhance hepatocyte functions when used as substrate matrix during culture [138] while also serving as an immune-protective material [124]. Immunostaining of the spheroids encapsulated in microgels after their formation verified the presence of collagen fibrils around both human HEK-293 and rat hepatocyte spheroids, suggesting the collagen fibrils did not originate from the rat hepatocytes and could supply biochemical and mechanical cues in microscale range (Figure 5-3e).

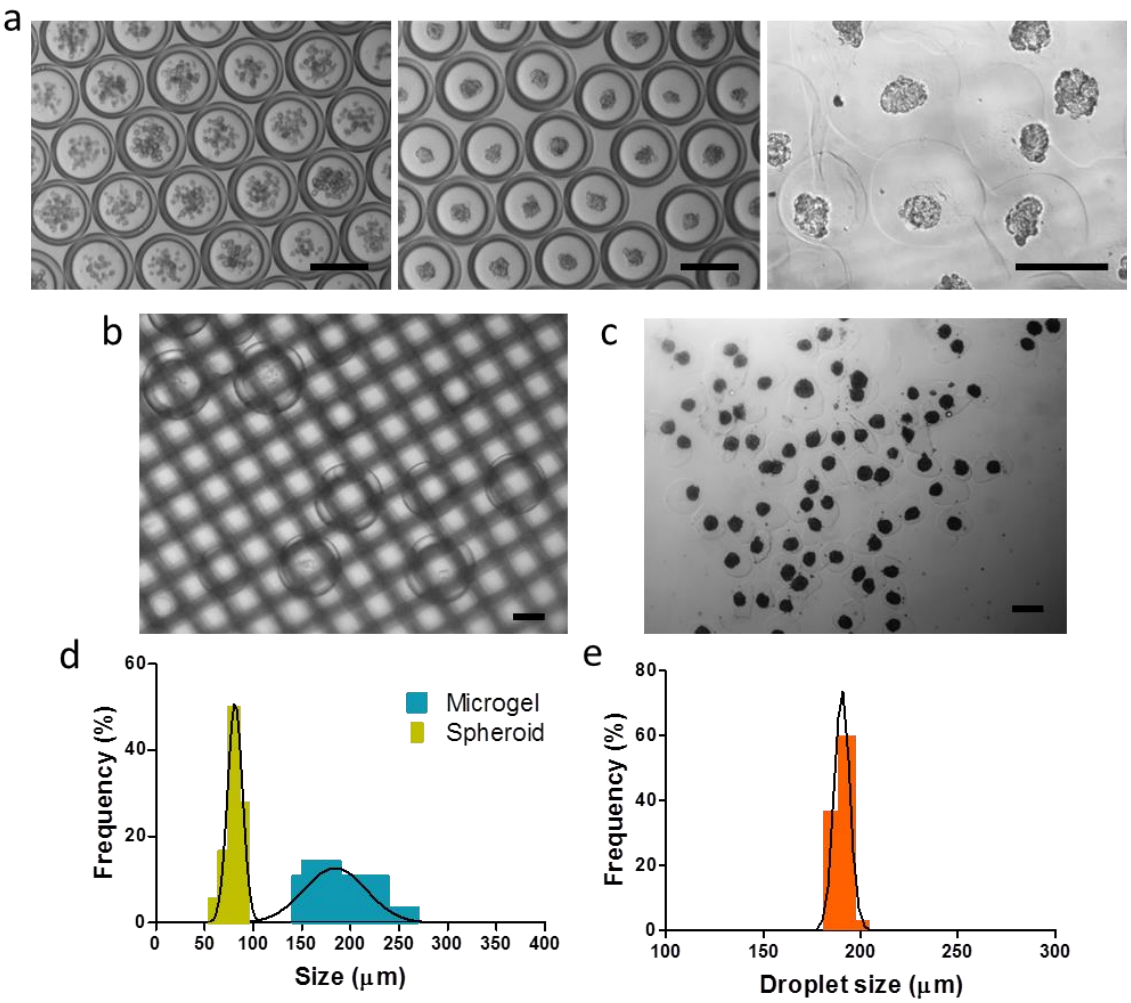
a
b
c
d
60
40
20
0
Frequency (%)
0
50
100
150
200
250
300
350
400
Size (μm)
Microgel
Spheroid
e
80
60
40
20
0
Frequency (%)
100
150
200
250
300
Droplet size (μm)

Figure 5-2: a) Microencapsulated spheroid production (Left & middle: Bright field image taken at time 0 & 4 h. Right: Microgel formation after oil removal). (Scale bar = 200 μm) b) DE droplet trapped on top of a cell strainer while rinsed with calcium-containing solution. (Scale bar = 100 μm) c) Alginate microgels encapsulating single hepatocyte spheroid. (Scale bar = 200 μm) d) Size distribution of spheroid and microgel. e) Size distribution of DE droplet.

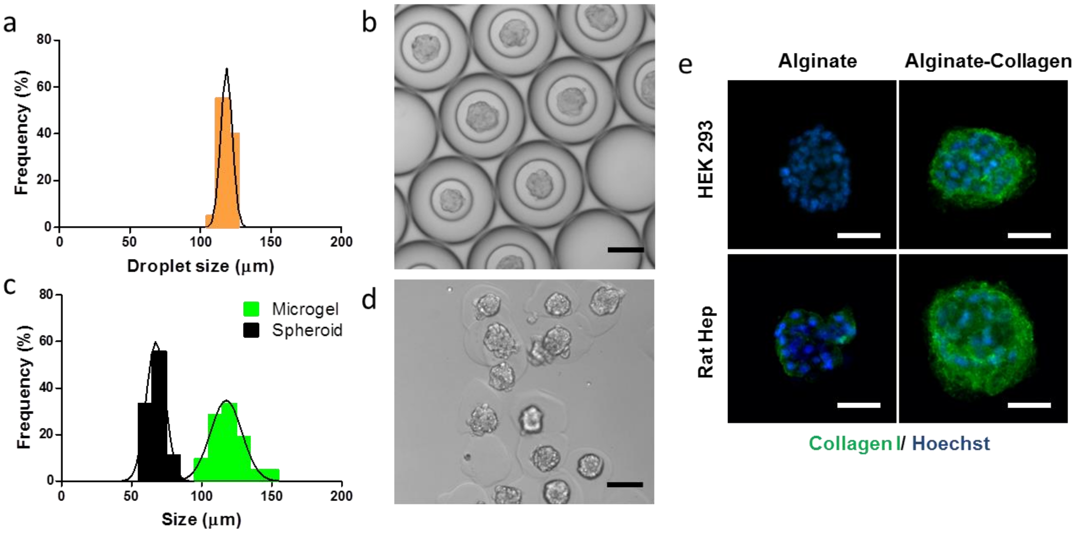

Figure 5-3: a & b) Size distribution of DE droplets produced from microfluidic device with 100 μm channel width and depth and the representative bright field image. c & d) Size distribution of microgel and spheroid produced from the 122 μm droplets and the representative bright field image. (Scale bar = 100 μm) e) Immunostaining of rat collagen I of HEK 293 and rat hepatocytes spheroid encapsulated in different materials. (Scale bar = 50 μm)

5.3.2 Characterization of hepatocytes cultured in 2D and 3D

Maintaining long-term hepatocyte functions has been the major obstacle of liver tissue engineering. Collagen sandwich is the current gold standard of culturing hepatocytes in 2D [138]. In a collagen sandwich configuration, hepatocytes were situated betwen two layers of collagen gel and exposed to microenvironment cues in a pseudo-3D configuration where they displayed normal cubic cell shape with tight cell-cell junctions after 7 days of culture, a feature that was lost when the top collagen layer was absent (Figure 5-4a). Using hepatocytes cultured in the collagen sandwich configuration

(Col-sandwich) as a 2D control, the performance of the microencapsulated hepatocyte spheroids with different microscale niche was compared. After 24 days of culture, hepatocyte spheroids maintained their compact, spherical morphology and viability in alginate-collagen (Alg-col) microgels, whereas the two features were lost in hepatocyte spheroids encapsulated in alginate (Alg) microgels (Figure 5-4b). Hepatocytes cultured in Col-sandwich could also maintain the morphology and viability over the course of 24 days. 5(6)-Carboxy-2′,7′-dichlorofluorescein diacetate (CDFDA) staining indicated the activity of the MRP-2 transporter and formation of bile canaliculi in all three cases. In the case of Col-sandwich, channel-like canaliculi were observed in some regions, whereas the spheroid samples displayed patchy and increased amount of signals. Functional assessments showed that the amount of albumin synthesized by hepatocytes per day in Alg-col was higher than the other two cases on day 12, 16 and 18 (Figure 5-5a), and the cumulative amount of albumin synthesized was also significantly higher than the other two cases (Figure 5-5b). Hepatocytes encapsulated in Alg-col synthesized significantly more urea on a few days but there was not significant difference in the cumulative level of release (Figure 5-5c & 5-5d). Lastly, cytochrome P450 3A4 (CYP3A4) luminogenic assay revealed that the basal level of CYP3A4 activity of hepatocytes in Alg-col was ~4-5 fold & ~15 fold higher than the those in Alg and Col-sandwich at day 16 and 24 respectively (Figure 5-5e). The induction of CYP3A4 activity (3-5 fold) upon 10 μM dexamethasone exposure of all three cases conformed with results reported in literature (Figure 5-5f) [139]. Overall, the results of this experiment showed that hepatocytes in Alg-col exhibited the highest functions, while those in Alg and Col-sandwich performed similarly but inferiorly. The results also implied that both 3D culture configuration with extensive cell-cell interactions and a conducive matrix microenvironment are important to maintaining hepatocyte functions. Given that other proteins such as fibronectin and hyaluronic acid can be incorporated in our system readily, our technology holds promise to screen for optimal matrix microenvironment for spheroid culture in many applications.

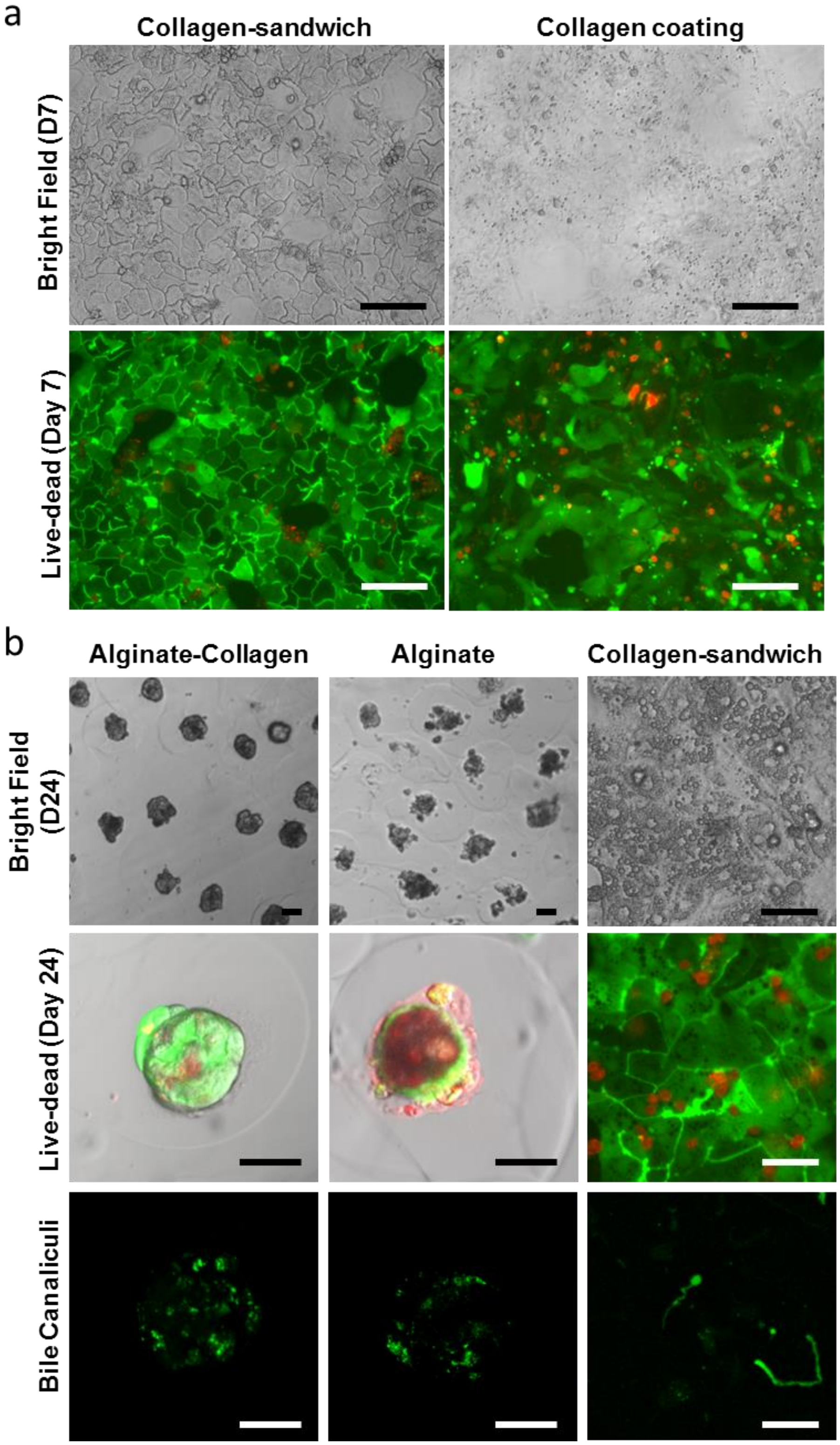

a
Collagen-sandwich
Collagen coating
Bright Field (D7)
Live-dead (Day 7)
b
Alginate-Collagen
Alginate
Collagen-sandwich
Bright Field (D24)
Live-dead (Day 24)
Bile Canaliculi

Figure 5-4: a) Characterization (morphology and live-dead staining) of hepatocyte cultured in collagen sandwich configuration or on collagen coating only for 7 days. (Scale bar = 100 μm) Hepatocytes cultured in Col-sandwich exhibited cubic cell shape while the ones cultured on a single collagen coating displayed elongated, fibroblast-like shape. b) Characterization (morphology, live-dead staining at Day 24 and staining for bile canaliculi) of hepatocyte cultured in different conditions. (Scale bar = 50 μm)

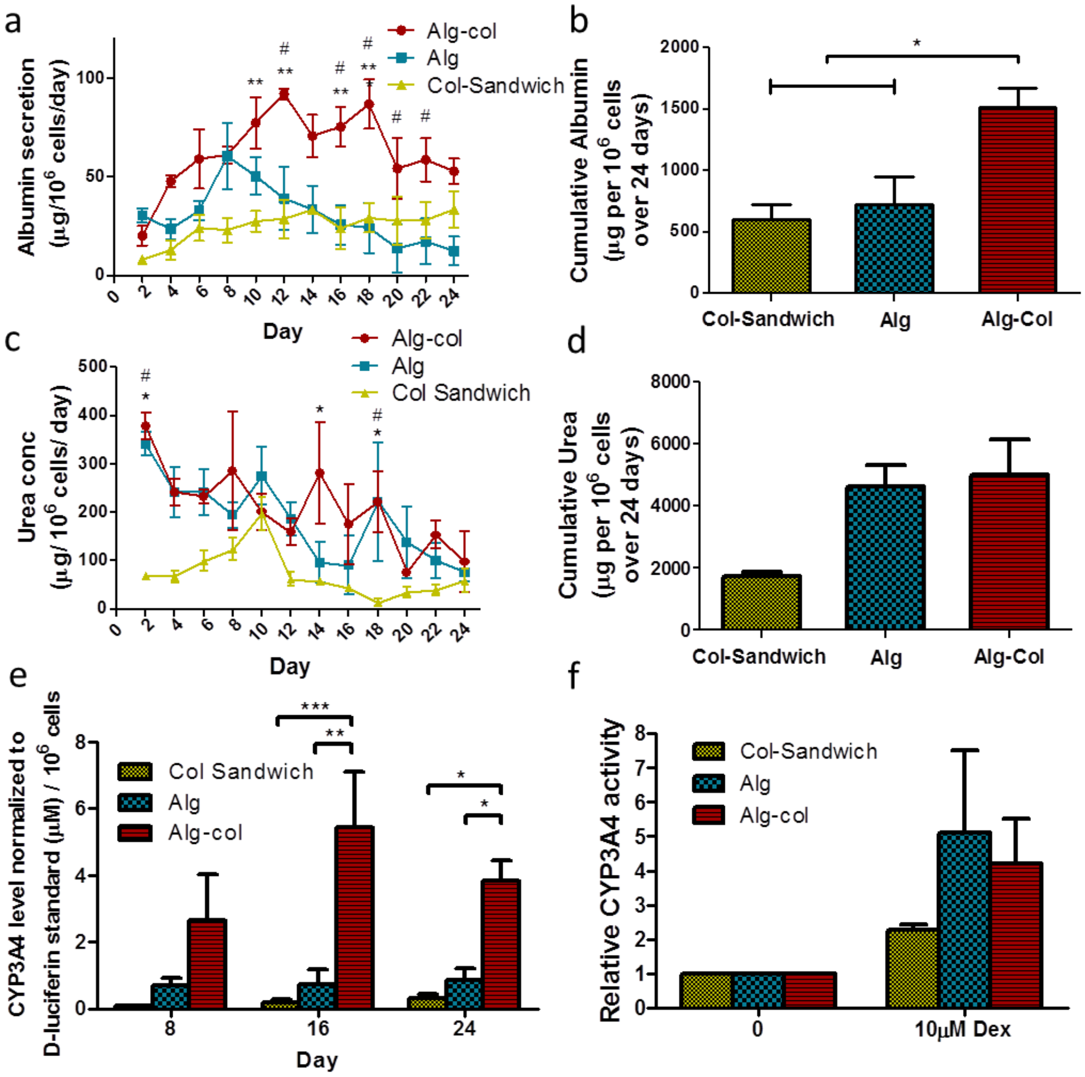

Figure 5-5: a) Daily albumin release (#p<0.05 between Alg and Col-Sandwich, **p<0.01 between Alg-col and Col-Sandwich). b) Cumulative albumin release of 3 conditions for 24 days (*p<0.05) c) Daily urea secretion (#p<0.05 between Alg and Col-Sandwich, *p<0.05 between Alg-col and Col-Sandwich).). d) Cumulative urea secretion of 3 conditions for 24 days. e) Basal CYP3A4 activity measured by a luminogenic assay. f) Induction of CYP3A4 activity after treatment with 10 μM Dex for 72 h.

5.3.3 Investigation of the co-culture of EPC and Hep

As a first step of the co-culture experiment, different media formulations were tested to determine the optimal cell culture conditions for both types of cells. EGM-2, the culture medium for EPC, was mixed with hepatocyte medium at assorted ratios for screening. The proliferation and viability of EPC decreased as the fraction of hepatocyte medium increased while hepatocyte viability was poor when they were cultured in EGM-2 (Figure 5-6b & 5-6c). The cumulative albumin and urea secretions were not significantly different when the hepatocyte medium constituted 50 or 66% of the co-culture medium (Figure 5-6d & 5-6e). Consequently, a 1:1 mixture of EGM-2 and hepatocyte medium was selected to best preserve the functions and viability of EPC and hepatocytes respectively.

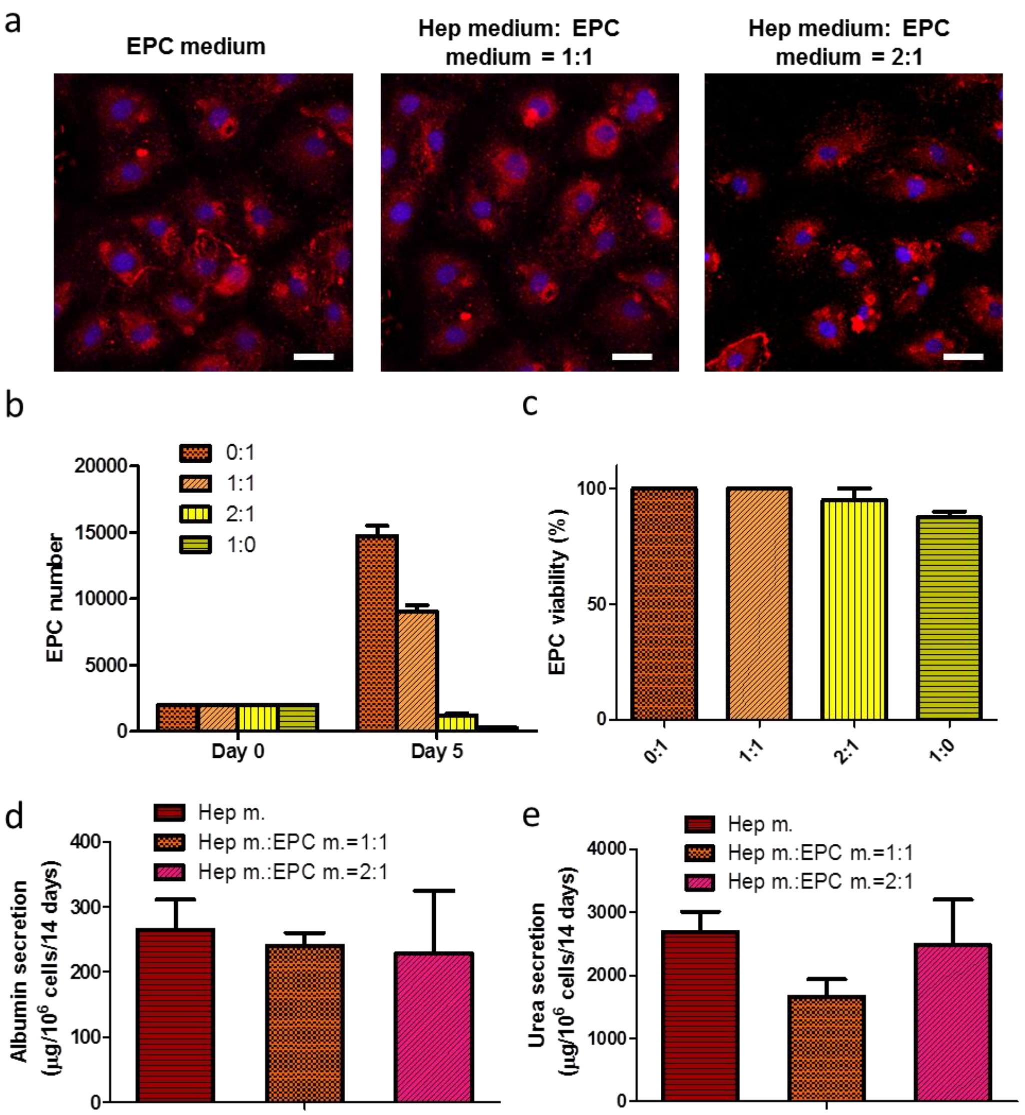

Figure 5-6: a) Immunostaining of von Willibrand factor (vWF), an EPC marker, of EPC cultured in various media. (Scale bar = 25 μm) b & c) EPC number and viability after culture in various media for 5 days. d & e) Cumulative albumin and urea secretion of hepatocytes cultured in various media for 14 days.

Next, various ratios (5:1, 3:1, 1:1, 1:3) of hepatocytes and EPC were mixed and encased into DE droplets to generate co-culture spheroids encapsulated in alginate microgels. Before loaded into droplets, the two cell types were labelled with different celltracker markers to assess their organization in the composite spheroid (Figure 5-7a). Analysis on the fluorescent images taken with the spheroids showed that at low hepatocyte to EPC ratio, EPC tended to envelop individual hepatocytes. When their numbers were approximately equal, the two cell types distributed evenly. As hepatocyte fraction increased, hepatocytes preferentially aggregated, leaving the EPC on the periphery. Functional assessments showed that EPC improved hepatocyte performance (syntheses of albumin and urea, basal activity of CYP3A4) significantly when the ratio of hepatocyte to EPC was 5:1 (Figure 5-7 b–d). The performance declined as EPC fraction increased. Whilst our data confirmed that EPC could support hepatocyte functions in a co-culture spheroid configuration, the influence was only observed at certain cell-to-cell ratio. At some other ratios (1:1 and 1:3) the effect was even opposite where hepatocyte performance was below that of control. One possible explanation is that, as EPC fraction increased, homocellular interactions among hepatocytes were disrupted which could not be substituted with heterocellular influence from EPC. Further study is required to prove this hypothesis.

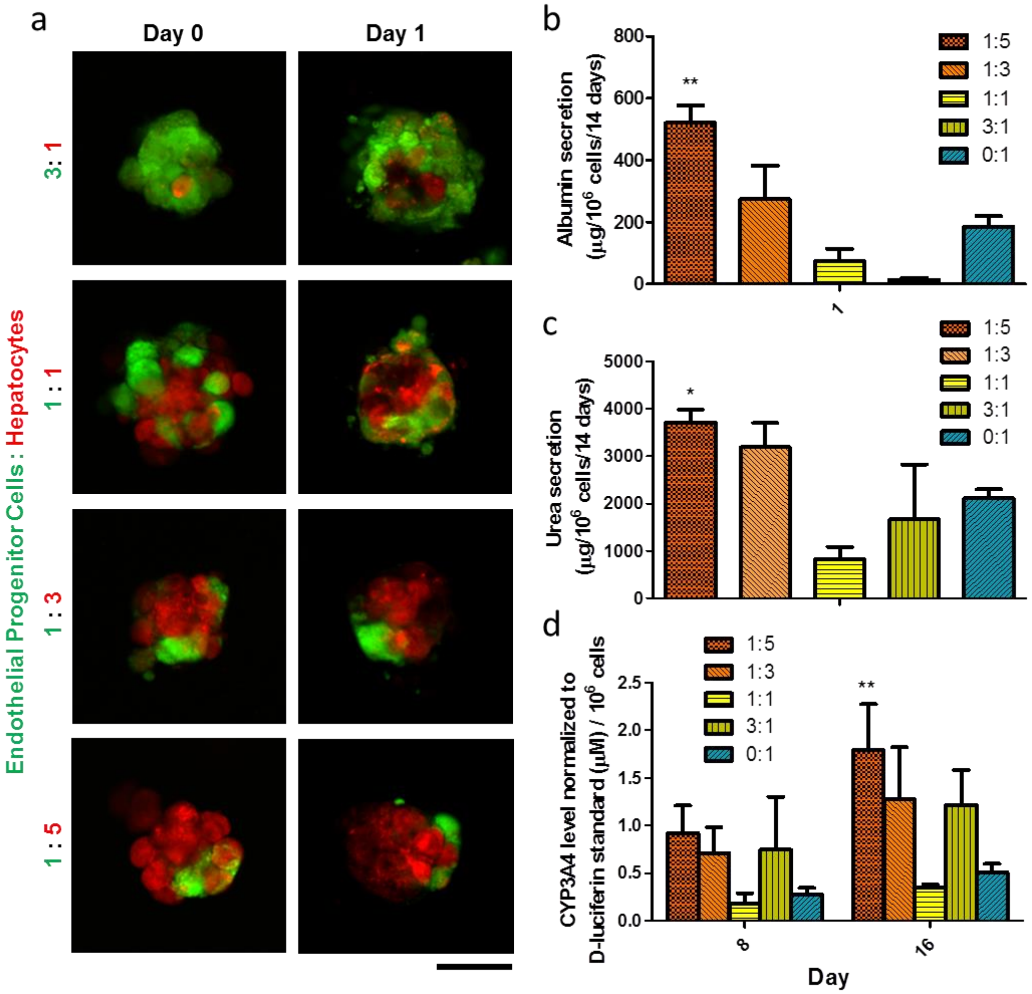

Figure 5-7: a) Tracking of cell organization in the composite spheroids at different co-culture ratios. (Scale bar = 50 µm) b) Cumulative albumin release for 14 days ($p<0.01$ between 1:5 and 1:1/3:1/0:1). c) Cumulative urea secretion for 14 days (*$p<0.05$ between 1:5 and 1:1/3:1/0:1). d) Basal CYP3A4 activity measured by a luminogenic assay (**$p<0.01$ between 1:5 and 0:1).**

5.3.4 Combination of heterocellular influence and conducive matrix cue

Finally, we aimed at investigating whether conducive matrix cues would complement heterocellular interactions to further increase hepatocyte performance synergistically. Hepatocyte spheroids encapsulated in Alg-col (Hep in Alg-col), co-culture spheroids (5:1 ratio) encapsulated in Alg (HepEPC in Alg) and Alg-col (HepEPC in Alg-col) were generated and analyzed (Figure 5-8a). The spheroids were immunofluorescently stained to discern the two distinct types of cells. Staining for albumin and von Willibrand factor (vWF) indicated strong staining from heptaocytes and the presence of EPC. The viability of all three cases was well preserved at day 14 and formation of bile canaliculi was also observed. The amount of cumulative albumin synthesized was comparable between Hep in Alg-col and HepEPC in Alg and significantly higher in HepEPC in Alg-col (Figure 5-8b) while the difference in urea secretion was not significantly different (Figure 5-8c). For basal CYP3A4 activity, the levels of three cases were not significantly different at day 8, however HepEPC in Alg-col recorded significantly higher level of activity (~2 times of other groups) at day 16 (Figure 5-8d). Applying 10 μM dexamethasone to HepEPC in Alg-col induced CYP3A4 activity by 5 fold which was again consistent with literature data (Figure 5-8e) [139]. Overall, our data suggested that matrix cues from collagen exerted a similar supporting effect to co-culture with EPC on hepatocytes, and hepatocytes responded to both types of influence when they were supplied simultaneously. This example is a clear manifestation of the capability of our technology in optimizing both cell-cell and cell-extracellular matrix interactions for hepatocyte spheroid encapsulation.

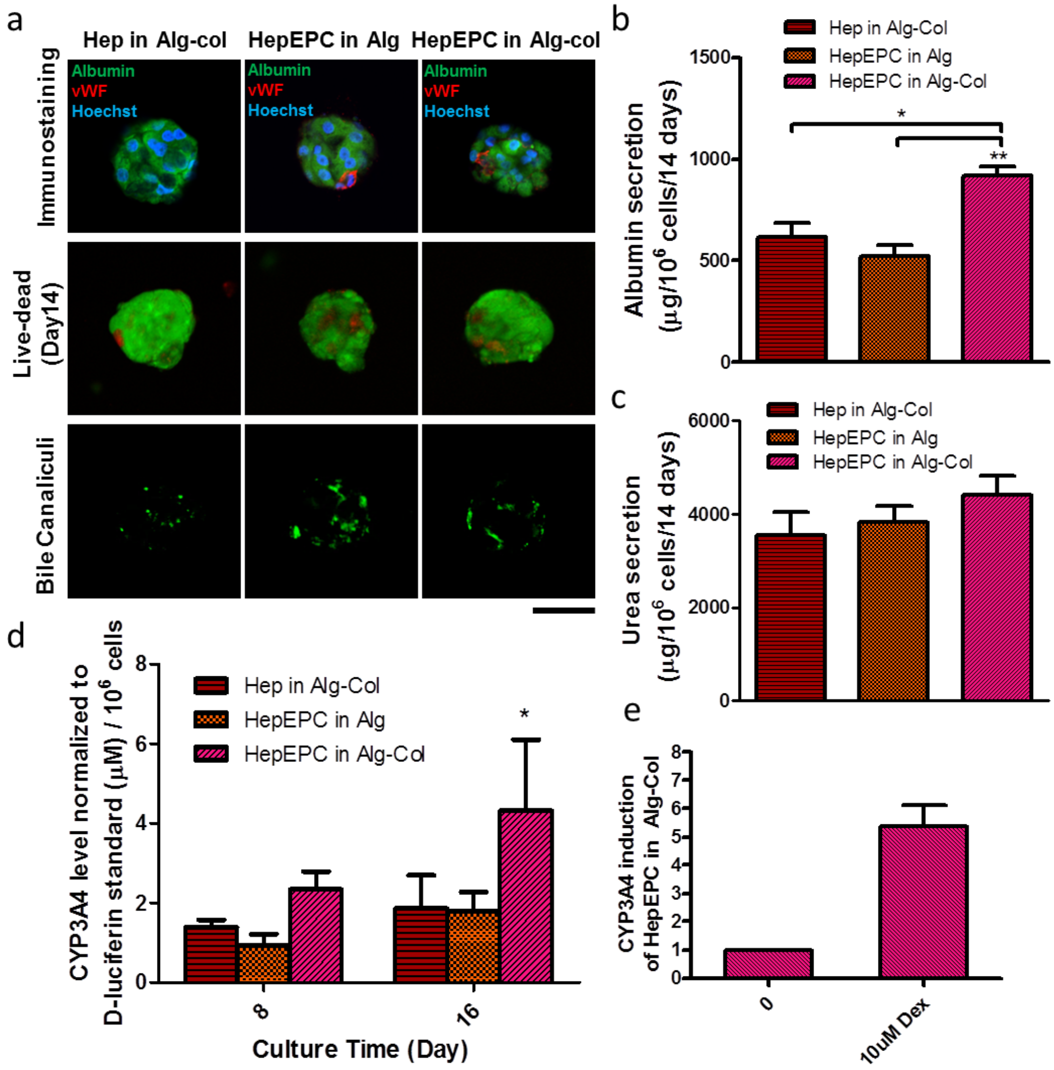

Figure 5-8: a) Characterization (immunostaining against hepatocyte (albumin) and EPC (vWF) markers, live-dead staining and staining of bile canaliculi) of single or co-culture spheroids cultured in different conditions. (Scale bar = 50 μm) b) Cumulative albumin release for 14 days. c) Cumulative urea secretion for 14 days. d) Basal CYP3A4 activity measured by a luminogenic assay (*$p<0.05$ between HepEPC in Alg-col and HepEPC in Alg). e) Induction of CYP3A4 activity after treatment with 10 μM Dex for 72 h.

5.4 Discussion

Microencapsulated hepatocyte spheroids can be applied in the fluidized bed of biroeactor for bioartificial liver, direct injection into the peritoneal space or drug screening platform [56, 140]. Our technology, in particular, offers certain benefits over traditional microencapsulation technology. First of all, the microgel size is smaller than 200 μm containing a spheroid of ~80 μm. This is hard to achieve with existing technology as the needle/nozzle size would be restrained by the size of spheroids encapsulated and shear force exerted on cells, resulting in a size range of 500 – 1000 μm of the microgel/microcapsule generated [127]. Reducing the microgel/microcapsule size would definitely be advantageous as the hydrogel layer has proven a significant barrier to the diffusion of large molecules. Literature data showed that it took 15 min versus 1 h for the release of bovine albumin serum to reach equilibrium from alginate gels of 400 μm and 1 mm in diameter respectively [141]. Our data showed that it took longer, though not significantly, for albumin to diffuse out from the 300 μm microgels than the 122 μm ones, demonstrating microgels with larger surface-to-volume ratio enables faster diffusion (Figure 5-9). Since many of the liver's substrates for detoxification and synthetic products are large molecules, the presence of a diffusion barrier associated with the immobilization materials may explain why so few, if not none, of the existing bioartificial livers have attained satisfactory results in clinical trials [119]. From a clinical point of view it is also important to decrease the total device volume by using smaller microgels in order to reduce patients’ extracorporeal plasma compartment and hence prevent hypotension occurring in patients [142]. Secondly, perhaps more importantly, our technology produces microgels containing single spheroid, in contrast to a Poisson-distributed fashion. The latter scenario will lead to possible agglomeration of multiple spheroids within a single microgel/microcapsule, compromising molecular transport to and from a fused spheroid. There is wide consensus that necrosis in spheroid core will occur if the spheroid size is larger than ~150 μm [68], which is likely to happen in the event of spheroid fusion within the microgel/microcapsule. Our high-throughput technology also circumvents the need to purify the microencapsulated spheroids from empty capsules. This would be crucial if a sufficient number (in the order of million/billion) of microgels/microcapsules are to be generated with high yield and uniformity to satisfy GMP for clinical applications. Last but not least, the DE technology we embraced provides one-step generation of microencapsulated hepatocyte spheroids whereas other technologies require formation of spheroid before microencapsulation [74]. The biochemical composition of the encapsulation materials and cell composition in spheroid could be flexibly tuned to enhance and maintain hepatocyte functions. The use of EPC as a novel supporting cell type to enhance hepatocyte functions open up new opportunities in maintainig long-term hepatocyte functions by co-culture with cell types that are not immortalized or obtained via invasive means. Nevertheless, the fact that at certain co-culture ratios the beneficial effect was lost means further research should be devoted into studying the mechanism of the phenomenon and optimizing the process. The potential of forming co-culture spheroids in DE droplets could also facilitate the high-throughput generation of miniaturized, injectable liver-bud for use in liver replacement therapy.

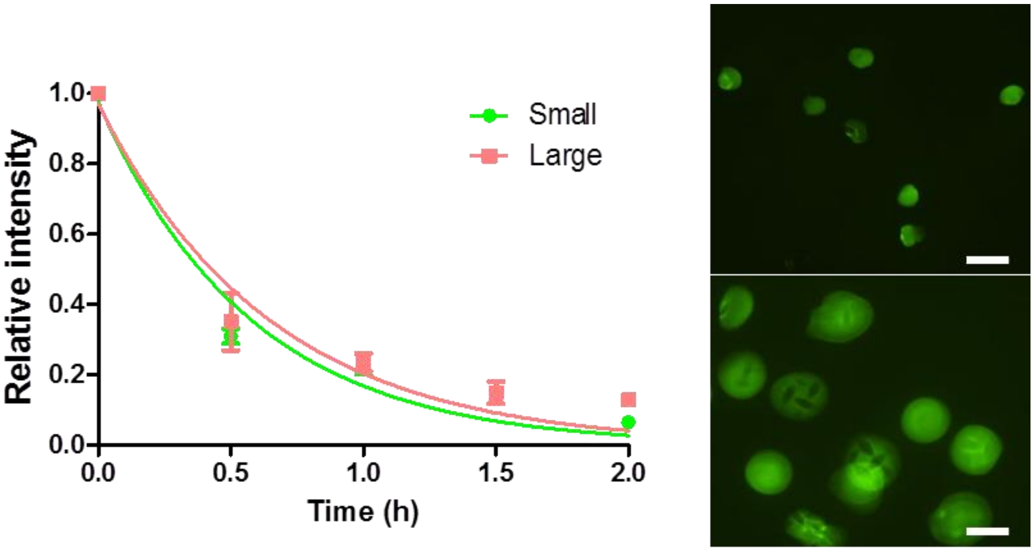

Figure 5-9: Relative intensity of albumin-FITC encapsulated in microgels of different size. The total intensity of the gel at each time point was substracted with the intensity at equilibrium (5 days) and normalized with the intensity at time 0. Gaussian nonlinear fitting was shown on the graph. The top and bottom figure on the right shows the fluorescent images of small and large gel. (Scale bar = 200 μm)

5.5 Conclusions

In this study, we demonstrated the efficient one-step production of microencapsulated hepatocyte spheroids with high yield, flexibility and uniformity via the generation of microfluidics DE droplet. We showed that the incorporation of collagen in the encapsulation materials and EPC (hepatocyte to EPC ratio = 5:1) as a novel supporting cell source would enhance the long-term performance of hepatocytes. In the broader sense of biomanufacturing, we envisioned the technology can be widely adopted to screen for optimal matrix environment and cell composition for spheroid culture and scaled up to manufacture microencapsulated spheroid for various liver tissue engineering and medical applications.

References

1. Kobel, S. and M.P. Lutolf, *Biomaterials meet microfluidics: building the next generation of artificial niches.* Curr Opin Biotechnol, 2011. **22**(5): p. 690-7.

2. Romanova, E.V., et al., *Small-volume analysis of cell-cell signaling molecules in the brain.* Neuropsychopharmacology, 2014. **39**(1): p. 50-64.

3. Macarron, R., et al., *Impact of high-throughput screening in biomedical research.* Nat Rev Drug Discov, 2011. **10**(3): p. 188-95.

4. Mayr, L.M. and P. Fuerst, *The future of high-throughput screening.* J Biomol Screen, 2008. **13**(6): p. 443-8.

5. V.G., Y., et al., *Micro- and Nanoscale Technologies in High-Throughput Biomedical Experimentation*, in *NanoScience in Biomedicine*, S. D., Editor 2009, Springer Berlin Heidelberg. p. 314-346.

6. Michael, S., et al., *A robotic platform for quantitative high-throughput screening.* Assay Drug Dev Technol, 2008. **6**(5): p. 637-57.

7. Zhang, Y., H.F. Chan, and K.W. Leong, *Advanced materials and processing for drug delivery: the past and the future.* Adv Drug Deliv Rev, 2013. **65**(1): p. 104-20.

8. Rolland, J.P., et al., *Direct fabrication and harvesting of monodisperse, shape-specific nanobiomaterials.* J Am Chem Soc, 2005. **127**(28): p. 10096-100.

9. Glangchai, L.C., et al., *Nanoimprint lithography based fabrication of shape-specific, enzymatically-triggered smart nanoparticles.* J Control Release, 2008. **125**(3): p. 263-72.

10. Dendukuri, D., et al., *Continuous-flow lithography for high-throughput microparticle synthesis.* Nat Mater, 2006. **5**(5): p. 365-9.

11. Nge, P.N., C.I. Rogers, and A.T. Woolley, *Advances in microfluidic materials, functions, integration, and applications.* Chem Rev, 2013. **113**(4): p. 2550-83.

12. Whitesides, G.M., *The origins and the future of microfluidics.* Nature, 2006. **442**(7101): p. 368-73.

13. Zhang, W., et al., *PMMA/PDMS valves and pumps for disposable microfluidics.* Lab Chip, 2009. **9**(21): p. 3088-94.

14. Iliescu, C., et al., *A practical guide for the fabrication of microfluidic devices using glass and silicon.* Biomicrofluidics, 2012. **6**(1): p. 16505-1650516.

15. Cate, D.M., et al., *Recent developments in paper-based microfluidic devices.* Anal Chem, 2015. **87**(1): p. 19-41.

16. Hansen, C. and S.R. Quake, *Microfluidics in structural biology: smaller, faster em leader better.* Curr Opin Struct Biol, 2003. **13**(5): p. 538-44.

17. Gao, Y., et al., *Plasmonic Mach-Zehnder interferometer for ultrasensitive on-chip biosensing.* ACS Nano, 2011. **5**(12): p. 9836-44.

18. Sharei, A., et al., *A vector-free microfluidic platform for intracellular delivery.* Proc Natl Acad Sci U S A, 2013. **110**(6): p. 2082-7.

19. Bhatia, S.N. and D.E. Ingber, *Microfluidic organs-on-chips.* Nat Biotechnol, 2014. **32**(8): p. 760-72.

20. Truskey, G.A., et al., *Design considerations for an integrated microphysiological muscle tissue for drug and tissue toxicity testing.* Stem Cell Res Ther, 2013. **4 Suppl 1**: p. S10.

21. R.K., S., et al., *Designer emulsions using microfluidics.* Materials Today, 2008. **11**(4): p. 18-27.

22. Teh, S.Y., et al., *Droplet microfluidics.* Lab Chip, 2008. **8**(2): p. 198-220.

23. Abate, A.R. and D.A. Weitz, *High-order multiple emulsions formed in poly(dimethylsiloxane) microfluidics.* Small, 2009. **5**(18): p. 2030-2.

24. Ward, T., et al., *Microfluidic flow focusing: drop size and scaling in pressure versus flow-rate-driven pumping.* Electrophoresis, 2005. **26**(19): p. 3716-24.

25. Hindson, B.J., et al., *High-throughput droplet digital PCR system for absolute quantitation of DNA copy number.* Anal Chem, 2011. **83**(22): p. 8604-10.

26. Brouzes, E., *Droplet microfluidics for single-cell analysis.* Methods Mol Biol, 2012. **853**: p. 105-39.

27. Xu, X., et al., *Single-cell exome sequencing reveals single-nucleotide mutation characteristics of a kidney tumor.* Cell, 2012. **148**(5): p. 886-95.

28. Lawson, D.A., et al., *Single-cell analysis reveals a stem-cell program in human metastatic breast cancer cells.* Nature, 2015. **526**(7571): p. 131-5.

29. Chen, F., et al., *Chemical transfection of cells in picoliter aqueous droplets in fluorocarbon oil.* Anal Chem, 2011. **83**(22): p. 8816-20.

30. Lian, M., et al., *Monodisperse alginate microgel formation in a three-dimensional microfluidic droplet generator.* Biomicrofluidics, 2012. **6**(4): p. 44108.

31. Bosenberg, M.W. and J. Massague, *Juxtacrine cell signaling molecules.* Curr Opin Cell Biol, 1993. **5**(5): p. 832-8.

32. Blagovic, K., et al., *Engineering cell-cell signaling.* Curr Opin Biotechnol, 2013. **24**(5): p. 940-7.

33. Takeichi, M., *Morphogenetic roles of classic cadherins.* Curr Opin Cell Biol, 1995. **7**(5): p. 619-27.

34. Hurtado, S.P., et al., *Connexin expression and gap-junction-mediated cell interactions in an in vitro model of haemopoietic stroma.* Cell Tissue Res, 2004. **316**(1): p. 65-76.

35. Scheer, N., et al., *An instructive function for Notch in promoting gliogenesis in the zebrafish retina.* Development, 2001. **128**(7): p. 1099-107.

36. Rossello, R.A. and D. H, *Cell communication and tissue engineering.* Commun Integr Biol, 2010. **3**(1): p. 53-6.

37. Keller, G.M., *In vitro differentiation of embryonic stem cells.* Curr Opin Cell Biol, 1995. **7**(6): p. 862-9.

38. Wang, W., et al., *3D spheroid culture system on micropatterned substrates for improved differentiation efficiency of multipotent mesenchymal stem cells.* Biomaterials, 2009. **30**(14): p. 2705-15.

39. Zhang, L., et al., *Chondrogenic differentiation of human mesenchymal stem cells: a comparison between micromass and pellet culture systems.* Biotechnol Lett, 2010. **32**(9): p. 1339-46.

40. Reynolds, B.A. and R.L. Rietze, *Neural stem cells and neurospheres--re-evaluating the relationship.* Nat Methods, 2005. **2**(5): p. 333-6.

41. Rosso, F., et al., *From cell-ECM interactions to tissue engineering.* J Cell Physiol, 2004. **199**(2): p. 174-80.

42. Flemming, R.G., et al., *Effects of synthetic micro- and nano-structured surfaces on cell behavior.* Biomaterials, 1999. **20**(6): p. 573-88.

43. Lukashev, M.E. and Z. Werb, *ECM signalling: orchestrating cell behaviour and misbehaviour.* Trends Cell Biol, 1998. **8**(11): p. 437-41.

44. Taipale, J. and J. Keski-Oja, *Growth factors in the extracellular matrix.* FASEB J, 1997. **11**(1): p. 51-9.

45. Aplin, A.E. and R.L. Juliano, *Integrin and cytoskeletal regulation of growth factor signaling to the MAP kinase pathway.* J Cell Sci, 1999. **112 (Pt 5)**: p. 695-706.

46. Hutmacher, D.W., *Scaffold design and fabrication technologies for engineering tissues--state of the art and future perspectives.* J Biomater Sci Polym Ed, 2001. **12**(1): p. 107-24.

47. Mallick, K.K. and S.C. Cox, *Biomaterial scaffolds for tissue engineering.* Front Biosci (Elite Ed), 2013. **5**: p. 341-60.

48. Engler, A.J., et al., *Matrix elasticity directs stem cell lineage specification.* Cell, 2006. **126**(4): p. 677-89.

49. Dalby, M.J., N. Gadegaard, and R.O. Oreffo, *Harnessing nanotopography and integrin-matrix interactions to influence stem cell fate.* Nat Mater, 2014. **13**(6): p. 558-69.

50. Zeilinger, K., et al., *[Liver cell culture in bioreactors for in vitro drug studies as an alternative to animal testing].* ALTEX, 2000. **17**(1): p. 3-10.

51. Kim, W.R., et al., *Burden of liver disease in the United States: summary of a workshop.* Hepatology, 2002. **36**(1): p. 227-42.

52. Allen, J.W., T. Hassanein, and S.N. Bhatia, *Advances in bioartificial liver devices.* Hepatology, 2001. **34**(3): p. 447-55.

53. Uchida, S., et al., *An injectable spheroid system with genetic modification for cell transplantation therapy.* Biomaterials, 2014. **35**(8): p. 2499-506.

54. Allen, J.W. and S.N. Bhatia, *Improving the next generation of bioartificial liver devices.* Semin Cell Dev Biol, 2002. **13**(6): p. 447-54.

55. Navarro-Alvarez, N., et al., *Intramuscular transplantation of engineered hepatic tissue constructs corrects acute and chronic liver failure in mice.* J Hepatol, 2010. **52**(2): p. 211-9.

56. Miranda, J.P., et al., *Extending hepatocyte functionality for drug-testing applications using high-viscosity alginate-encapsulated three-dimensional cultures in bioreactors.* Tissue Eng Part C Methods, 2010. **16**(6): p. 1223-32.

57. Landry, J., et al., *Spheroidal aggregate culture of rat liver cells: histotypic reorganization, biomatrix deposition, and maintenance of functional activities.* J Cell Biol, 1985. **101**(3): p. 914-23.

58. Lazar, A., et al., *Extended liver-specific functions of porcine hepatocyte spheroids entrapped in collagen gel.* In Vitro Cell Dev Biol Anim, 1995. **31**(5): p. 340-6.

59. Bhatia, S.N., et al., *Effect of cell-cell interactions in preservation of cellular phenotype: cocultivation of hepatocytes and nonparenchymal cells.* FASEB J, 1999. **13**(14): p. 1883-900.

60. Stevens, K.R., et al., *InVERT molding for scalable control of tissue microarchitecture.* Nat Commun, 2013. **4**: p. 1847.

61. Lin, P., et al., *Assessing porcine liver-derived biomatrix for hepatic tissue engineering.* Tissue Eng, 2004. **10**(7-8): p. 1046-53.

62. LeCluyse, E.L., et al., *Cultured rat hepatocytes.* Pharm Biotechnol, 1996. **8**: p. 121-59.

63. Tuschl, G., et al., *Serum-free collagen sandwich cultures of adult rat hepatocytes maintain liver-like properties long term: a valuable model for in vitro toxicity and drug-drug interaction studies.* Chem Biol Interact, 2009. **181**(1): p. 124-37.

64. Khang, G., et al., *Preparation and characterization of natural/synthetic hybrid scaffolds.* Adv Exp Med Biol, 2003. **534**: p. 235-45.

65. Baraniak, P.R. and T.C. McDevitt, *Scaffold-free culture of mesenchymal stem cell spheroids in suspension preserves multilineage potential.* Cell Tissue Res, 2012. **347**(3): p. 701-11.

66. Korff, T. and H.G. Augustin, *Integration of endothelial cells in multicellular spheroids prevents apoptosis and induces differentiation.* J Cell Biol, 1998. **143**(5): p. 1341-52.

67. Bosnakovski, D., et al., *Chondrogenic differentiation of bovine bone marrow mesenchymal stem cells (MSCs) in different hydrogels: influence of collagen type II extracellular matrix on MSC chondrogenesis.* Biotechnol Bioeng, 2006. **93**(6): p. 1152-63.

68. Lin, R.Z. and H.Y. Chang, *Recent advances in three-dimensional multicellular spheroid culture for biomedical research.* Biotechnol J, 2008. **3**(9-10): p. 1172-84.

69. Lee, E.J., et al., *Spherical bullet formation via E-cadherin promotes therapeutic potency of mesenchymal stem cells derived from human umbilical cord blood for myocardial infarction.* Mol Ther, 2012. **20**(7): p. 1424-33.

70. Franko, A.J. and R.M. Sutherland, *Oxygen diffusion distance and development of necrosis in multicell spheroids.* Radiat Res, 1979. **79**(3): p. 439-53.

71. Kurosawa, H., *Methods for inducing embryoid body formation: in vitro differentiation system of embryonic stem cells.* J Biosci Bioeng, 2007. **103**(5): p. 389-98.

72. Hsiao, A.Y., et al., *384 hanging drop arrays give excellent Z-factors and allow versatile formation of co-culture spheroids.* Biotechnol Bioeng, 2012. **109**(5): p. 1293-304.

73. Choi, Y.Y., et al., *Controlled-size embryoid body formation in concave microwell arrays.* Biomaterials, 2010. **31**(15): p. 4296-303.

74. Wilson, J.L., et al., *Alginate encapsulation parameters influence the differentiation of microencapsulated embryonic stem cell aggregates.* Biotechnol Bioeng, 2014. **111**(3): p. 618-31.

75. Shendure, J. and E. Lieberman Aiden, *The expanding scope of DNA sequencing.* Nat Biotechnol, 2012. **30**(11): p. 1084-94.

76. Kosuri, S. and G.M. Church, *Large-scale de novo DNA synthesis: technologies and applications.* Nat Methods, 2014. **11**(5): p. 499-507.

77. Quan, J., et al., *Parallel on-chip gene synthesis and application to optimization of protein expression.* Nat Biotechnol, 2011. **29**(5): p. 449-52.

78. Yang, G. and S.G. Withers, *Ultrahigh-throughput FACS-based screening for directed enzyme evolution.* Chembiochem, 2009. **10**(17): p. 2704-15.

79. Antipov, E., et al., *Highly L and D enantioselective variants of horseradish peroxidase discovered by an ultrahigh-throughput selection method.* Proc Natl Acad Sci U S A, 2008. **105**(46): p. 17694-9.

80. Tawfik, D.S. and A.D. Griffiths, *Man-made cell-like compartments for molecular evolution.* Nat Biotechnol, 1998. **16**(7): p. 652-6.

81. Griffiths, A.D. and D.S. Tawfik, *Miniaturising the laboratory in emulsion droplets.* Trends Biotechnol, 2006. **24**(9): p. 395-402.

82. Aharoni, A., et al., *High-throughput screening of enzyme libraries: thiolactonases evolved by fluorescence-activated sorting of single cells in emulsion compartments.* Chem Biol, 2005. **12**(12): p. 1281-9.

83. Wu, H.W., C.C. Lin, and G.B. Lee, *Stem cells in microfluidics.* Biomicrofluidics, 2011. **5**(1): p. 13401.

84. Zhang, Y., et al., *A programmable microenvironment for cellular studies via microfluidics-generated double emulsions.* Biomaterials, 2013. **34**(19): p. 4564-72.

85. Saaem, I., et al., *Error correction of microchip synthesized genes using Surveyor nuclease.* Nucleic Acids Res, 2012. **40**(3): p. e23.

86. Quan, J. and J. Tian, *Circular polymerase extension cloning of complex gene libraries and pathways.* PLoS One, 2009. **4**(7): p. e6441.

87. Kim, C., et al., *Generation of core-shell microcapsules with three-dimensional focusing device for efficient formation of cell spheroid.* Lab Chip, 2011. **11**(2): p. 246-52.

88. Riess, J.G. and M.P. Krafft, *Advanced fluorocarbon-based systems for oxygen and drug delivery, and diagnosis.* Artif Cells Blood Substit Immobil Biotechnol, 1997. **25**(1-2): p. 43-52.

89. Lu, H.F., et al., *Three-dimensional co-culture of rat hepatocyte spheroids and NIH/3T3 fibroblasts enhances hepatocyte functional maintenance.* Acta Biomater, 2005. **1**(4): p. 399-410.

90. Schukur, L., et al., *Directed differentiation of size-controlled embryoid bodies towards endothelial and cardiac lineages in RGD-modified poly(ethylene glycol) hydrogels.* Adv Healthc Mater, 2013. **2**(1): p. 195-205.

91. Kitagawa, F., et al., *Chondrogenic differentiation of immortalized human mesenchymal stem cells on zirconia microwell substrata.* Tissue Eng Part C Methods, 2013. **19**(6): p. 438-48.

92. Shin, S.R., et al., *Cell-laden microengineered and mechanically tunable hybrid hydrogels of gelatin and graphene oxide.* Adv Mater, 2013. **25**(44): p. 6385-91.

93. Dawson, E., et al., *Biomaterials for stem cell differentiation.* Adv Drug Deliv Rev, 2008. **60**(2): p. 215-28.

94. Chung, C. and J.A. Burdick, *Influence of three-dimensional hyaluronic acid microenvironments on mesenchymal stem cell chondrogenesis.* Tissue Eng Part A, 2009. **15**(2): p. 243-54.

95. Yang, F., et al., *The effect of incorporating RGD adhesive peptide in polyethylene glycol diacrylate hydrogel on osteogenesis of bone marrow stromal cells.* Biomaterials, 2005. **26**(30): p. 5991-8.

96. Faulkner-Jones, A., et al., *Development of a valve-based cell printer for the formation of human embryonic stem cell spheroid aggregates.* Biofabrication, 2013. **5**(1): p. 015013.

97. Lee, K.H., et al., *Diffusion-mediated in situ alginate encapsulation of cell spheroids using microscale concave well and nanoporous membrane.* Lab Chip, 2011. **11**(6): p. 1168-73.

98. Yoon, S., et al., *Droplet-based microfluidic system to form and separate multicellular spheroids using magnetic nanoparticles.* Lab Chip, 2013. **13**(8): p. 1522-8.

99. Yu, L., M.C. Chen, and K.C. Cheung, *Droplet-based microfluidic system for multicellular tumor spheroid formation and anticancer drug testing.* Lab Chip, 2010. **10**(18): p. 2424-32.

100. Sakai, S., et al., *Cell-enclosing gelatin-based microcapsule production for tissue engineering using a microfluidic flow-focusing system.* Biomicrofluidics, 2011. **5**(1): p. 13402.

101. Tung, Y.C., et al., *High-throughput 3D spheroid culture and drug testing using a 384 hanging drop array.* Analyst, 2011. **136**(3): p. 473-8.

102. Jeong, G.S., et al., *Surface tension-mediated, concave-microwell arrays for large-scale, simultaneous production of homogeneously sized embryoid bodies.* Adv Healthc Mater, 2013. **2**(1): p. 119-25.

103. Lee, W.Y., et al., *The use of injectable spherically symmetric cell aggregates self-assembled in a thermo-responsive hydrogel for enhanced cell transplantation.* Biomaterials, 2009. **30**(29): p. 5505-13.

104. Luebke-Wheeler, J.L., et al., *E-cadherin protects primary hepatocyte spheroids from cell death by a caspase-independent mechanism.* Cell Transplant, 2009. **18**(12): p. 1281-7.

105. Takagi, J., et al., *Structure of integrin alpha5beta1 in complex with fibronectin.* EMBO J, 2003. **22**(18): p. 4607-15.

106. Donzelli, E., et al., *Mesenchymal stem cells cultured on a collagen scaffold: In vitro osteogenic differentiation.* Arch Oral Biol, 2007. **52**(1): p. 64-73.

107. Clausell-Tormos, J., et al., *Droplet-based microfluidic platforms for the encapsulation and screening of Mammalian cells and multicellular organisms.* Chem Biol, 2008. **15**(5): p. 427-37.

108. Matsunaga, Y.T., Y. Morimoto, and S. Takeuchi, *Molding cell beads for rapid construction of macroscopic 3D tissue architecture.* Adv Mater, 2011. **23**(12): p. H90-4.

109. Lin, R.Z., et al., *Magnetic reconstruction of three-dimensional tissues from multicellular spheroids.* Tissue Eng Part C Methods, 2008. **14**(3): p. 197-205.

110. Hong, S., et al., *Collagen microsphere production on a chip.* Lab Chip, 2012. **12**(18): p. 3277-80.

111. Tumarkin, E. and E. Kumacheva, *Microfluidic generation of microgels from synthetic and natural polymers.* Chem Soc Rev, 2009. **38**(8): p. 2161-8.

112. Chia, S.M., et al., *Engineering microenvironment for expansion of sensitive anchorage-dependent mammalian cells.* J Biotechnol, 2005. **118**(4): p. 434-47.

113. Fritschy, W.M., G.H. Wolters, and R. van Schilfgaarde, *Effect of alginate-polylysine-alginate microencapsulation on in vitro insulin release from rat pancreatic islets.* Diabetes, 1991. **40**(1): p. 37-43.

114. Lim, G.J., et al., *Cell microencapsulation.* Adv Exp Med Biol, 2010. **670**: p. 126-36.

115. Uludag, H., P. De Vos, and P.A. Tresco, *Technology of mammalian cell encapsulation.* Adv Drug Deliv Rev, 2000. **42**(1-2): p. 29-64.

116. Gauvin, R., et al., *Hydrogels and microtechnologies for engineering the cellular microenvironment.* Wiley Interdiscip Rev Nanomed Nanobiotechnol, 2012. **4**(3): p. 235-46.

117. Pareta, R., et al., *Immunoisolation: where regenerative medicine meets solid organ transplantation.* Expert Rev Clin Immunol, 2012. **8**(7): p. 685-92.

118. Carpentier, B., A. Gautier, and C. Legallais, *Artificial and bioartificial liver devices: present and future.* Gut, 2009. **58**(12): p. 1690-702.

119. Struecker, B., N. Raschzok, and I.M. Sauer, *Liver support strategies: cutting-edge technologies.* Nat Rev Gastroenterol Hepatol, 2014. **11**(3): p. 166-76.

120. Iwata, H. and Y. Ueda, *Pharmacokinetic considerations in development of a bioartificial liver.* Clin Pharmacokinet, 2004. **43**(4): p. 211-25.

121. Kinasiewicz, A., et al., *Culture of C3A cells in alginate beads for fluidized bed bioartificial liver.* Transplant Proc, 2007. **39**(9): p. 2911-3.

122. David, B., et al., *In vitro assessment of encapsulated C3A hepatocytes functions in a fluidized bed bioreactor.* Biotechnol Prog, 2004. **20**(4): p. 1204-12.

123. Jitraruch, S., et al., *Alginate microencapsulated hepatocytes optimised for transplantation in acute liver failure.* PLoS One, 2014. **9**(12): p. e113609.

124. No da, Y., G.S. Jeong, and S.H. Lee, *Immune-protected xenogeneic bioartificial livers with liver-specific microarchitecture and hydrogel-encapsulated cells.* Biomaterials, 2014. **35**(32): p. 8983-91.

125. Ambrosino, G., et al., *Isolated hepatocytes versus hepatocyte spheroids: in vitro culture of rat hepatocytes.* Cell Transplant, 2005. **14**(6): p. 397-401.

126. Selden, C., et al., *Evaluation of encapsulated liver cell spheroids in a fluidised-bed bioartificial liver for treatment of ischaemic acute liver failure in pigs in a translational setting.* PLoS One, 2013. **8**(12): p. e82312.

127. Tomei, A.A., et al., *Device design and materials optimization of conformal coating for islets of Langerhans.* Proc Natl Acad Sci U S A, 2014. **111**(29): p. 10514-9.

128. Chan, H.F., et al., *Rapid formation of multicellular spheroids in double-emulsion droplets with controllable microenvironment.* Sci Rep, 2013. **3**: p. 3462.

129. Bale, S.S., et al., *Long-term coculture strategies for primary hepatocytes and liver sinusoidal endothelial cells.* Tissue Eng Part C Methods, 2015. **21**(4): p. 413-22.

130. Bhatia, S.N., M.L. Yarmush, and M. Toner, *Controlling cell interactions by micropatterning in co-cultures: hepatocytes and 3T3 fibroblasts.* J Biomed Mater Res, 1997. **34**(2): p. 189-99.

131. Vozzi, F., et al., *Connected culture of murine hepatocytes and HUVEC in a multicompartmental bioreactor.* Tissue Eng Part A, 2009. **15**(6): p. 1291-9.

132. Yu, H., et al., *Improved tissue-engineered bone regeneration by endothelial cell mediated vascularization.* Biomaterials, 2009. **30**(4): p. 508-17.

133. Stroncek, J.D., et al., *Comparison of endothelial cell phenotypic markers of late-outgrowth endothelial progenitor cells isolated from patients with coronary artery disease and healthy volunteers.* Tissue Eng Part A, 2009. **15**(11): p. 3473-86.

134. Kang, S.D., et al., *Isolation of functional human endothelial cells from small volumes of umbilical cord blood.* Ann Biomed Eng, 2013. **41**(10): p. 2181-92.

135. Yamaoka, M., et al., *Enhancement of albumin production by hepatocyte growth factor in rat hepatocytes: distinction in mode of action from stimulation of DNA synthesis.* Liver, 1998. **18**(1): p. 52-9.

136. Urbich, C., et al., *Soluble factors released by endothelial progenitor cells promote migration of endothelial cells and cardiac resident progenitor cells.* J Mol Cell Cardiol, 2005. **39**(5): p. 733-42.

137. Brown, M.A., et al., *Characterization of umbilical cord blood-derived late outgrowth endothelial progenitor cells exposed to laminar shear stress.* Tissue Eng Part A, 2009. **15**(11): p. 3575-87.

138. Dunn, J.C., R.G. Tompkins, and M.L. Yarmush, *Long-term in vitro function of adult hepatocytes in a collagen sandwich configuration.* Biotechnol Prog, 1991. **7**(3): p. 237-45.

139. Li, C.Y., et al., *Micropatterned cell-cell interactions enable functional encapsulation of primary hepatocytes in hydrogel microtissues.* Tissue Eng Part A, 2014. **20**(15-16): p. 2200-12.

140. Fitzpatrick, E., et al., *Coculture with mesenchymal stem cells results in improved viability and function of human hepatocytes.* Cell Transplant, 2015. **24**(1): p. 73-83.

141. L., C., R. A., and H. D., *Improving cell encapsulation through size control.* J Biomater Sci Polym Ed, 2002. **13**(7): p. 783-96.

142. Jalan, R., S. Sen, and R. Williams, *Prospects for extracorporeal liver support.* Gut, 2004. **53**(6): p. 890-8.

Biography

Hon Fai Chan was born in Hong Kong, China on June 30th 1988. He graduated from University of Hong Kong with a Bachelor degree in Biomedical Engineering (First Class Honor).

Publications:

1. **“High-Throughput Screening of Microchip-synthesized Genes in Programmable Double-Emulsion Droplets”** **Chan HF***, Ma S*, Zhang Y, Leong KW (in preparation) (* contributed equally)
2. **“Efficient one-step production of microencapsulated single or co-culture hepatocyte spheroids with enhanced functions”** **Chan HF**, Zhang Y, Leong KW (submitted)
3. **"Scaffold-free, Human Mesenchymal Stem Cell-Based Tissue Engineered Blood Vessels“.** Jung Y, Ji H, Chen Z, **Chan HF**, Atchison L, Klitzman B, Truskey GA, and Leong KW Scientific Reports (in press)
4. **“3D Printing of Highly Stretchable and Tough Hydrogels into Complex, Cellularized Structures** “. S Hong*, D Sycks*, **HF Chan***, S Lin, GP Lopez, F Guilak, KW Leong, X Zhao Advanced Materials 27 (27), 4034-4034 (* contributed equally)
5. **“A Novel Fluorosurfactant for Emulsion-based Biological Applications”**. Chiu Y, **Chan HF**, Phua KKL, Zhang Y, Juul S, Knudsen B, Leong KW ACS Nano. 2013
6. **“Harnessing Localized Ridges for High-Aspect-Ratio Hierarchical Patterns with Dynamic Tunability and Multifunctionality”**. Cao C, **Chan HF**, Zang J, Leong KW, Zhao X. Adv Mater. 2013 Dec 12.

7. **"Rapid formation of multicellular spheroids in double-mulsion droplets with controllable microenvironment"**. **Chan HF**, Zhang Y, Ho YP, Chiu YL, Jung Y, Leong KW. Sci Rep. 2013 Dec 10;3:3462
8. **"Magnetoactive sponges for dynamic control of microfluidic flow patterns in microphysiological systems"**. Hong S, Jung Y, Yen R, **Chan HF**, Leong KW, Truskey GA, Zhao X. Lab Chip. 2014 Feb 7;14(3):514-21.
9. **"Design Considerations for an Integrated Microphysiological Muscle Tissue for Drug and Tissue Toxicity Testing"**. Truskey GA, Achneck HA, Bursac N, **Chan HF**, Cheng CS, Fernandez C, Hong S, Jung Y, Koves T, Kraus WE, Leong K., Madden L, Reichert WE, Zhao X. Stem Cell Research & Development. 2013 4(Suppl 1):S10
10. **"A programmable microenvironment for cellular studies via microfluidics-generated double emulsions"**. Zhang Y, Ho YP, Chiu YL, **Chan HF**, Chlebina B, Schuhmann T, You L, Leong KW. Biomaterials. 2013 Jun;34(19):4564-72. Epub 2013 Mar 21.
11. **"Advanced materials and processing for drug delivery: the past and the future"**. Zhang Y, **Chan HF**, Leong KW. Adv Drug Deliv Rev. 2013 Jan;65(1):104-20.. Epub 2012 Oct 23. Review